A Study on the Deformation Behaviour of the Cathode Collector Bar at High Temperature and Low Stress Levels

Mémoire

Femi Richard Fakoya

Maîtrise en génie civil
Maître ès sciences (M.Sc)

Québec, Canada

Résumé

L'étude de la déformation de la barre collectrice dans les conditions subies au sein de la cellule de réduction d'aluminium est d'une grande importance pour l'optimisation de l'efficacité et l'augmentation de la durée de vie de la cellule. Ce mémoire nous informe des résultats d'un programme expérimental réalisé sur une barre de collectrice en acier. Le but, est d' étudier son comportement en tenant compte de ses propriétés thermiques, mécaniques et de fluage. Des essais ont été effectués en compression à de basses tensions, de 0,5 à 2MPa et à une température élevée, de 900°C. Différents comportements ont été observés à de faibles contraintes, jusqu'à 2MPa, cela peut être justifié par le temps et le niveau de pression appliqué. L'inspection métallographique a montré l'apparition d'oxydation et de la corrosion sur des échantillons testés, ceci est dû à l'environnement agressif des conditions du test. D'importants efforts et modifications ont été fournis pour éradiquer cet effet et pour améliorer l'exactitude des données de test de fluage obtenus.

Abstract

The study of the deformation behaviour of the collector bar at conditions experienced within the aluminium reduction cell is of great importance to optimizing the efficiency and increasing the life span of the cell. This mémoire communicates the results of an experimental program carried out on the steel collector bar material (AISI 1006) to investigate its behaviour in relation to its thermal, mechanical and the creep properties. Tests were carried out in compression at low stresses, 0.5 to 2 MPa and high temperature, 900 °C. Different behaviour was observed at low stresses up to 2 MPa, which can be characterised by time and applied stress level. Metallographic inspection showed effect of oxidation and corrosion on tested samples due to the aggressive environment of the test condition, major efforts and modification were made to eradicate this effect and to improve the accuracy of obtained creep test data.

Table of Contents

List of Figures

List of Tables

Acknowledgement

First and foremost, I would like to thank God for the strength and ability to carry out this study as a partial fulfilment requirement for the Master degree programme in civil engineering from the Université Laval.

I also want to acknowledge the financial support of Natural Sciences and Engineering Research Council of Canada (NSERC) and Alcoa through the Industrial Research Chair MACE^3. I would like to also thank the CQRDA and the Aluminium Research Centre-REGAL for partial financial support.

Special thanks to my thesis director, Professor Mario Fafard and co-director Professor Houshang Alamdari for the opportunity to be part of the research group and for their guidance and support throughout this research work.

My appreciation also goes to Dr. Donald Picard, Mr Guillaume Gauvin, Mr Hugues Ferland from the REGAL group, at Laval University for their technical support, and also Mrs Lyne Dupuis for her administrative support. I couldn't have gotten through without them.

I would also like to extend my appreciation to Dr. Donald Ziegler from Alcoa Canada Primary Metals for the scientific discussions and to Mr André Ferland, and Mrs Maude Larouche from Laval University for their help with the microstructural investigation.

Finally, special thanks to my family and my dear wife, Mrs Damilola O. Oyelade for their moral support, encouragements and for standing by me through it all. They made it possible and worth the effort. Thank you to all my colleagues at REGAL group – Laval University and MACE^3; it has been an amazing experience and time spent with everyone.

1. Introduction

1.1. Basics of aluminium production

Aluminium is the second most produced metal in the world next to iron. It is presently regarded as the third most commonly available element after oxygen and silicon due to the abundant availability of its principal ore, bauxite in the earth crust. Alumina (Al_2O_3) is firstly obtained from bauxite by Bayer process, a method well described in literature. After many attempts by previous scientists, in 1886, Charles Martin Hall and Paul Héroult independently and almost simultaneously discovered the process of extracting pure aluminium metal from its alumina by electrolysis process at high temperature of about 970 °C. The overall cell reaction can be expressed as:

$$2\mathrm{Al_2O_3}\left(dissolved\right)+3C\left(s\right)4Al\left(l\right)+3C\mathrm{O_2} \tag{1.1}$$

This process, now popularly referred to as Hall-Héroult process is well described by several authors [1–3], and is as illustrated in Figure **1**.**1**.

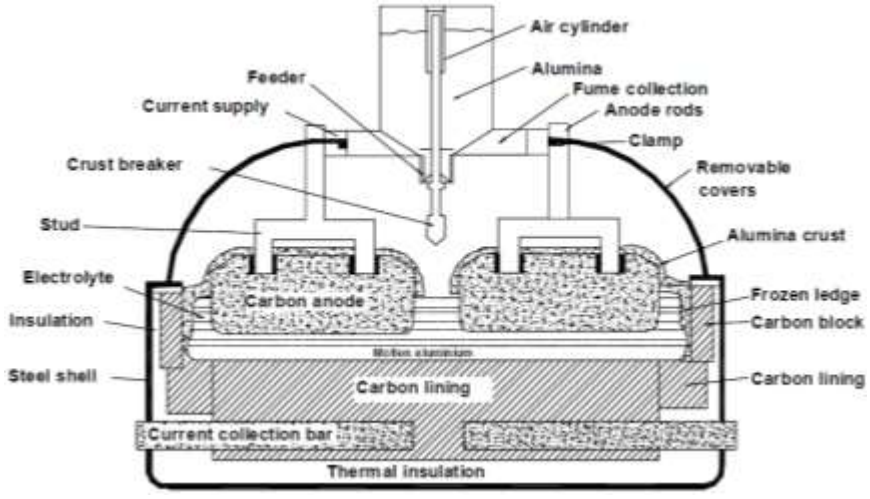

Figure 1.1: Cross sectional schema of an industrial Hall-Héroult electrolytic cell with prebaked anodes. [1]

The basic principle of the Hall-Héroult process has remained unchanged over the last decade. However, its efficiency has increased tremendously and continuously after many refinements and improvements through scientific and technological progress. It is

currently the most widely used method for large scale production of aluminium metal within the industry.

Cost related factors acts as a driving force for the continuous interest from the aluminium industry. Efforts of researchers aim to reduce energy consumption, improve efficiency, maximize productivity and obtain a longer service life of the cell. This has led to new development within the industry, one of which involves an increasing lifespan of the cell from 1000 days in the early years (1948) to close to 2500 days (presently) [2]. Continuous efforts are also dedicated towards full and accurate computerisation of the smelting cell, looking at global and individual components of the cell, their properties, how they function, and the best approach to upgrading their performance in view of optimisation.

Major developments in improving the energy efficiency and the lifespan of the cell were mainly due to the improvements in material quality, operational procedures, innovations in the cell design as well as process automation [2,3]. This approach takes into account, a wide range of complex phenomena such as the behaviour of the anode, the cathode assembly, heat loss, chemical reactions and thermal effects during operation of the cell. This thereby highlighted the need to understand and characterise the behaviour of major and specific components of the cell at operating conditions.

The following sections give a short breakdown of the Hall-Héroult cell, stating the basic motivation for the study on the material behaviour of the cathode collector bar at the cell operating conditions with an eye towards characterisation.

1.2. Breakdown concept of aluminium production

1.2.1. Hall-Héroult cell

The Hall-Héroult cell is governed by Faraday´s law of electrolysis. It is a process where aluminium metal is separated from oxygen by passing an electric current through a melt composed essentially of dissolved alumina in cryolite at temperatures up to around 970 °C (Figure 1.1). Typical cells are operated at low voltages (e.g. 4-5 V) and high electrical currents (e.g. 100 -350 kA) [1,2]. High electrical current enters the reduction cell from the top of the cell through the anode structure, passes through the cryolite bath, through a

molten aluminium metal pad, enters the carbon block, and exits the cell through the collector bars.

1.2.2. The cathode assembly

The longevity of the cell at operating conditions is determined by the first material to fail in the cell lining [2]. The entire lower cell construction is usually referred to as the cathode (Figure 1.2a) and is well described in literature [2–4]. In this study, the cathode assembly can be simply described as being made up of three major parts, consisting of the aluminium metal pad, the carbon blocks and the steel collector bars (Figure 1.2b).

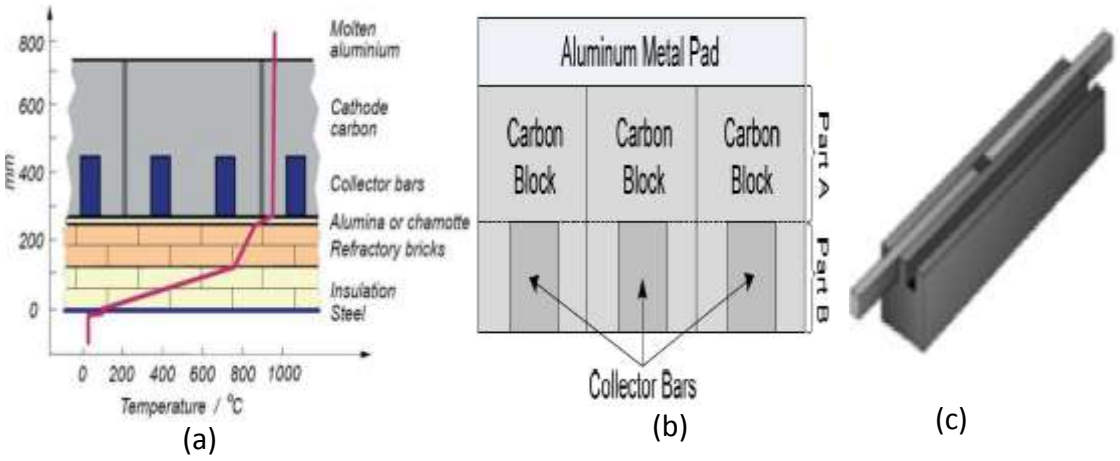

Figure 1.2: A typical cathode assembly, (a) the cathode (b) side cut away of multiple cells showing the aluminium pad, (c) two collector bars embedded in the carbon block. [2–4]

The carbon block are preformed rectangular blocks made up of carbon composite and occupies the full width between in sidewalls of the cell. In a conventional cathode today, the base of each carbon block is embedded with one or two steel rail bars (collector bar) that extend to the open ends of the steel shell and through each side of the electrolytic cell to connect with the bus bar (Figure 1.2c).

1.2.3. The steel collector bar

The collector bar serves as an electrical current collector and runs horizontally through the entire bottom lining. It is made of low carbon steel with carbon content of about 0.08 %C to obtain and maximise good conductivity and ductility properties of the bar. Steel however, has high thermal conductivity and deforms at high temperatures. The steel cathode collector bars are attached to the carbon blocks using cast iron poured during sealing operations (see Figure 1.3c), carbon glue, or rammed carbonaceous paste. The method of pouring cast iron to seal the collector bar to the carbon block is preferred and more popular as it facilitates good contact and reduces the electrical resistance at this interface, thereby reducing the overall voltage drop in the cathode assembly.

1.3. Problem

1.3.1. Introduction

There is a continuous fundamental need of the aluminium industry to better understand the degradation mechanism of the electrolysis cell lining in order to further improve its conception. The average life of the aluminium reduction cell is presently at about 2500 days for most smelters. This is less than the maximum life (about 3000 – 4000 days) that could be achieved if limitations were only due to the erosion of the carbon blocks [2,3].

However, many other mechanisms also contribute to the pre-mature failure of the cell lining, and in order to maximise the service life of the cell, a better knowledge of these mechanisms is required.

1.3.2. Failure mechanism in the cathode assembly

During operation, the cathode blocks are subjected to the action of high temperature and chemical process, which promote the degradation, heaving of the carbon blocks and cracking the cathodes. Many phenomena contribute to the heaving of the carbon blocks including stresses induced by thermal expansion, sodium swelling and chemical reaction inside the carbon blocks and side materials. However, these mechanisms and their effects have been well studied in literature [2,5].

1.3.3. Deformation of the steel collector bar

At high temperature, the cathode collector bar undergoes thermal expansion and exhibits greater expansion than in the carbon block (Figure 1.3a). During the sealing operation of attaching the collector bar to the carbon block, the expansion of the bar is not monotonic in behaviour. In the vicinity of 750 - 900 °C, the collector bar contracts, leading to the gap evolution (Figure 1.3b). The contact resistance between the collector bar and the cathode block has been previously estimated at 10 Ωmm^2 contributing roughly 100mV to the cell voltage drop in the cathode assembly [4].

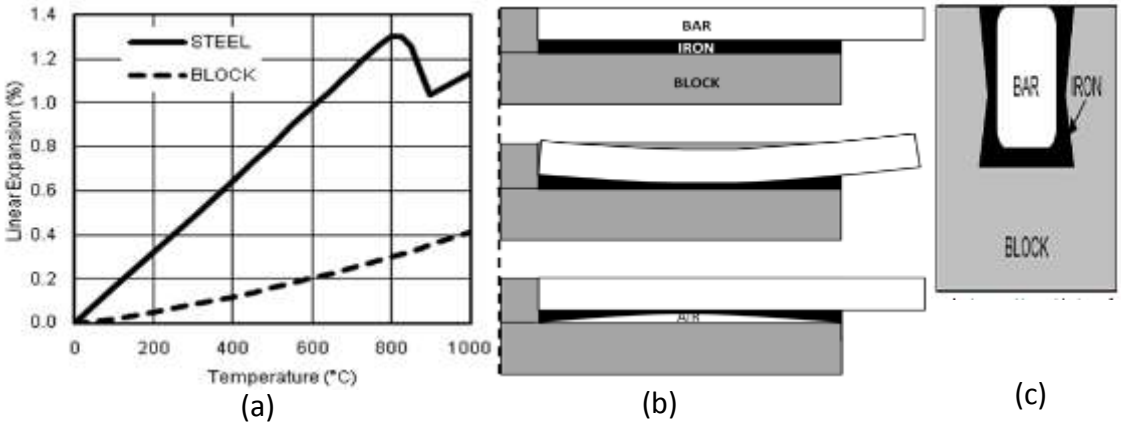

Figure 1.3: Effect of thermal expansion on the cathode assembly. (a): deformation curve for the carbon block and the steel collector bar; (b): deformation and gap evolution, (c) assembly of the carbon block, cast iron and steel bar. [4].

The voltage drop over the cathode assembly due to increase in electrical contact resistance of its components is an important indicator of the cathode´s condition. As the cell gets older, the cathode voltage drop increases in a more or less regular manner [4]. This increase in contact resistance of the cathode assembly is also a consideration in the design of the pot-to-pot electrical busbar as it impacts the current distribution.

Autopsies also showed that the heaving of the cathode carbon block induces a considerable deformation profile in the collector bar (Figure 1.4), majorly due to the temperature gradient and lower constraints at the end of the bar [2]. This leads not only to

elastic contractions but also creep of the cathode collector bar over the service life of the cell [5]. The total strain can be expressed such that:

$$\varepsilon = \varepsilon^{th} + \varepsilon^{e} + \varepsilon^{cr} \quad (1.2)$$

ε denotes total strain, ε^{th} thermal strain, ε^{e} elastic strain and ε^{cr} creep strain [2,5,6].

The creep/relaxation behaviour is a nearly incompressible phenomenon. The deformation along the transverse section of the collector bar causes a decrease in the stress level at the steel/cast iron/cathode block interfaces, thereby further increasing the electrical resistance induced at this interface. This also contributes to the overall contact voltage drop (CVD) in the cathode assembly hence reducing the energy efficiency of the cell.

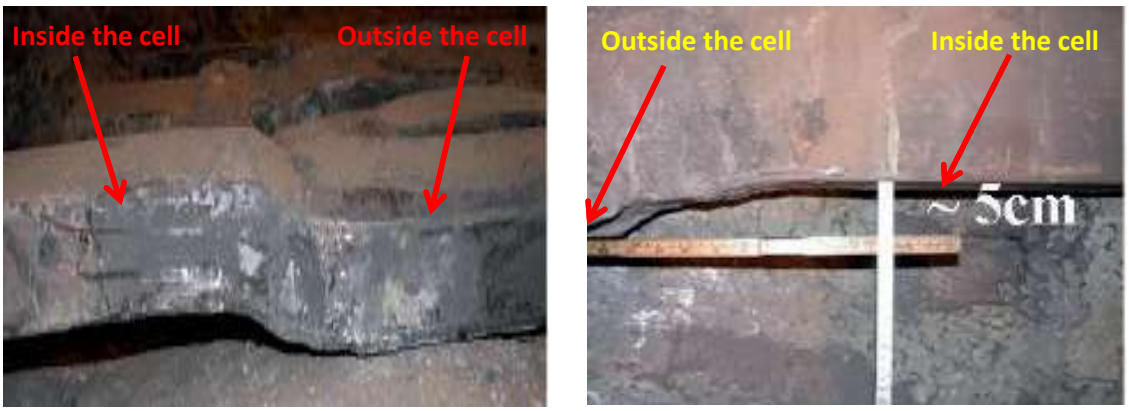

(a) (b)

Figure 1.4: Deformation of the collector bar: (a) deformed collector bar, (b) measurement of deformed collector bar after service life. [2]

Steel has excellent strength properties at ambient conditions, but loses its strength and stiffness with increasing temperature. At high temperature, deformation becomes more pronounced even at low stress level as the yield strength becomes significantly lower. A more dominating creep effect also begins to occur with time at high temperature.

In order to have a good understanding of the material behaviour of the collector bar at operating temperature (around 960 °C), it is necessary to identify parameters not only for thermal expansion and elastic behaviour, but also for the creep behaviour of the metal.

1.4. Deformation behaviour and properties of metals

1.4.1. Thermal properties

Metals, as all materials, deform in response to a change in temperature. This deformation behaviour is termed as thermal expansion. The level of deformation by the change in temperature is commonly used to determine the material´s coefficient of thermal expansion. This data are well stated in the literature [7,8] for different materials and at different temperatures. It can be obtained by expressions such as:

$$\alpha_{th} = \frac{\Delta l}{l_0 * \Delta T} \tag{1.3}$$

where α_{th} denotes thermal expansion coefficient, l_0 initial length, Δl change in length due to change in temperature ΔT .

1.4.2. Mechanical properties - stress – strain – time relationships

Metals subjected to a uniaxial force will undergo deformation which may be time-dependent or not. The properties of metals and their alloys are highly influenced by their microstructure. Their deformation behaviour is dependent on the applied stress and temperature which influence the microstructure of the metal. Deformation of metals through application of mechanical loads in tension or in compression is as illustrated in Figure 1.5.

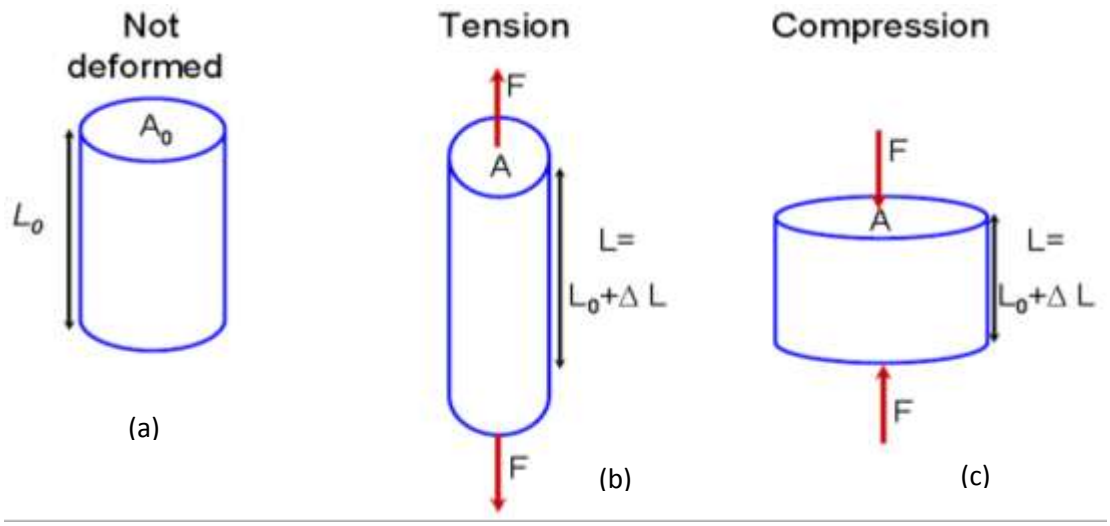

Figure 1.5: Sketch of a material under various modes of applied load: (a) no load, (b) in tension, and (c) in compression

A simply applied load □ is distributed on the surface area A of a specimen resulting in distributed stress σ, which can be expressed such as:

$$\sigma = \frac{F}{A} \tag{1.4}$$

This results in deformation of such material where the new length is calculated such as:

$$L = L_0 + \Delta L \tag{1.5}$$

where L_0 is the original length (also referred as gage length) before deformation, ΔL is the change in length and L is the final length upon deformation. The strain ε can be obtained by:

$$\varepsilon = \frac{\Delta L}{L_0} \tag{1.6}$$

In a general form, the strain increases with increasing level of stress. The stress-strain data plots are typical for explaining the deformation characteristic of many materials and for obtaining their mechanical properties [9]. This process is well described in literature and as illustrated in Figure 1.6.

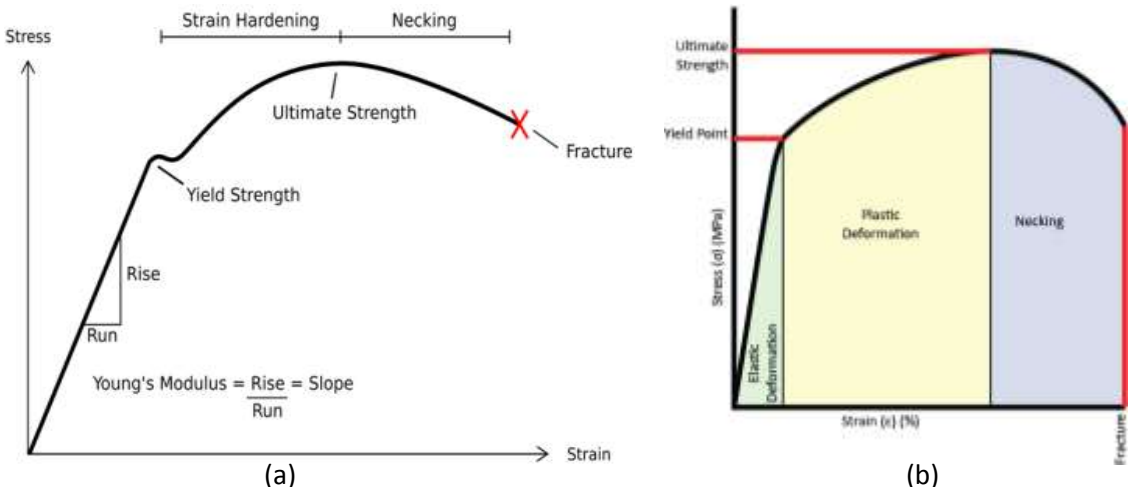

Figure 1.6: Stress – Strain curve, typical for a material in tension: (a) material behaviour and parameters along the curve, (b) types and regions of occurring deformation. [8,9].

Strain regions of elastic, plastic, necking and fracture can be observed in Figure 1.6b. This is characteristic for a ductile metal in elongation, but slightly different in compression as necking is not observed in such case. The essential region of the curve can be briefly explained as follows:

Elastic deformation is a reversible process where material regains its original dimension on removal of applied load. The deformation behaviour governed by the Hooke´s law such that:

$$\varepsilon^e = \sigma / E \tag{1.7}$$

where σ is the applied stress in the elastic domain, E the modulus of elasticity (Young´s modulus) and ε^e is the elastic strain. Apart from elastic deformation that disappears on removal of stress, even more deformation behaviour can occur with increasing stress range above the yield strength of such material. These types of deformation are usually referred to as "inelastic deformation" and can be either "plastic deformation" (occurring at stresses beyond yield stress and time independent) or "creep deformation" (occurring on application of constant stress over a time period) or action of both.

Plastic deformation is a permanent strain occurring at region above the yield strength σ_Y of the material. At onset of plastic deformation, a small increase in stress causes a relatively large additional deformation independent of time. This process of further

deformation is called yielding (occurring strain hardening), where the peak value is the ultimate strength of the material before tending towards fracture.

In addition to time independent elastic and plastic deformation described earlier, materials also undergo inelastic deformation at constant stress by mechanisms that result in markedly time-dependent behaviour called creep. This behaviour is represented by a curve where the strain varies with time (Figure 1.7). In this curve, there is a region of instant elastic deformation ε^e, (instantly recoverable on removal of stress), primary creep strain (mainly recoverable with time), secondary creep strain (steady state and permanent strain), and the tertiary creep strain tending towards rupture.

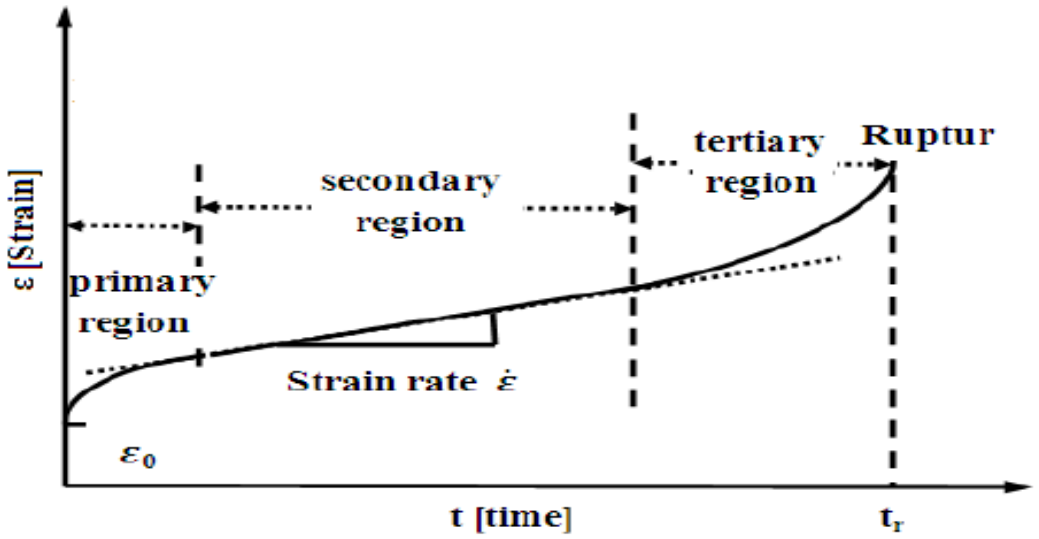

Figure 1.7: Schematics of a typical uniaxial creep curve. [9]

Fracture and rupture as described in Figure 1.6 and 1.7 respectively are terms related to damage which is not experienced by the cathode collector bar in the cell. Therefore it has not been considered in this work.

1.5. Scope of work - objectives

To sustain the continuous increase in the cell´s service life, the characterization of the material behaviour of the collector bar is a major factor that must be taken into consideration, especially for developing an accurate numerical model of the cell.

Therefore, the study of the deformation behaviour of the collector bar at conditions experienced within the aluminium reduction cell is of great importance to further optimize the energy efficiency and increase the life span of the cell.

There is a lack of sufficient relevant data in the literature to fully characterize the deformation behaviour of the collector bar at operating condition. Hence, in this study, an experimental procedure was carried out on the steel collector bar material (AISI 1006) to investigate its deformation behaviour in relation to its thermal, elastic and creep properties. The tests were carried out in compression at high temperature and low stress levels to reproduce conditions experienced within the reduction cell. The following objectives and considerations were set out in order to achieve this:

- state of art literature review of previous researches on the material properties of the metals at high temperature, phenomenon of creep in metals, time-dependent deformation theories and rheological models of creep theories;
- experimental investigations, by carrying out compressive creep tests at constant temperature of 900 °C and at different constant stress levels of 0.5, 1, 1.5 and 2 MPa;
- considerations for the effect of thermal expansion and phase change;
- considerations for the effect of corrosion and oxides;
- microstructural inspections on both virgin and tested samples;
- fit of suitable models and obtaining material parameters.

1.6. Structure of thesis content

The second chapter covers a state of art literature review looking at previous researching and discussing findings of existing data in relation to material properties of metal at high temperature, the creep phenomenon, creep theories and rheological models used in representing deformation behaviours of metals.

Chapter three looks at the experimental program from material selection, preparations including test set up and procedures, limitations and considerations for environmental factors having effect on deformation behaviour. Chapter four shows the results obtained

including those of corrosion tests, thermal expansion at heating period, creep tests and metallography inspections. It also looks at the analysis of obtained experimental results, discussing observations in the deformation behaviour at different stress levels up to 2 MPa and the outcome of the microstructural investigation carried out on virgin and tested samples.

The last chapter, chapter six, summarises all observations from methodology, obtained results and analysis approach, drawing conclusions based on chapter four. Theories discussed to try to explain observed behaviour and recommendations for future research were also looked at.

2. Literature Review

2.1. Background

Metals generally deform when subjected to high temperature and applied stress conditions. Hence, cathode collector bar, subjected to developed stresses at elevated temperature of up to 960 °C, undergoes not only elastic deformation but also creep of the bar over the service life of the cell. Good understanding of the time-dependent stress – strain relationship are therefore required to study, understand and model the behaviour of the bar at such high temperature conditions of the cell.

A literature review on the material properties of metals at high temperatures, physical mechanism of creep, characteristic creep behaviour at elevated temperature and low stress levels, and general model representations of such behaviour was deemed necessary. In line with the objectives of this work, this was carried out and summarised in this chapter.

2.2. Material Properties at High Temperature

2.2.1. Introduction

Although steel has excellent strength properties at ambient conditions, it loses its strength and stiffness with increasing temperature. At high temperature, deformation becomes more pronounced even at very low stress level, as its properties changes significantly.

The response of steel structure exposed to high temperature is governed by its thermal and mechanical properties. These temperature-dependent parameters, consisting mainly of thermal strain coefficient, Young's modulus, Poisson´s ratio and creep data, are required to model the deformation behaviour of the cathode collector bar in the cell. These properties are, however, also majorly affected by the microstructure and composition of the material and should firstly be considered.

2.2.2. Effect of carbon content on material properties

The weakening influence of carbon in carbon steel has been suggested by previous studies [10–12]. The amount of carbon in a metal has a reasonable effect on its thermal, mechanical and creep deformation properties. The carbon content of a steel bar has a

major influence on the temperature range at which phase change occurs during thermal expansion. However, it also has a major effect on the mechanical and deformation properties of the metal. This will be further discussed later on.

Weinberg [10] measured a decrease in the ultimate tensile strength (UTS) of steel with carbon content up to about 1.0 %C while Wray [11], also carried out series of experiments in tension to describe the effect of carbon content on the plastic deformation behaviour of plain carbon steel at elevated temperature up to (1300 °C).

Pines and Sirenko [12] observed that the creep strength of austenite steel decreased continually with increasing carbon up to about 1.0 %C. Ruano et al [13] also related the change in creep strength of steel to the measured increase in the self-diffusivity of iron with carbon. Ruano further suggested that an increase in self-diffusivity is an indicative of weaker interatomic bonding as results showed that the austenitic iron lattice is expanded by the addition/increase in carbon.

2.2.3. Thermal properties

Major parameters influencing the temperature rise in steel are thermal conductivity and specific heat (or heat capacity). The thermal conductivity decreases with increasing temperature in an almost linear fashion (Figure 2.1a) while the specific heat increases with increasing temperature and have a large spike occurring at 750 °C (Figure 2.1b).

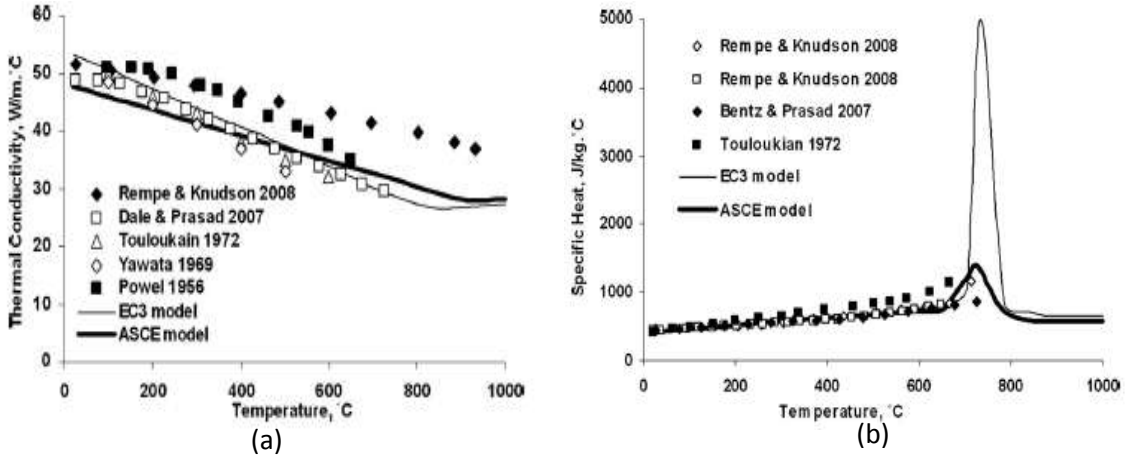

Figure 2.1: Effect of increasing temperature on low carbon steel thermal properties (a) thermal conductivity, (b) specific heat. [8]

The spike in the specific heat at about 750 °C is due to phase change occurring in the steel microstructure, the point at which transition of atomic structure from a face centred cubic (FCC) to a body centred cubic (BCC) begins to occur. This also corresponds with the deformation behaviour of steel where carbon steel undergoes linear thermal expansion with increasing temperature (Figure 2.2a).

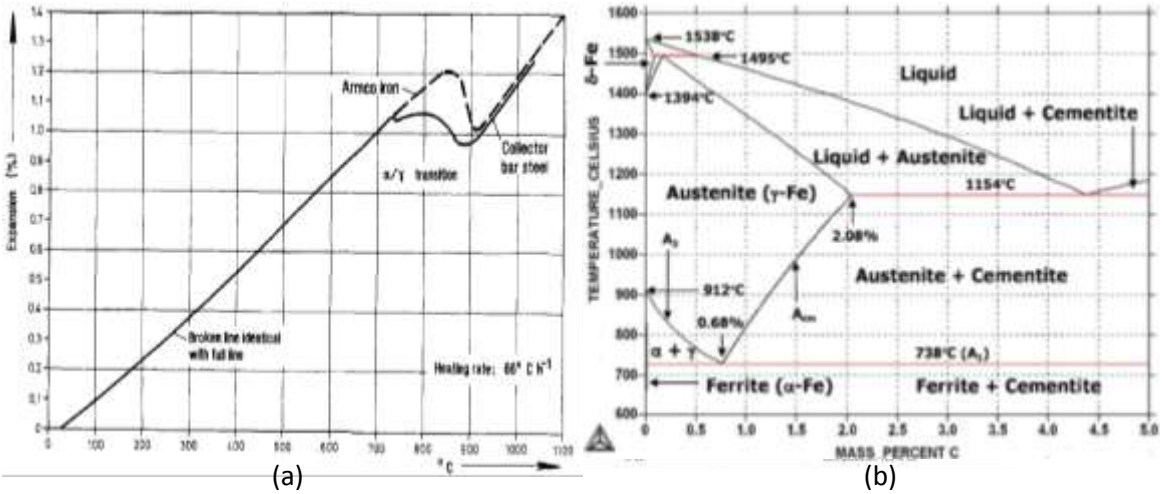

Figure 2.2: Effect of temperature on steel deformation properties: (a) variation of thermal strain with temperature, (b) iron – carbon phase diagram. [7]

At a certain temperature, the linear expansion changes and material begins to contract over a short range of temperature before any further increase. This contraction region is a result of the occurring phase transformation, where material moves from ferrite to austenite temperature region. Due to high dependence of the material properties on the microstructure (e.g. material composition), the carbon content of the steel bar has a major influence on the point at which the phase transformation begins (Figure 2.2b).

At carbon content above 0.02 %, a phase change from ferrite to austenite associated to a contraction, starts to occur at about 730 °C and finishes between 800 °C and 900 °C for carbon content up to 0.3 %. A thermal strain of up to 1.2 % with the occurrence of a phase change has been predicted by different models and measured in different tests at temperatures up to 900 °C [7,8].

2.2.4. Mechanical properties

The mechanical properties of metals are generally represented within the stress–strain diagram (see Figure 1.6). Strength tests are usually conducted either in transient (constant load, increasing temperature rate) or at steady state (constant temperature, increasing load rate) to obtain the stress-strain plot where the mechanical properties such as Young´s modulus, yield strength, strain hardening parameter, ultimate strength and even fracture parameters can be estimated.

Tensile strength test is the most popular method used [8,9,14,15] to obtain the mechanical properties for most metals and their alloys. There is limited data found in literature for tests in compression. However, it is generally assumed that the Young´s modulus, derived based on tensile strength tests are the same for compression state. For low carbon steel in tension, both yield strength and elastic modulus decreases significantly at higher temperatures above 300 °C. Existing data at different temperatures shows an elastic modulus of about 13.5 GPa and a yield strength of 18 MPa (at a loading rate of 0.01 s-1) have been measured in different tests at 900 °C (Figure 2.3) [8].

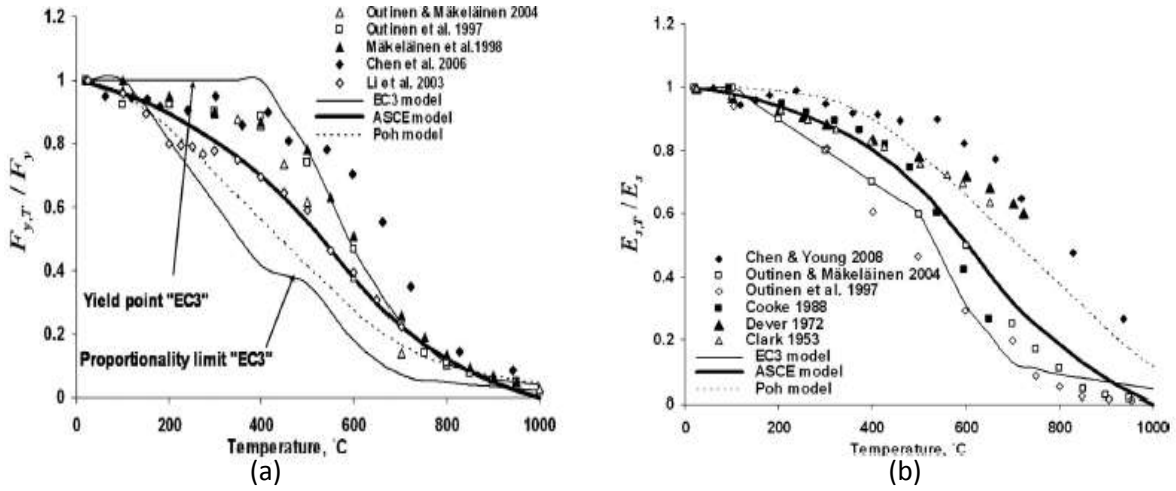

Figure 2.3: Normalised data of mechanical properties at different temperatures: (a) yield strength vs. temperature, (b) Elasticity modulus vs. temperature. [8]

Compression test data on the collector bar material (AISI 1006) showed great influence and dependence of its deformation behaviour and mechanical properties on temperature up to 850 °C for strain rates ranging from 0.1 to 50 s^{-1}. At constant temperature of 850 °C, the yield stress increases with increasing strain rate such that, yield stresses of 50, 85 and 150 MPa were obtained for strain rates of 0.1, 3, and 50 s^{-1} respectively [16].

European standard, EC-3 distinguished the proportionality limit of a material as the end of the linear elastic portion of the stress – strain curve (Figure 1.6), point after which it becomes nonlinear elastic before the yield limit is reached. This approach was deemed necessary to partly account for creep strain in test sample subjected to strength test at high temperatures [15].

2.2.5. Creep properties

Deformation properties influencing response of steel structures at elevated temperatures are thermal strain and creep at high temperatures. A brief introduction to the creep deformation behaviour of materials was carried out in chapter one (see Figure 1.7). A study on the creep rate of the collector bar at low loads ranging from 1 to 5 MPa [7] concluded that the collector bar slowly deformed under small forces experienced in the cell at temperatures above 700 °C. From several data provided in this study (Figure 2.4),

it can be concluded that the creep rate is around 0.002 %/h at 900 °C under a load of 1.3 MPa, a rate corresponding to almost 1 % creep in three weeks [7].

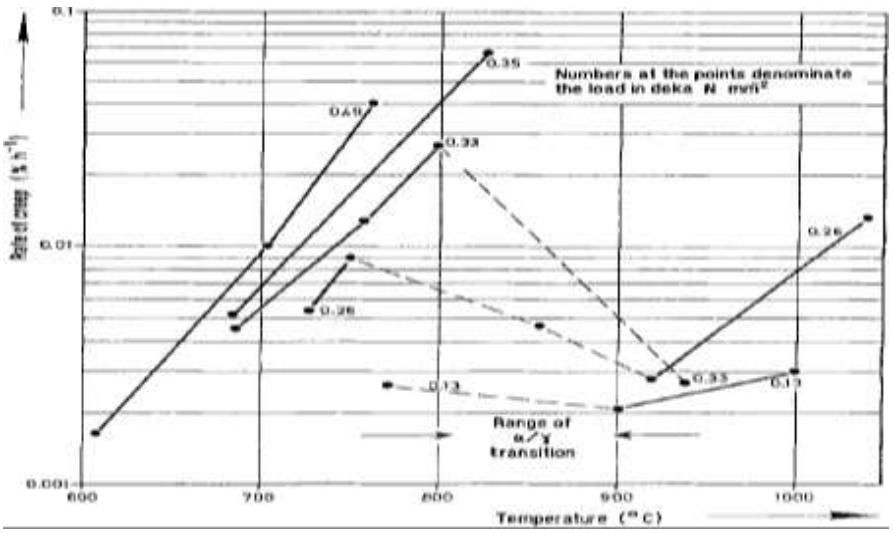

Figure 2.4: Creep rate data at different stresses & temperatures. [7]

To fully understand the creep deformation behaviour and properties of a material, it is necessary to study the creep phenomenon including the mechanism, physical laws and models used to represent and explain such behaviour.

2.3. The phenomenon of creep

Creep is a time-dependent deformation where under constant stress, the strain varies with time $\left(\varepsilon^{cr} = \frac{d\varepsilon}{dt}\right)$. Creep of solid may be exhibited in the visco-elastic range where the creep strain may be completely (or almost completely) recovered on removal of the stress, or in visco-plastic range, where the creep deformation is permanent. In the latter case (permanent deformation), an elastic component also exists but this may be trivial by comparison [9].

A typical creep curve can be characterised by three stages; primary, secondary and tertiary (see Figure 1.7). In the initial stage “primary creep”, the strain is relatively high

but slows down with increasing time (decreasing strain rate) and eventually reaches a steady state named "secondary creep" (constant strain rate). In the final stage "tertiary creep", the creep strain accelerates (increase in strain rate) towards failure. This final stage is mostly observed in a tensile test rather than compression due to the "Necking" effect.

Creep strains are derived from steady state tests during which the stress is kept constant. The extent of creep deformation in a given material is dependent on and can be characterised by the applied stress level and temperature level at which the test is being carried out. An increasing level of creep strain can be obtained in response to an increased level of the applied stress and/or temperature (Figure 2.5).

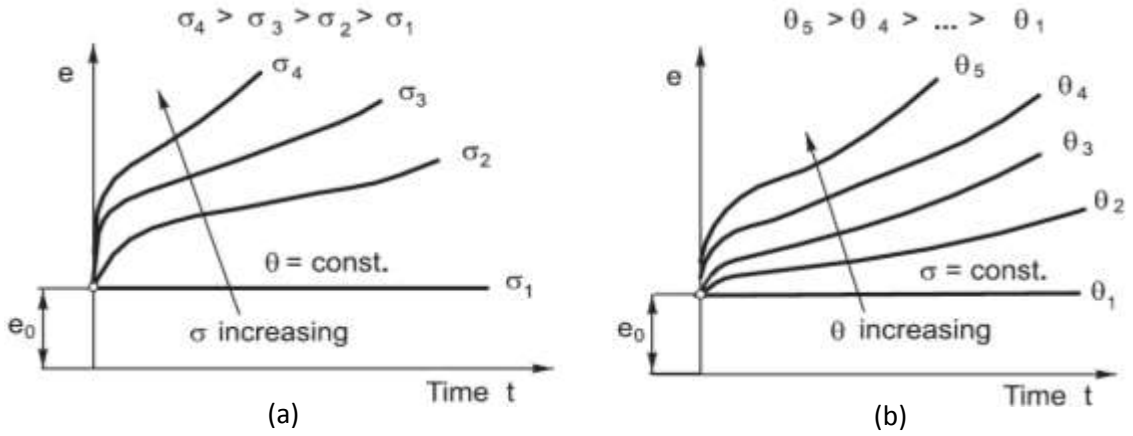

Figure 2.5: Schematic view of a typical creep curves for various stresses and temperature levels. (a): increasing stress level, (b) increasing temperature level. [8]

There is a stress level (σ_1 in Figure 2.5a), popularly referred to as "threshold stress", and a temperature level (θ_1 in Figure 2.5b), where the resulting creep strain is very small or negligible. Below these levels, no creep strain is considered to occur [17]. Increasing temperature above threshold (θ_1 in Figure 2.5b) leads to a stress driven atomic rearrangement in the microstructure of the material hence acting creep deformation over time. Such case is referred to as thermally activated creep process, which takes into account, the dependence of both stress and temperature and is governed by the Arrhenius equation:

$$\dot{\varepsilon} = A\sigma e^{\left(-\frac{Q}{RT}\right)} \tag{2.1}$$

A depends mainly on the material, Q is the activation energy which can be altered due to a sufficient shift in temperature or stress, σ is the applied stress, $\dot{\varepsilon}$ is the strain rate and T is the temperature [18,19].

The secondary creep stage is considered as the most understood of the creep stages and deemed important for explaining the creep deformation behaviour of metals [18]. The stress dependence parameter n, of the creep curve for this stage depends on the creep rate and the applied stress. This has been well explained by different creep mechanisms in literature. A creep rate - time curve (Figure 2.6) is generally used to give a clearer identification and understanding of the creep curve and to determine the dominating creep mechanism.

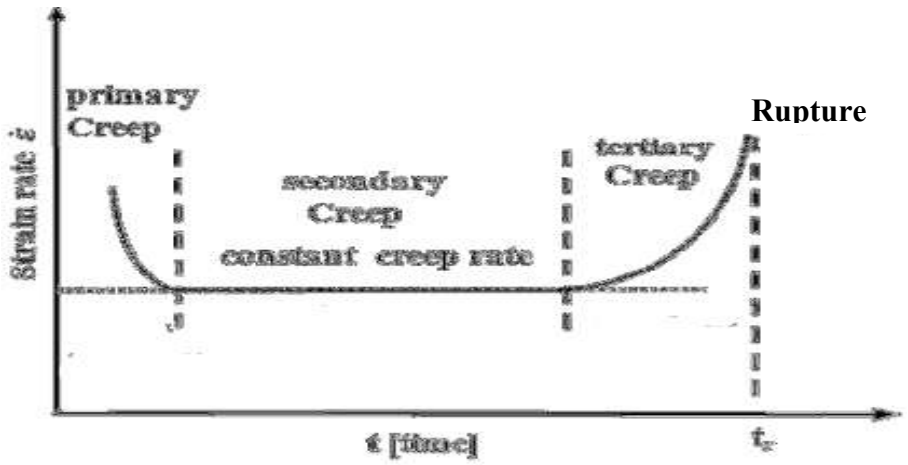

Figure 2.6: Schematic view of a typical uniaxial creep rate curve. [18]

Similar and derived from the creep curve, the creep rate versus time curve has a primary creep stage, where the creep rate decreases with time $\left(\frac{d\varepsilon^{cr}}{dt} < 0\right)$. A clear section of the secondary creep stage is observed where the strain rate reaches a near constant $\left(\frac{d\varepsilon^{cr}}{dt} =\right.$

$0\big)$ and also referred to as "minimum strain rate". In the final stage, tertiary creep, the strain rate accelerates towards rupture $\left(\frac{d\varepsilon^{cr}}{dt} > 0\right)$.

A general equation for the secondary creep rate in crystalline material is often derived from Arrhenius equation above such that:

$$\dot{\varepsilon} = \frac{A_2 \sigma^n}{d^q T} e^{(-\frac{Q}{RT})} \tag{2.2}$$

where d is the average grain diameter, T absolute temperature, n the stress coefficient, q the grain size coefficient and Q is the activation energy [19].

Generally for metals under constant load, creep is expected to become noticeable at temperatures corresponding to 30 % of the melting temperature ($0.3T_m$) for pure metals and 40 % ($0.4T_m$) for alloy metals [19]. For the cathode collector bar material sample (AISI 1006) used in this study, the melting point is at approximately 1400 °C. Therefore the creep strain should become evident at temperature starting from 566 °C and above.

Earlier published works focused on creep behaviour of metals and observed that the physical mechanism causing deformation is quite different from that in other solids. In crystalline materials such as metals, the creep curve is related to possible action of a group of mechanisms which depends not only on certain temperature and stress ranges but also depends on the structure of the alloy, its composition and the pre-history of the sample/material [13,20,21].

Therefore it is important to further investigate and understand the mechanism causing creep in crystalline material particularly in steel metals. This is considered and summarised in the next section.

2.4. Physical mechanisms of creep:

2.4.1. Microstructural behaviour

Polycrystalline metal aggregates consist of crystal grains with characteristic arrangement of atoms within them. The basic mechanism of deformations of these grains is that its part slips relative to each other. This slip occurs in places close to the packing of atoms and may be understood by taking into account the motion of crystal defects, known as dislocations [9].

Dislocation slip and grain boundary sliding are important mechanisms that determine material´s mechanical behaviour. Dislocations are linear defects in the crystal structure of metals and are largely responsible for the material´s inelastic deformation. Elaborate interactions between the defects in a crystal structure can lead to complex forms of mechanical behaviour.

For example, in response to a stress applied on a material, the crystal structure consisting of atoms, vacancies, dislocations within the solid material moves relative to one another in a time-dependent manner, resulting in creep deformation (Figure 2.7). Such atomic motion occurs more rapidly at higher temperature and constitutes a broad category of behaviour process called diffusion.

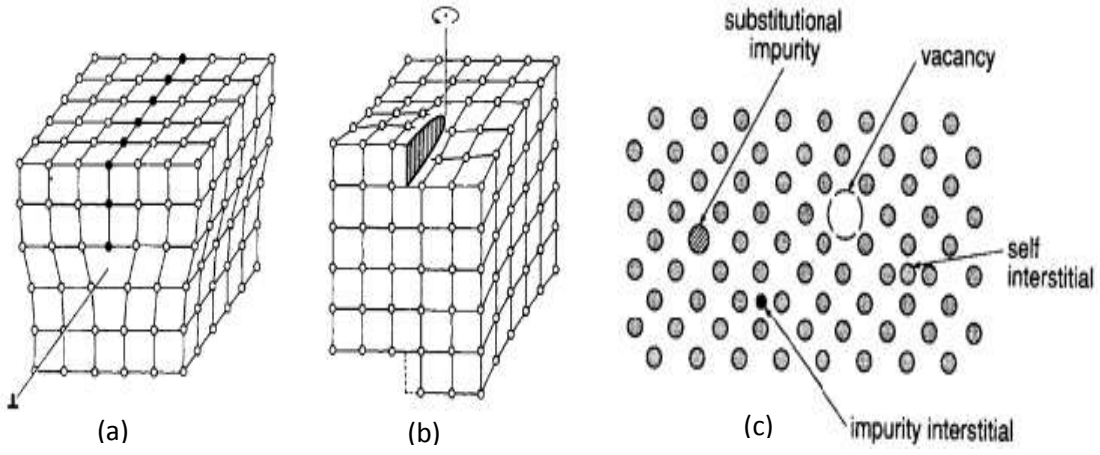

Figure 2.7: Defects in a metallic crystalline structure, (a) line dislocation, (b) dislocation screw, (c) point defects. [9]

At low temperature (below $0.3T_m$), creep deformation occurs at a very slow time pace as the amount and distribution of the defects in the crystal structure remains almost uniform (dislocation slip/slide mechanism). However, at high temperature, creep deformation occurs at a faster rate as vacancies in the crystal structure diffuse to the location of dislocations and causes them to accelerate to adjacent slip plane.

Variety of physical mechanisms, explaining creep process in metal and its dependence on the applied stress and temperature, have been widely studied in literature [18]. They may however, be grouped into two terms as "diffusional flow" and "dislocation flow". Considerations are sometimes given for grain boundary sliding (GBS) to be a distinct mechanism.

2.4.2. Dislocation slip mechanism

This creep mechanism is a kinetic process occurring at low temperatures between 0.1Tm and 0.3Tm. Below the ideal shear strength, flow of dislocations by glide motion can occur, provided a sufficient number of independent slip systems are available (Figure 2.8). This will cause the material to undergo work hardening until the stress required to flow equals the applied stress. However, this motion can be limited by obstacles such as solutes, precipitates or even grain boundaries [18].

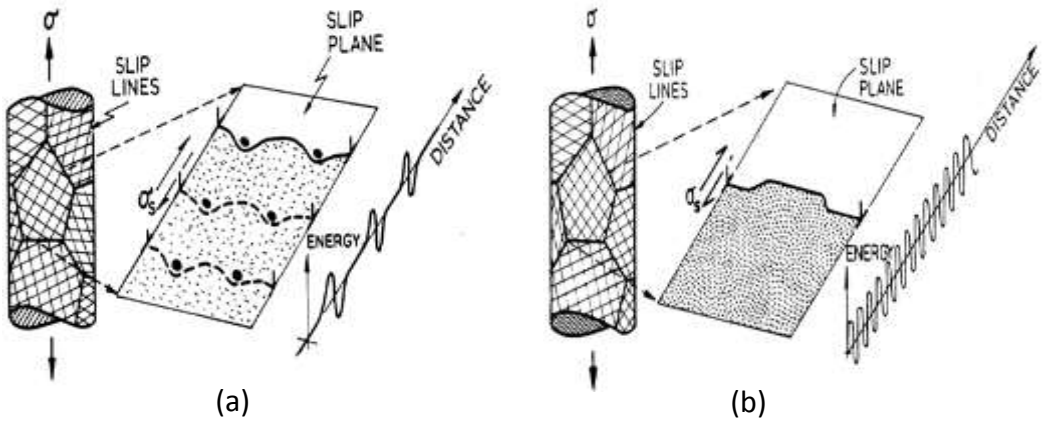

Figure 2.8; Mechanism of dislocation slip. (a) motion obstructed by obstacles (b) slip of weak grain boundary. [18]

2.4.3. Diffusional creep

This creep mechanism occurs at low stresses and relatively high temperature (above 0.6Tm). It involves the movement of vacancies in the crystal lattice (Figure 2.9). This can occur as a result of spontaneous formation of vacancies near the grain boundaries that are approximately normal to the applied stress. The uneven distribution thus created results in movement (diffusion) of the vacancies to regions of lower concentration. This leads to a mass transfer in the material structure, causing an overall deformation of the material.

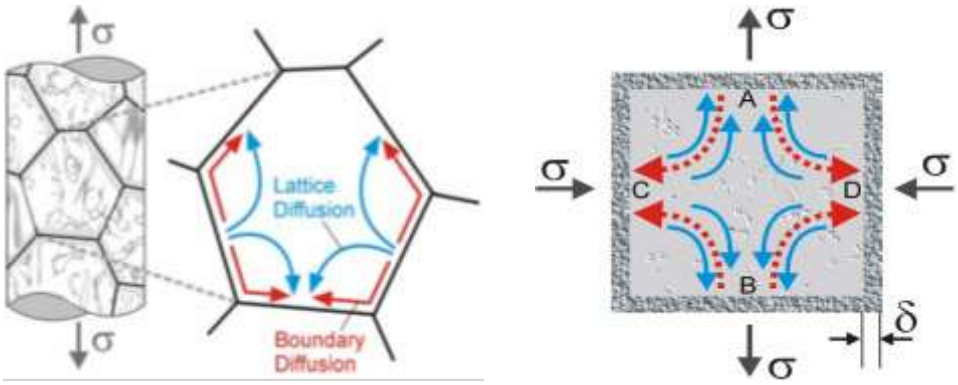

(a) (b)

Figure 2.9: Mechanism of diffusion creep, (a) lattice and boundary diffusion of vacancies and atoms respectively (b) response of defects to an applied stress. [18]

Physical laws of diffusional flow mechanism are explained either by (a) lattice diffusion (Nebarro – Herring creep), or (b) grain boundary diffusion (Coble creep). Nebarro Herring creep occurs if the vacancies move through the crystal lattice while Coble creep occurs if the vacancies move along grain boundaries instead and represented by:

$$\dot{\gamma} = A_{NH}\left(\frac{D_{sd}Gb}{kT}\right)\left(\frac{b}{q}\right)^{q=2}\left(\frac{\tau}{G}\right)^{n=1} \quad or \quad \dot{\gamma} = A_{Coble}\left(\frac{D_{sd}Gb}{kT}\right)\left(\frac{b}{q}\right)^{q=3}\left(\frac{\tau}{G}\right)^{n=1} \tag{2.3}$$

where they both have a strain rate $\dot{\gamma}$ approximately proportional to the stress τ, a stress exponent (n) of 1 (i.e. linear behaviour), an inverse proportionality to the square of the average grain diameter (for Nebarro, grain dependence q = 2 and for Coble, q = 3), the shear modulus G and the Burger´s vector constant b [18,19].

2.4.4. Power law creep - dislocation climb

This creep mechanism occurs at intermediate temperatures ($0.3T_m$ - $0.6T_m$) and relatively high stress level. This process employs the flow of dislocations by both glide motion and climb over obstacles through movement of vacancies (Figure 2.10). In response to an applied stress on a material, an edge dislocation moves along the crystal plane by stepwise slip process (glide). On encountering an obstacle, such as a precipitate particle or an immobile entanglement of other dislocations, further deformation requires that the dislocation move to another lattice plane. This motion is termed "climb" and requires rearrangement of atoms by vacancy diffusion. The climb process is time-dependent and considered to have a more dominating effect in the creep deformation behaviour of the material. The cumulative effect of a large number of such climb events permits more slip (glide), hence permitting more macroscopic deformation to occur [18,19].

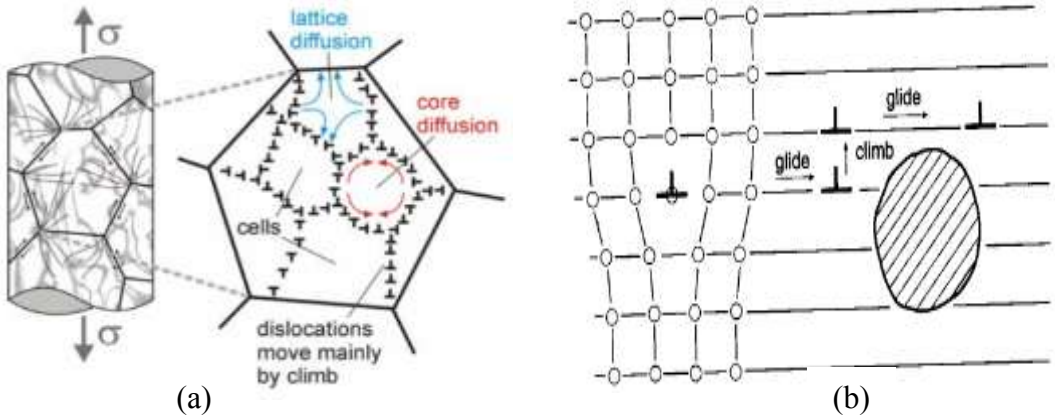

Figure 2.10: Climb plus glide controlled creep mechanism in power law (a) effect of lattice diffusion + dislocation climb (controlling effect), (b) Dislocation climb + glide effect. [18].

The resistance to the climb process is such that considerable high stress is required for deformation to occur. Hence, the power law creep theory has a strong stress dependence factor n, with values ranging from three to eight. The representative equation can be expressed such that [19]:

$$\dot{\gamma} = A_2 \left(\frac{D_v G b}{kT}\right)\left(\frac{\tau}{G}\right)^n \tag{2.4}$$

2.4.5. Harper - Dorn creep

Creep experiments are difficult to carry out at low stresses. This is because strain rates are very low and a very high level of precision is required. This made it very difficult to predict and develop an accurate physical mechanism at such conditions. However, Harper and Dorn in a study in 1957 proposed a physical mechanism to predict creep of metals at low stress level and high temperature (above $0.6T_m$). Numerous creep tests were performed on aluminium of high purity and large grain sizes [19,22]. Results of the investigation lead to the conclusions that (a) the steady state creep rate increased linearly with the applied stress (i.e. stress exponent n =1), (b) no dependence on grain size, (c) similar to power law, dislocation-climb is the controlling mechanism and the activation energy was that of self-diffusion (Figure 2.11).

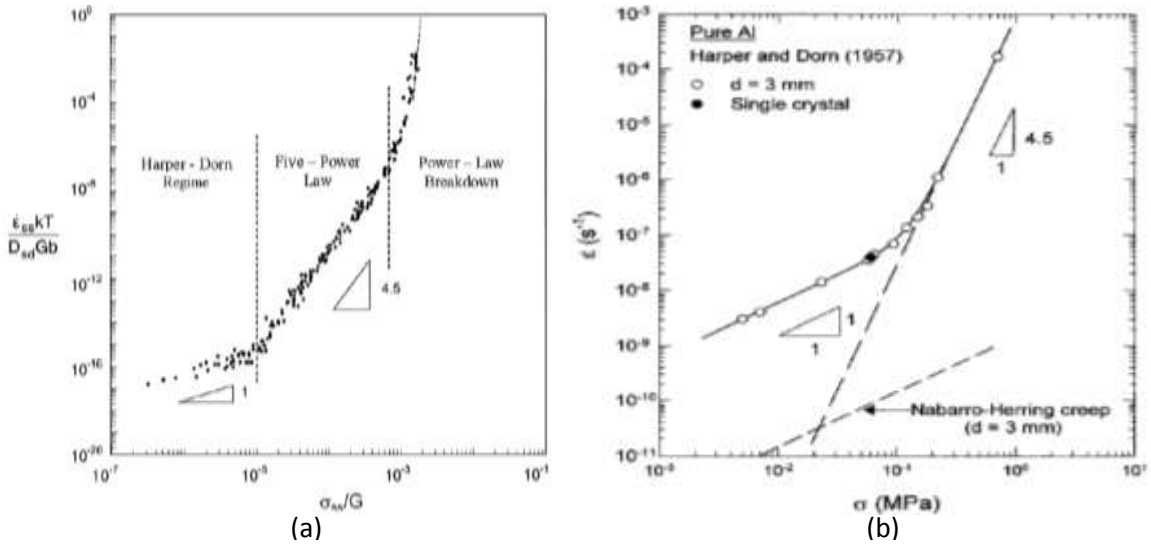

Figure 2.11: Creep strain rate – stress plot (a) physical laws occurring at different stress and strain rate region, (b) Evidence of Harper Dorn and Nebarro creep laws. [19].

The relationship between the applied stress and the steady state creep rate for the Harper-Dorn creep can be phenomenologically described similar to power law as:

$$\dot{\gamma} = A_{HD}\left(\frac{D_{sd}Gb}{KT}\right)\left(\frac{\sigma}{G}\right)^{n=1} \quad (2.5)$$

A_{HD} is Harper Dorn constant and a stress exponent (n) of 1 [19].

Similar observations were also reported some years later by other investigators, although the effect of dynamic recrystallization was also observed for tests at high temperatures above $0.6T_m$ [22,23].

2.5. Representation of creep behaviour models

2.5.1. Background

The fundamental problem of modelling creep behaviour is the representation of the stress – strain – time relationship. This is a complex phenomenon and has large number of factors influencing it. Several models and theories other than those identified in the previous section have been developed to describe creep behaviour in a wide range of real materials; they will be looked at further on in this study.

The record of creep behaviour and regions within the creep curve has been discussed earlier in this chapter. Some of the physical mechanisms and laws developed to understand them were also considered. Various models to represent these creep behaviour have been widely studied in the literature [24–30]. A few of such relevant models for metals were reviewed here with respect to applicable creep regions and their ability to represent the dependence of stress, temperature and internal variables parameters of the creep curve are summarised here.

2.5.2. Phenomenological models

Phenomenological models are theories of creep, developed based on the observation of experimental creep curves, obtained by testing a number of identical specimens under creep / relaxation condition. The models are based on the study of the stress – strain – time deformation behaviour of metals in the laboratory at required conditions (different stress and temperature levels). It purely tries to characterise the stress – strain and or the

strain - time curves obtained from experimental data by using known phenomena and obtaining its parameters by curve fitting and regression.

Stress - strain rate curve parameter plays a significant role in modelling the creep behaviour. Steel may be considered as an isotropic incompressible material, where similar to plasticity theory, the creep behaviour may be divided into volumetric and deviatoric (or shear) parts. Only the applied deviatoric (shear) stress, causing deformation of the material (deviatoric strain), will be considered in this study.

Models based on phenomenological behaviour of metals uses physical quantities or try to introduce meaning to the used parameters and its applications are only possible for given conditions. Different phenomenological models for stress-strain behaviour have been proposed by many authors [24–30]. These models are further looked at in the next section.

2.5.3. Empirical models

Empirical creep models were generally derived using observed data from relationship between stress – strain – time in the creep test. The parameters involved, e.g. the stress exponent n, can be determined by curve fitting of the test data. Each region of the creep curve, (primary, secondary and tertiary) can be described by its own special equation. Different groups of fundamental equations were developed along the line of logarithmic form, sine-hyperbolic form, polynomial form and exponential form. Each form was reviewed to describe models for both primary and secondary creep. This is summarised in Table 2.1.

Table 2.1: Review of various applicable models developed to represent the creep of metals

Creep Law Form	**Primary creep**	**Secondary creep**	**Discussion**
Logarithmic	$\varepsilon = \varepsilon_0 + A[\log(1+Bt)]^{2/3}$	$\varepsilon = Alog(t) + Bt + C$	A, B, and C are parameter constant. Proposed by (Philips et al, 1905) and (Weaver et al, 1936). This model was found majorly suitable in creep behaviour of metal at very low temperatures in ranges below half the melting temperature. A clear

			disadvantage of the model is that stress and temperature dependencies of the parameters are not explicitly accounted for.
Sine - hyperbolic	$\varepsilon = A + Bsinh\left[\mathrm{C}\left(\frac{t}{t_0}\right)^{1/3}\right]$	$\varepsilon = \varepsilon_0 + sinh\left(\frac{\sigma}{\sigma_0}\right) + \left(v_0 sinh\left(\frac{t}{t_0}\right)\right) * t$	Proposed by (Parker et al, 1958) and developed for secondary creep by Nadai – McVetty in 1943. Due to the nature of this relation (hyperbolic function), it defines a linear relation between creep rate and stress at low stress values. To describe the temperature dependencies, additional Arrhenius term should be multiplied to this relation.
Polynomial	$\varepsilon = A * \sigma^n * t^p$	$\varepsilon = A + Bt^{1/3} + Ct$	n and p are parameter constant. Model developed by (Norton, 1929) and (Bailey, 1935), (Andrade, 1914) and (Cottrell-Ayetkin, 1947). The advantage of this model is its power law relation used to describe the stress variable dependent to the elevated temperature. Major disadvantage is the lack of its explicit consideration of the temperature and the fixed exponent of 1/3, limiting its acceptability.
Exponential	$\varepsilon = A[1 - \exp(-Bt)]$	$\varepsilon = A[1 - exp(B - Ct^n)]$ $\varepsilon = f(s) * \sigma^n * exp\left(\frac{Q_a}{RT}\right)$	R is a gas constant, Q_a is the activation energy and T is the absolute temperature. Proposed by Sherby, Dorn, 1953. The disadvantage of the primary creep model is that temperature and stress dependencies are not explicitly modelled. It has however served as a pioneer to the development of the Garofalo creep model for the whole creep curve (i.e. secondary and even tertiary stage).The model for secondary creep describes the effect of certain test parameters such as temperature and stress on creep behaviour. It contains nearly all parameter dependencies used in a creep experiment.

In summary of Table 2.1, the mathematical form of all creep relations described above were categorised in forms of exponential, power law, or sine – hyperbolic relations. The explicit forms of this law, which are a function of time, are not applicable for finite element analysis. However, Taylor expansion helps to reduce all creep models to either power law or exponential form.

More developments were seen in modelling of creep behaviour especially in research results reported between 2000 and 2012. Researches focused more on modification and

extension of previous developed models discussed in Table 2.1. A major attempt to describe the creep process was further concentrated more or less on using the exponential approach based on the idea of the Kelvin – Voigt viscoelastic model which are well described in literature [31–33].

2.5.4. Viscoelastic models

The creep behaviour of metals can be represented by models comprising of springs and dashpots to represent elastic and viscous strain respectively. Viscoelastic models proposed by Kelvin - Voigt in 1898 are simple rheological models developed on the idea of the exponential creep law form (Table 2.2). The goal of rheological models is to relate, by laboratory testing, each component of stress to each component of strain while, in the process, introducing a few material properties as is necessary to capture the fundamental behaviour with sufficient accuracy for engineering purposes. Various combinations of these mechanical models such as spring and dashpots can be used (Table 2.2) to simulate a wide range of time-dependent behaviour. Different viscoelastic models are popularly used and well described in literature [30–35]; some of which are also listed in Table 2.2.

Table 2.2: List of existing viscoelastic models.

Model	**Property**	**Stress – strain – time relation in 1D**	**Element representation**
Spring	Elastic	$\varepsilon = \frac{\sigma}{E_e}$	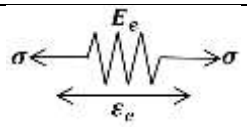
Dashpot	Viscous	$\varepsilon(t) = \frac{\sigma . t}{\eta_v}$	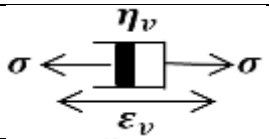
Maxwell	Viscoelastic	$\varepsilon(t) = \frac{\sigma}{E_e} + \frac{\sigma . t}{\eta_v}$ $\sigma(t) = G\gamma(t) + \eta_v \frac{d\gamma(t)}{dt}$	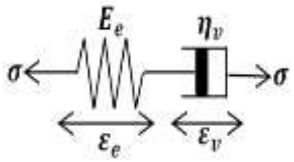

Kelvin - Voigt	Viscoelastic	$\varepsilon(t) = \frac{\sigma}{E_e}\left[1 - exp - \frac{E_e.t}{\eta_v}\right]$ $\gamma(t) = \frac{\sigma_0}{G} + \frac{\sigma_0}{\eta_v}.t$	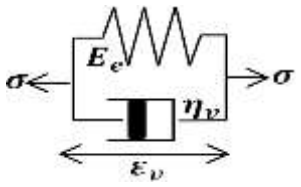
Generalized Kelvin	Viscoelastic	$\varepsilon(t) = \frac{\sigma}{E_v} + \frac{\sigma}{E_e}\left[1 - exp - \frac{E_e.t}{\eta_v}\right]$	
Generalized Maxwell	Viscoelastic	$\varepsilon(t) = \frac{\sigma}{E_e}\left[1 - exp - \frac{E_e.t}{\eta_v}\right] + \frac{\sigma.t}{\eta_v}$	
Burger	Viscoelastic	$\varepsilon(t) = \frac{\sigma}{E_v} + \frac{\sigma}{E_e}\left[1 - exp - \frac{E_e.t}{\eta_v}\right] + \frac{\sigma.t}{\eta_p}$	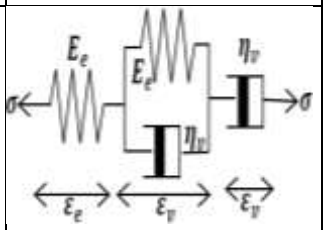

where σ =stress, ε =strain, E_e =Young´s modulus, G =shear modulus, γ =shear strain η_v =viscosity, and t =time.

Different rheological models have been introduced for the mathematical description of the stress-train-time behaviour of metals. However, the basic creep behaviour of metals at high temperature can best be described according to Maxwell, Kelvin-Voigt, Burger (Table 2.2) and the introduction of Bingham (elastoviscoplastic) models.

Maxwell model, proposed by James Maxwell in 1868, combines the elastic element (spring) to the viscous element (dashpot) in series. On application of stress, the elastic element produces instantaneous strain. As the stress remains constant over a certain period of time, viscous flow will occur; this is also referred to as delayed strain. Thus the elastic deformation completely disappears in favour of the viscous component, thereby inducing permanent strain.

Kelvin - Voigt model combines elastic element (spring) to viscous element (dashpot) in parallel. The set-up of this model means elastic and viscous elements can only be deformed together and to the same extent. Hence, unlike Maxwell, instantaneous

deformation on application of stress is not represented. Under a constant load, at the beginning, the dashpot sustains the load alone and gradually transfers the load to the spring.

Both Maxwell and Kelvin - Voigt model are linear viscoelastic models capable of giving a good representation of the regions within a creep curve as described earlier. The elements of Kelvin-Voigt gives a good representation of the primary creep strain region (recoverable strain), while the elastic and viscous element of Maxwell gives a good representation of the elastic strain region and the secondary creep strain region (irreversible viscous flow) respectively. However, for a Kelvin-Voigt element of an established rheological model subjected to an applied stress, the viscous element could also experience a continuous viscous flow; meaning the primary creep strain region may not be fully reversible.

Plastic strain (permanent deformation) behaviour occurs in metals when the applied stress is greater than the yield stress and requires incorporation of an additional element (plastic slider) other than the elastic and viscous element used in Kelvin Voigt and Maxwell models. However, at high temperatures, metals lose their yield strength and can undergo a continuous viscous flow (permanent strain deformation) even at low stresses below its yield stress. In such cases, the use of the elements of Kelvin-Voigt and Maxwell or their combination is still applicable without the additional plastic element.

Linear viscoelastic models have been extended to account for non-linear viscosity representing the effect of permanent strain in the deformation behaviour of metals. One of such approaches included slightly modifying and adding an additional term (n) to the Kelvin –Voigt model representing the primary creep strain region such that:

$$\varepsilon(t) = A * [1 - \exp(B - Ct^n)] \tag{2.6}$$

Garofalo [30] also described the instantaneous elastic, primary and secondary regions of the creep curve by adding linear terms (elasto -plastic part) to the Kelvin-Voigt model such that:

$$\varepsilon(t) = \varepsilon_0 + \varepsilon_t \left[1 - \exp\left(\frac{t}{t_r}\right)\right] + \dot{\varepsilon}_s * t \tag{2.7}$$

where ε_0 is the initial time independent elastic strain, ε_t is the transient (primary) creep strain, t_r is the transient time between primary and secondary creep part and $\dot{\varepsilon}_s$ is the strain rate of the secondary creep region.

Similar to Garofalo model, Burger rheological model combined the elements of Maxwell and Kelvin-Voigt model in series to account for the instantaneous elastic strain, recoverable strain (primary creep) and the permanent strain (secondary creep) region of the creep curve (Figure 2.12).

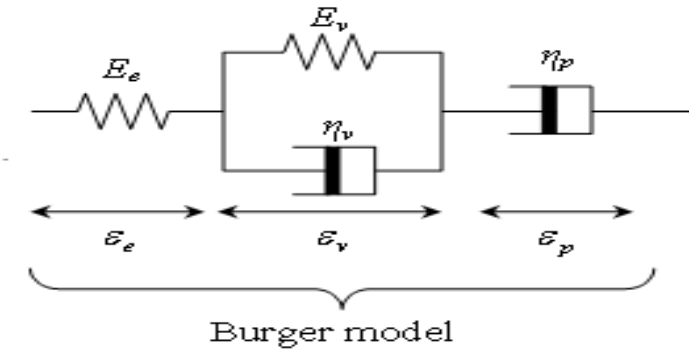

Figure 2.12: Burger viscoelastic creep model

The equation of the Burger model can simple be expressed in terms of stress and strain such that:

$$\boldsymbol{\varepsilon(t) = \sigma\left[\frac{1}{E_e} + \frac{1}{E_v}\left\{1 - exp\left(-\frac{E_v(t)}{\eta_v}\right)\right\} + \frac{t}{\eta_p}\right]} \tag{2.8}$$

where $\varepsilon(t)$ is the total strain, σ, is the constant applied stress, E_e, is the elastic modulus for the instantaneous elastic region, E_v is the modulus for the viscous recoverable region, η_v, is the viscous coefficient of the recoverable region, and η_p, is the viscous coefficient of the permanent strain region.

The differential stress – strain constitutive relation of the model can hence be expressed such as:

$$\sigma + \frac{E_e(\eta_v+\eta_p)+E_v\eta_p}{E_eE_v}\dot{\sigma} + \frac{\eta_v\eta_p}{E_eE_v}\ddot{\sigma} = \eta_p\dot{\varepsilon} + \frac{\eta_v\eta_p}{E_v}\ddot{\varepsilon} \quad (2.9)$$

Equation (2.9) is a second order derivative and the determination of the creep integral core function is of importance. At the initial stage, the elastic region, where the stress is a constant σ_0 at time $t = 0$, the creep equation can simply be expressed in its integral core function:

$$\varepsilon(t) = J_0\sigma_0 + \sigma\int_0^t D(t-\tau)\,d\tau \quad (2.10)$$

where J_0 is the elastic compliance, $D(t-\tau)$ is the creep core function and the eigen function which reflects the rheological properties of the material can hence be expressed as:

$$D(t-\tau) = \frac{\dot{\varepsilon}(t-\tau)}{\sigma} \quad (2.11)$$

The Burger model can be considered suitable to adequately represent all regions of the creep curve, (including permanent strain due to viscous flow) for metals in deformation at high temperatures and at low stress levels below their yield strength. Maxwell models could also be sufficient to model the creep deformation behaviour of metals in cases where the primary creep strain is negligible. In situations where the applied stress is greater than the yield strength at a particular temperature, the occurring permanent strain (plastic deformation) requires a different model along the line of viscoplasticity.

2.5.5. Elastoviscoplastic models

The Bingham viscoplastic model consists of the Saint Venant rigid plastic element connected in parallel with a Newton viscous element. This model introduces the yield point which describes the transition from the state of rest flow.

The Bingham model equation is such that:

$$\sigma = \sigma_y + \eta_p * \varepsilon_p \quad (2.12)$$

where σ is the applied stress, σ_y is the yield stress, η_p is the viscous coefficient and ε_p is plastic strain.

Elastoviscoplastic models have been used to model stress – strain - time behaviour in cases where the applied stress exceeds the yield stress of on the material [32]. This model is a slightly modified version of the Burger model and consists of typical kelvin model in series with a Bingham model (Figure 2.13) [31–34].

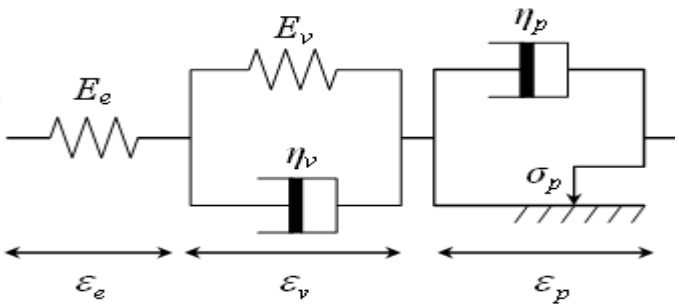

Figure 2.13: Elastoviscoplastic creep model

The time-dependent stress - strain relationship of the elastoviscoplastic model in 1D is as follows:

$$\varepsilon(t) = \frac{\sigma}{E_v} + \frac{\sigma}{E_e}\left[1 - exp - \frac{E_e.t}{\eta_v}\right] + \frac{(\sigma - \sigma_0).t}{\eta_v} \qquad (2.13)$$

2.6. Summary

This review focused on the deformation behaviour of metals (particularly low carbon steel) and their properties at elevated temperatures available in literature. The deformation behaviour of steel becomes more pronounced at high temperatures as metals tend to lose its strength and stiffness with increasing temperature. The material composition of steel, especially carbon, was described to have some influence on the temperature dependent properties consisting of thermal (thermal expansion coefficient),

mechanical (Young´s modulus) and creep (creep strength) which are needed to model the behaviour of the material.

For the cathode collector bar material (AISI 1006) low carbon steel, a linear thermal expansion of up to 1.2 % with occurrence of phase change in the form of contraction between 700 °C and 900 °C were predicted and measured in tests at temperatures up to 900 °C. Mechanical properties including yield strength and Young´s modulus decreases significantly with increasing temperatures above 300 °C. A Young´s modulus of about 13.5 GPa and yield strength of about 18 MPa were obtained from tests on low carbon steel at 900 °C. Analysis of Creep rate data on the collector bar at low loads ranging from 1 to 5 MPa shows that the bar slowly deforms under small forces at temperatures above 700 °C. A creep rate of about 0.002 %/h was obtained at 900 °C and 1.3 MPa corresponding to almost 1 % creep of the bar in three weeks.

The study of the creep phenomenon showed that a creep curve can be characterised by three main stages of primary, secondary and tertiary regions. The creep curves are derived from steady state tests where constant stress is applied on a material over a certain period of time while the corresponding strain are measured. The response of creep curve is dependent on the applied stress and temperature level.

A threshold stress level was described as the minimum stress level below which no creep occurs. Also, above a certain temperature level (usually $0.3T_m$), a thermal activation process represented by an Arrhenius equation begin and, involves grain movement within the microstructural arrangement of the material causing creep deformation in the material. Below this temperature level (0.3Tm), there is no creep or its effect is negligible. For the cathode collector bar material (AISI 1006) the melting point is at approximately 1400 °C, hence, the effect of creep can be observed at about 566 °C.

Studies on the physical mechanism of the creep showed that metals deform at microstructural level due to slips of the grain parts and can be best described by dislocation theory. Three physical mechanisms consisting of dislocation slip, diffusion flow (Nebarro Herring and Coble creep) and Power law (dislocation climb) was discussed as the major controlling creep mechanisms in metals and applicable at

combination of different stress and temperature levels. Similar to Nebarro and Coble creep, Harper Dorn also described the mechanism of creep at low stresses and high temperatures (above 0.6Tm) with a linear stress dependence n of 1. Power law however, was described to occur at higher stresses and intermediate temperatures ($0.3 – 0.6T_m$) and a nonlinear stress dependence ranging from 3 – 8.

Review of creep behaviour models were categorised into three main groups consisting of the phenomenological models, the empirical models and the rheological models. The phenomenological models are developed based on observations of experimental creep data while the empirical models are derived from the stress – strain - time relationship of creep data with its parameter determined by curve fitting and regression. Different empirical models developed along the line of logarithmic form, sine - hyperbolic form and exponential forms were reviewed, describing models for primary and secondary creep region as in Table 2.1.

The rheological models are developed along the line of representing experimental stress – strain – time results with combinations of mechanical elements such as spring, dashpot and sliders to represent elastic, viscous and permanent strain deformation behaviour. Various viscoelastic and elastoviscoplastic including Maxwell, Kelvin-Voigt, Burger and Bingham model were reviewed for their suitability to models the creep deformation behaviour of metals at high temperatures.

The approach of using rheological models has great advantages and is flexible in modelling even complicated material mechanical behaviour at different time effect. The main advantage of the rheological model approach is that it illustrates different constitutive relations in a graphical, accessible form and allows their transformation by changing the position of various rheological elements in the total scheme.

3. Experimental Program

3.1. Introduction

This chapter covers the overall description of the experimental investigations carried out on the cathode collector bar material. This includes the oxidation tests, the creep tests in compression and the microstructural analysis of a virgin and creep test samples. The process includes looking at the overall test design, material processing, experimental procedure, data collection and the use of guidelines from applicable standards.

3.2. Material

The cathode collector bar material was used as the test specimen in this investigation. The specimen is an AISI 1006, hot rolled low carbon steel with typical composition of 0.080 % Carbon, 0.25-0.40 % Manganese, 0.050 % Sulphur and 0.040 % Phosphorus. The cylindrical shaped specimens are 86 mm long x 29 mm diameter and have a mass of 431.9 g (Figure 3.1) in accordance to ASTM E209-00 and ASTM E139-11 for tests in compression at high temperatures.

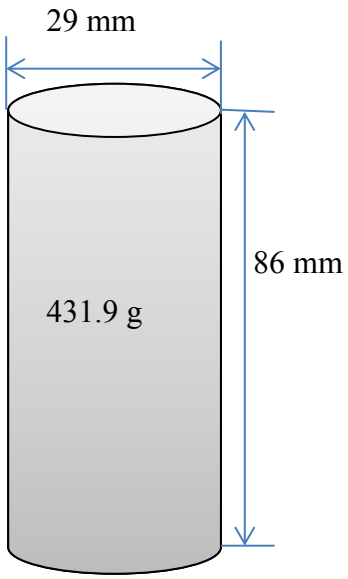

Figure 3.1: Schematic of the sample (AISI 1006) for the creep test in compression

3.3. Test set-up and procedure

3.3.1. Equipment and set-up

The compression creep tests were carried out at the REGAL laboratory in the department of civil and water engineering, Laval University, Quebec. The equipments used are as listed in table 3.1 and the test set-up described shortly after.

Table 3.1: List of equipment for the compression creep test

Equipment	Specification
Test bench	MTS landmark servo hydrodynamic test bench
Load cell	5, 10 and 250 kN MTS load cell.
Heating device	A three-zone resistance furnace, each zone furnished with a thermocouple by Winston Salem Thermocraft
Data collection device	Linear variable differential transformer (LVDT) and a precision linear encoder device (Heidenhain MT 1281).
Data storage	On line standalone desktop work station.

The test was carried out on an MTS landmark servo hydrodynamic test bench using three load cells with maximum capabilities of 250, 10 and 5 kN. The load cell was selected according to the test requirements. The required test temperature was attained in a flowing argon atmosphere of a three-zone resistance furnace, each zone with a thermocouple for temperature regulation and control. The argon flow rate was at 4 l/min. On line displacement data were taken by both the LVDT and the Heidenhain MT 1281. Water was used as coolant to regulate the temperatures in areas where the data taking device and load cells were located. The test bench and specimen set-up was as depicted in Figure 3.2.

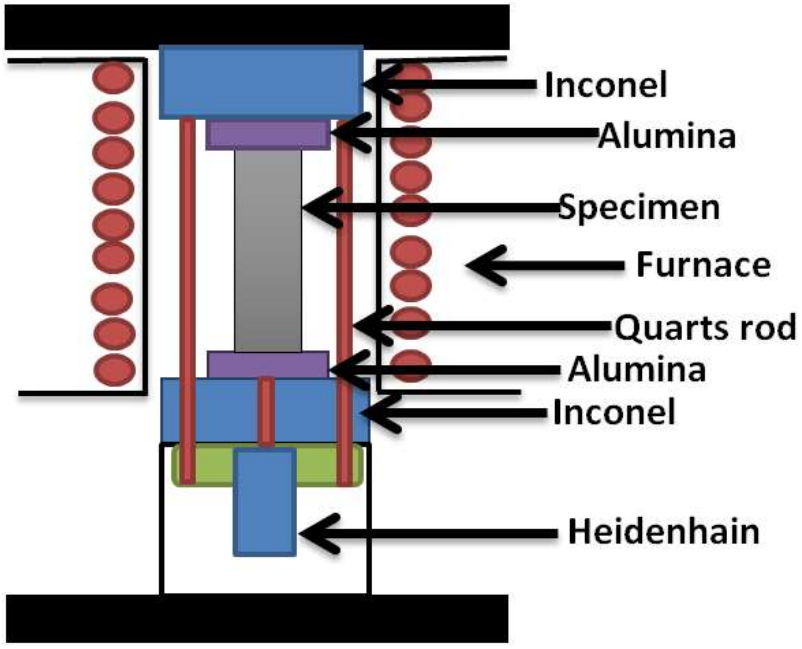

Figure 3.2: Schematic layout of creep test set-up

3.3.2. Procedure

The test procedure was in accordance to ASTM E 209-00 and E 139-11 and described in two stages. During the heating stage, the sample was subjected to an initial pre-stress of 0.08 MPa while heating to the required test temperature (at 900 °C) and left at this isothermal condition for about 4 hours. This was to ensure proper contact at all surfaces, uniform temperature distribution in the set-up, and to achieve steady state (signifying maximum grain size and hence steady microstructure). Thereafter, at the second stage, the required test load was instantaneously applied and kept constant on the sample for the creep test duration. For a test in compression, high precision in aligning sample within test set-up was essential to ensure a homogeneous stress distribution in sample.

The strain data were obtained and recorded every 10 seconds and represented with a graphical plot displayed on the stand-alone desktop workstation. The test was monitored at regular interval and terminated once a sufficient region of secondary creep had been observed. The strain estimation as a function of time is based on the full length of the sample, i.e. the vertical relative displacement of the two circular faces of the sample. The

effect of thermal expansion, contraction due to phase change took place prior to the creep test (i.e. during the heating stage) and oxidation behaviour of the material was observed all through the test duration.

3.4. Oxidation and metal loss test

Steels subjected to high temperatures in a corrosive environment experiences formation of oxide on their surfaces. Birosca et al. [36] carried out a study on the oxidation rate of low carbon steel at 650, 750, 900, 1000 and 1100 °C and showed that at all temperatures, the oxide thickness reaches a plateau level after a relatively short oxidation time. They also concluded that the higher the temperature level, the greater the oxide thickness [36].

A short investigation was carried out to check for oxidation and metal loss due to corrosive nature of the required test condition and environment. Two samples, one coated with refractory material (SEALMET) and the other uncoated, were placed in the MTS test bench set-up as described above without any load. The temperature was raised up to 900 °C and kept constant for 24 h. Weight measurements were taken before and after the test (Table 3.2). Though argon gas was injected into the furnace chamber, the effect of the presence of some air could still be observed and hence oxidation was a factor for consideration.

Table 3.2: Measurements of specimen for oxidation and metal loss test (grams)

Sample	Uncoated weight	Coated weight	Weight after test	Weight after cleaning	% weight loss
Coated	431.9	436.9	436.9	428.9	0.69
Plain	431.9	431.9	424.5	409.0	5.06

A metal loss of about 5.06 % in the uncoated sample compared to 0.69 % in the coated sample was observed. Due to the amount of weight loss by the uncoated sample, it was considered to coat all samples prior to test. The scale oxides of the coated samples were observed to be more closely attached to the sample after the test in comparison to that of the plain sample, where most of its scale appeared to have fallen off during the test. Some

blue and green stains were also observed on the coated material (Figure 3.3), indicating signs of corrosion leading to metal loss. Based on these observations, in preparation for the creep test, all other samples were coated to reduce effect of corrosion, metal loss and to ensure good strain measurement. Coating was applied by brush and special care was taken to ensure uniform coating on all samples used in the test.

(a) (b)

Figure 3.3: Corrosion test (a) coated and plain sample after test, (b) oxide scales detached off the sample

Due to the high corrosive nature of the test environment, residues of the test specimen and coatings usually remained stuck on the surface of the alumina support. This had to be properly cleaned off mainly by filing before carrying out each test. If proper care is not taken, this could lead to imbalance of specimen loading, unnecessary build-up of shear stress causing damage of the alumina, bringing test to an abrupt stoppage and also affecting the accuracy of final results obtained. Another major consideration for this procedure was to ensure uniform coating and consistency in weight of coating applied on all samples used for the test. Use of spray gun was considered.

3.5. Compression creep test

Generally for metals under constant load, creep of the bar is expected to become noticeable at temperatures corresponding to 30 % of the melting temperature ($0.3T_m$) for pure metals and 40 % ($0.4T_m$) for alloy metals [7]. For the sample used in this study (AISI 1006), the melting point is approximately 1400 °C hence, the creep strain was expected to become evident at temperature starting from 566 °C and above. All creep tests were carried out in compression at constant temperature of 900 °C for four (4) different applied stress levels of 0.5, 1, 1.5 and 2 MPa. Each test was performed three times to ensure repeatability. As a creep test in compression, and particularly at such low stress levels, the specimens were not expected to fail, hence tests were terminated once a significant amount of steady strain rate (secondary stage creep) was obtained.

3.6. Microstructural investigation

3.6.1. Preparation and procedure

Microstructural investigation was carried out to inspect the level of oxide formation and its effect on the deformation behaviour of the steel bar sample when exposed to creep at high temperature and low stresses. Microscopic inspection and composition analysis were carried out on virgin bar and creep tested samples. The test preparation and procedure were carried out in accordance to ASTM E3 – 11 and involved cutting a section of the sample, followed by grinding, and polishing of the surface of interest before finally examining it in a metallurgical scanning electron microscope (SEM).

A 5 mm sample was cut away from the top of each specimen (see Table 3.3) along its longitudinal length. The cutting was carried out using an abrasive cut-off blade with choice lubricant and cooling conditions. This was to make sure that the surface was not heated and the microstructure was not modified. An initial inspection was made on the circumferential surface (Figure 3.4) directly exposed to heat in the furnace during the creep test.

Table 3.3: List of samples for microstructural analysis

Sample
Virgin bar
Bar tested at 2 MPa, 900 °C for 230 h
Bar tested at 1.5 MPa, 900 °C for 280 h
Bar tested at 1 MPa, 900 °C for 240 h
Bar tested at 1 MPa, 900 °C for 72 h

Each of the 5 mm cut away sample was further dissected / sectioned (by machine sawing and continuous lubrication) into 4 uniform pieces along its circumference for further inspection along the cross sectional edges (Figure 3.4). The top edge where the steel sample which was directly in contact with the alumina when stress was applied during creep test was inspected (contact surface edge) and the circumferential edge directly exposed in furnace was also inspected (circumferential edge).

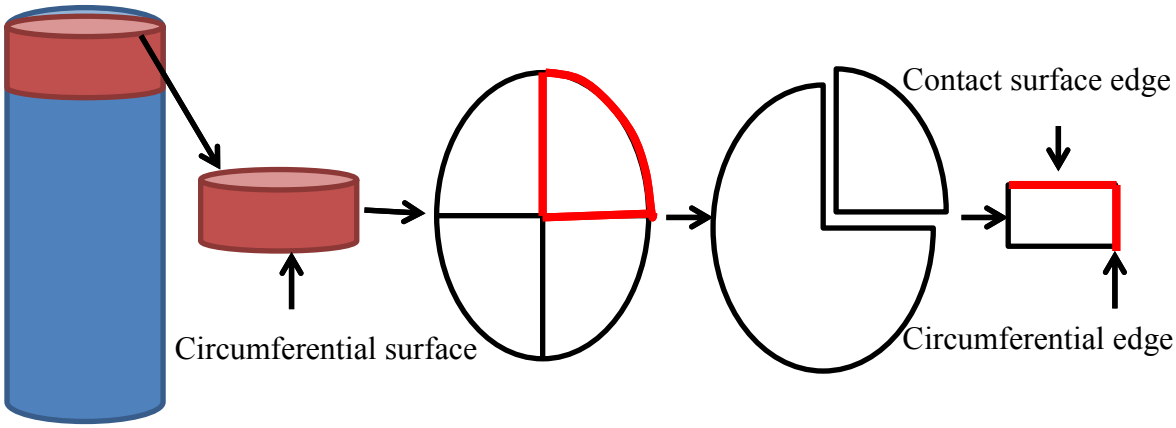

Figure 3.4: Cutting of the sample in preparation for the microstructural inspection

The cut samples were thoroughly cleaned to remove all grease, coolants and residues from the cut off blade on the sample. Prior to grinding and polishing, a 2 to 1 ratio mixture of samplkwick^{TM} powder and liquid respectively was prepared as a resin and poured into a small container holding the samples together. Particular attention was given

to the required surface for inspection. The resin mixture quickly solidified and was ejected from the container with the specimen in place within the resin.

Manual (hand held) grinding was carried out on the sample´s surface of interest using silicon carbide grinding paper of 240, 320 and 600 grain sizes respectively on a rotating disc with water lubricant. The specimen was moved back and forth across the rotating carbide paper to allow for even wear and rotated at 45 – 90^{o} till a flat surface with unidirectional grinding scratches was obtained. The samples were further manually polished with slurry of alumina by holding the surface of interest of the specimen by hand against the abrasive charged rotating steel wheel and moving the specimen in a circular path along the wheel against the direction of rotation of the wheel so as to obtain a scratch free finer surface (a mirror).

A thin layer of Gold and Palladium were added to the sample in a Technic Hummer 2 machine (Figure 3.5) to ensure good electrical conductivity of the sample when placed under the JEOL scanning electron microscope (Figure 3.6, SEM – JSM 840A) to reveal its microstructure.

Figure 3.5: Technic - Hummer 2 machine (a) set – up, (b) working procedure

Figure 3.6: JEOL SEM – JSM 840A, (a) Set – up, (b) working procedure

3.6.2. Microstructural inspection

Five samples were investigated as specified in Table 2.3. Initial investigation was carried out on the circumferential surface of a virgin bar and creep test samples at 2 and 1.5 MPa. Further investigation was carried out on the cross sectional surface of the samples looking at the contact surface edge and the circumferential edge, (see Figure 3.4) for pictorial description of referenced surface and edges inspected). The level of oxide formation and penetration on the surface and edges of the steel bar at point of interest was inspected and presented in chapter four.

4. Results and Discussion

4.1. Introduction

This chapter presents the results of experiments carried out on the AISI 1006 low carbon steel samples at high temperature and low stress levels. The material behaviour during the heating stage and applicable parameters were analysed. The preliminary creep test data at 900 °C and 1 MPa for a short period of time are presented. A few models discussed in chapter 2 were fitted to this experimental data to compare their suitability and to obtain applicable model parameters. Matlab® curve fitting tool was used for fitting the models to the experimental data. Characteristic data of the main creep tests at 900 °C and four different stress levels (0.5, 1, 1.5 and 2 MPa) for longer duration are also presented. Results of the metallographic inspection on virgin sample and four other creep tested samples at different stress level are also shown.

4.2. Thermal expansion and phase change

During the heating stage, the material was observed to expand almost linearly with increasing temperature up to 750 °C. This was followed by a contraction which began at 750 °C and ended at about 900 °C after which the temperature was kept constant (Figure 4.1).

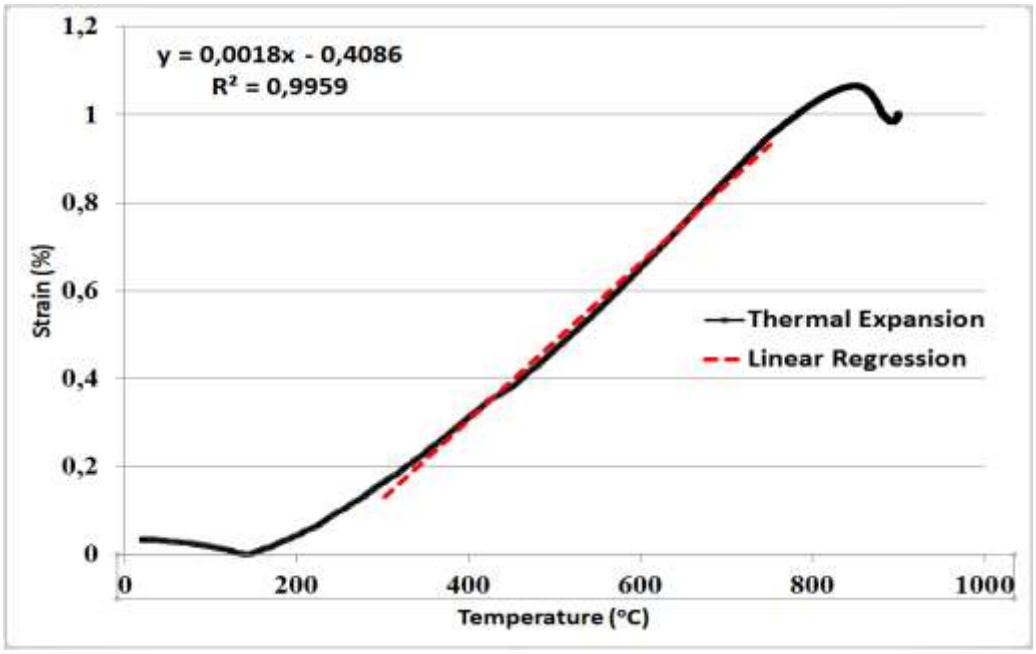

Figure 4.1: Thermal expansion and phase change during heating phase

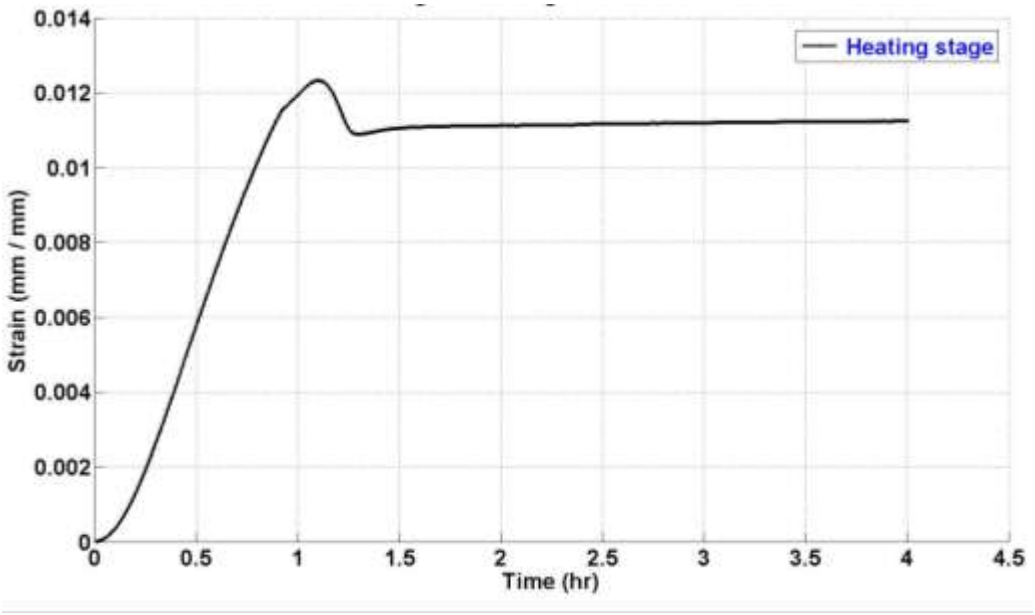

Figure 4.2: Strain vs time plot during heating stage

The expansion and contraction of the material at this temperature ranges suggest that it experienced both linear thermal expansion and phase transformation from ferrite to austenite state respectively. At 900 °C, the phase transformation tends to reach a stop

where the strain reaches a plateau over time (Figure 4.2). However, as the phase transformation occurs over a short temperature regime where both ferrite and austenite state seem to coexist, small ferrite phase may still exist at 900 °C (see Figure 2.2b for phase diagram). From this data, a maximum thermal strain of about 1.25 % was obtained. The coefficient of thermal expansion obtained from the gradient of the plot by linear regression gave a value of 18 x 10^{-6} per °C for this material. This could also be determined by the expression given in equation (1.3).

4.3. Compression creep test

4.3.1. Preliminary test – short duration

A preliminary creep test was carried out at 900 °C, the load of 1 MPa and kept constant for the test duration of 24 hours. During two hours of heating stage of the sample, a stress of 0.3 MPa was applied on the sample before commencing on the creep test afterward (Figure 4.3).

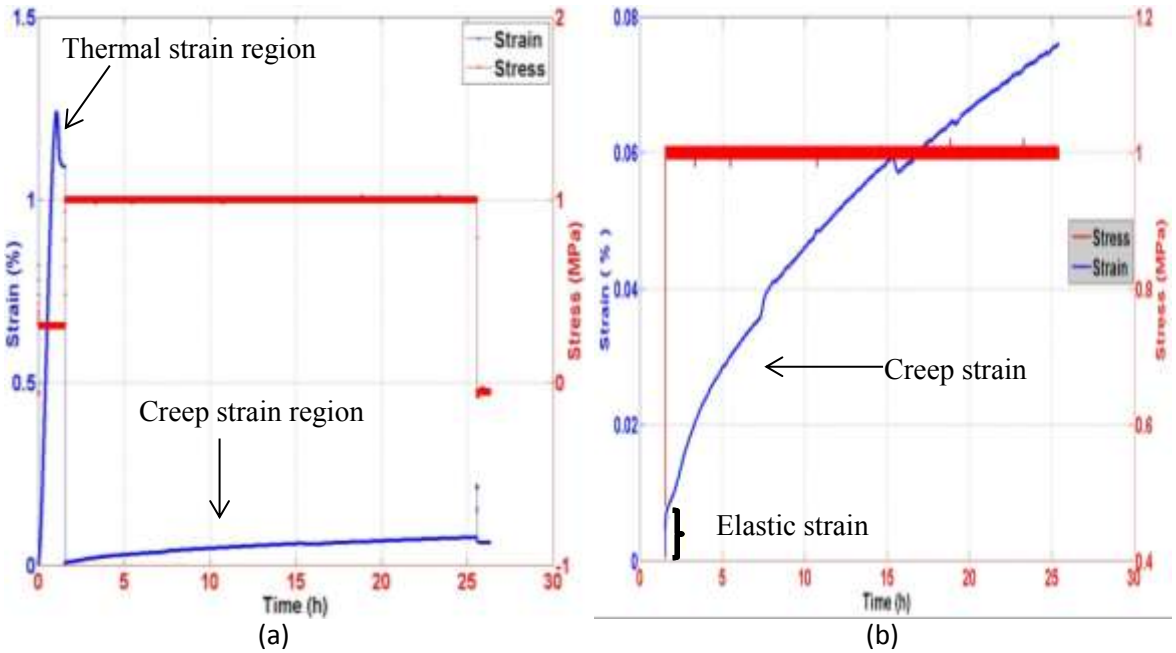

Figure 4.3: Preliminary creep test at 900 °C, at stress level of 1 MPa for 24 hours (a) total strain, (b) region of elastic and creep strain only

Figure 4.3a shows the total strain obtained relative to time. This includes thermal strain during the heating period, the elastic strain on quasi-instantly applied load and the creep strain at constant stress level over the duration of the test. It must be note that after the end of the heating period the displacement device has been reset before applying the load. In Figure 4.3b, region of thermal strain was excluded to give a more detailed view of the elastic and the creep region.

The elastic and the creep strains could be clearly identified in these figures. A total strain of 0.076 % was obtained while the value of the elastic strain was also determined from the curve as 0.0075 %. According to the stress - strain relationship, the value of the Young´s modulus was calculated to be 13.16 GPa using equation 1.7. However, this was not considered as the best approach to determine these parameters, hence, a more accurate approach of fitting a linear regression line of form ($y = mx + c$) was adopted.

By plotting the stress – strain graph of the elastic region, identified in the curve, a linear regression line was fitted to properly determine the value of the Young´s modulus parameter (Figure 4.4a). The gradient of the slope (m) gave a value of 1.2×10^{10} corresponding to a Young´s modulus value of 12 GPa. The correlation coefficient used to determine the goodness of the regression line fit to the curve was presented as the norm of residuals (R^2) and gave a value of 0.9968 (Figure 4.4a). An R^2 with a magnitude near one (1) represents a good fit and values closer to zero, a bad fit.

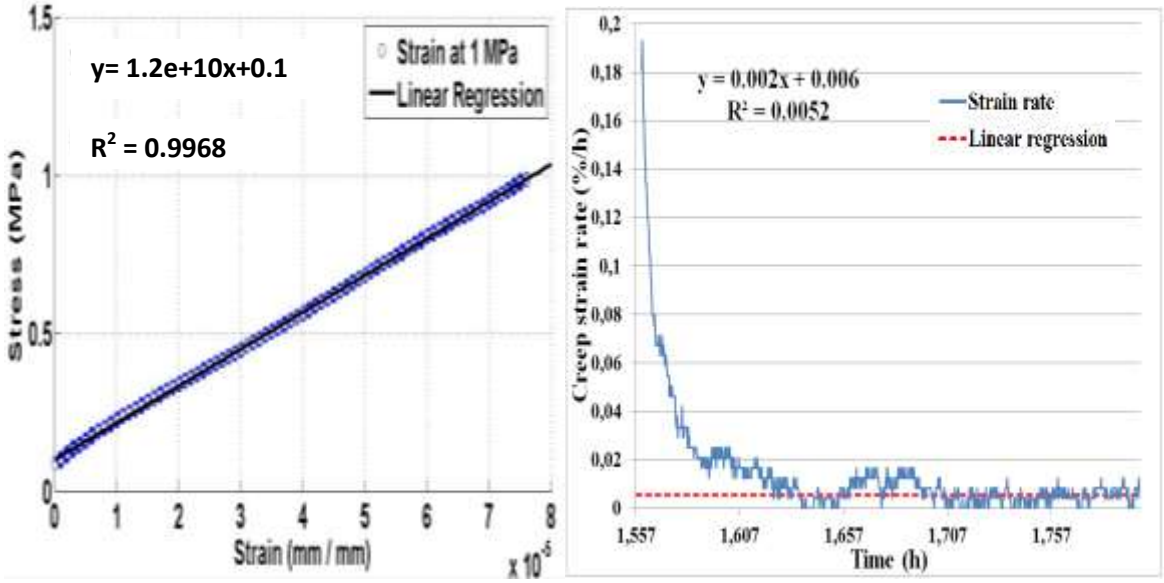

(a) (b)

Figure 4.4: Linear regression line fitting of preliminary creep data at 900 °C, at stress level of 1 MPa for 24 hours (a) stress – strain curve of the elastic region (b) creep strain rate – time curve

In a similar approach, based on the creep curve data, the creep strain rate at any given time was obtained by differentiating the creep strain with respect to the creep time (Figure 4.4b). It was noted that the curve appeared to reach a minimum constant rate after a short period of time; this minimum rate was taken as the creep strain rate at 0.006 %/h.

The strain response appeared to be highly sensitive to changes in the surrounding temperature. Any little change in room temperature had an impact on the temperature of the cooling water (used to protect the measuring devices) and hence the furnace temperature. A change in temperature as small as 3 °C within the furnace caused substantial increase in the strain and recovered back at normal furnace temperature (Figure 4.5). This corresponds well and can be associated to the effect of thermal expansion occurring at slight temperature change during the creep test.

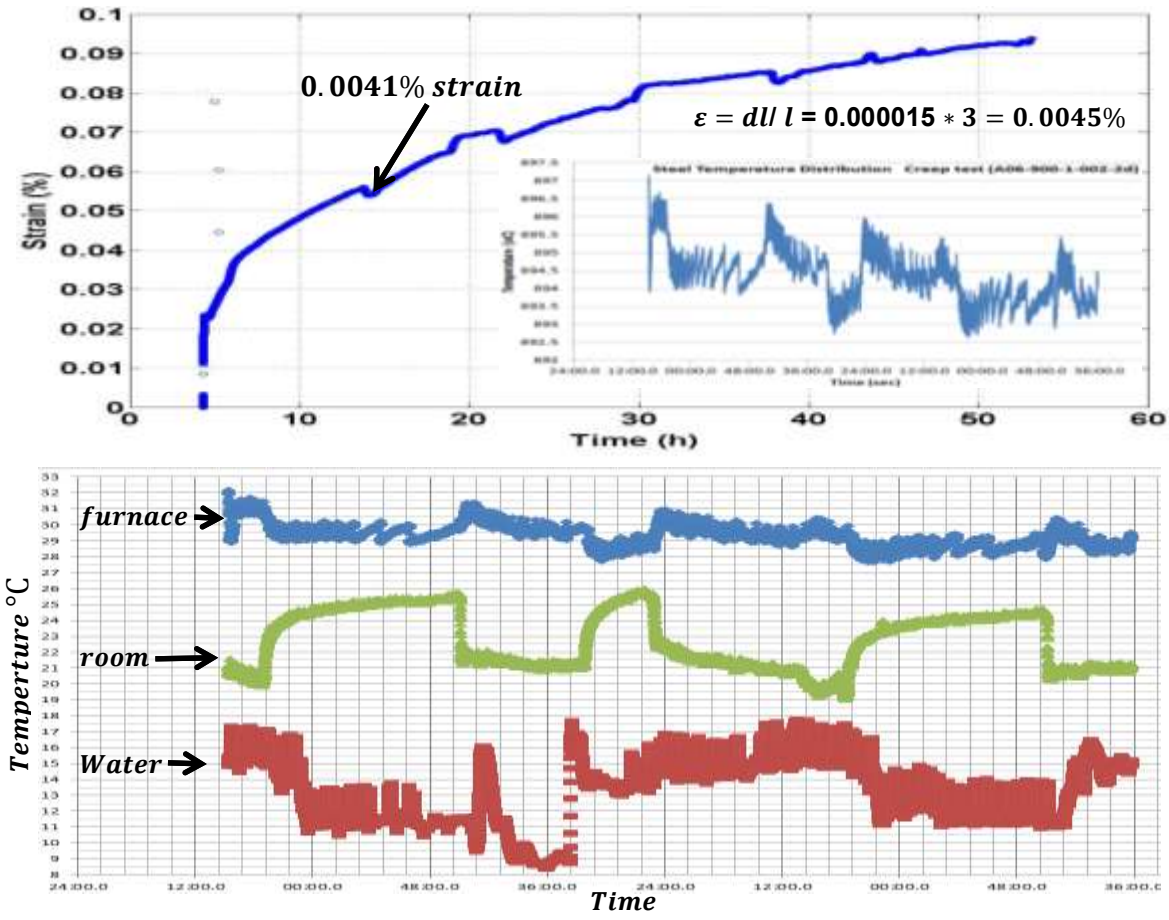

Figure 4.5: Change in creep strain due to change in temperature as effect of thermal expansion

4.3.2. Model curve fitting

Several creep laws proposed in literature were discussed in chapter 2. Three of these models including (a) power law, (b) exponential model and (c) Burger model were fitted to the experimental data using the Matlab curve fitting tool.

4.3.2.1. Power law

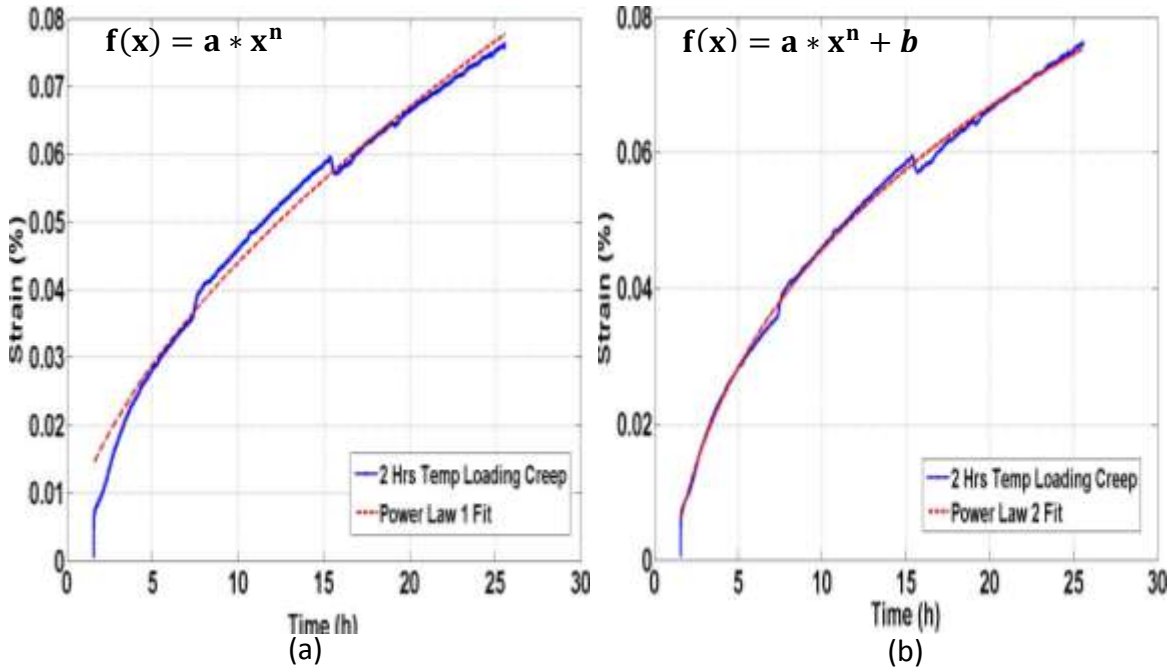

Figure 4.6: Curve fitting of power law models: (a) power law, (b) modified power law

The power law model fit in Figure 4.6a gave a fit that tends to favour a linear steady increase profile in comparison to the modified power law model presented in Figure 4.6b which gave a better fit for the whole curve. This suggested that at least two regions exist in the creep curve and one needs an additional term to properly represent the curve. The fit model parameters and goodness of fit values are given in Table 4.1.

Table 4.1: Power law models and goodness of fit parameters

Creep Data	**Model**	**a** (%)	***n***	**b** (%)	**SSE** (%)	**R^2**	**RMSE** (%)
Preliminary creep test	$f(x) = a * x^n$	0.0109	0.605	-	0.3725	0.9867	0.002076
	$f(x) = a * x^n + b$	0.0503	0.284	0.051	0.0486	0.9983	0.000750

4.3.2.2. Exponential models

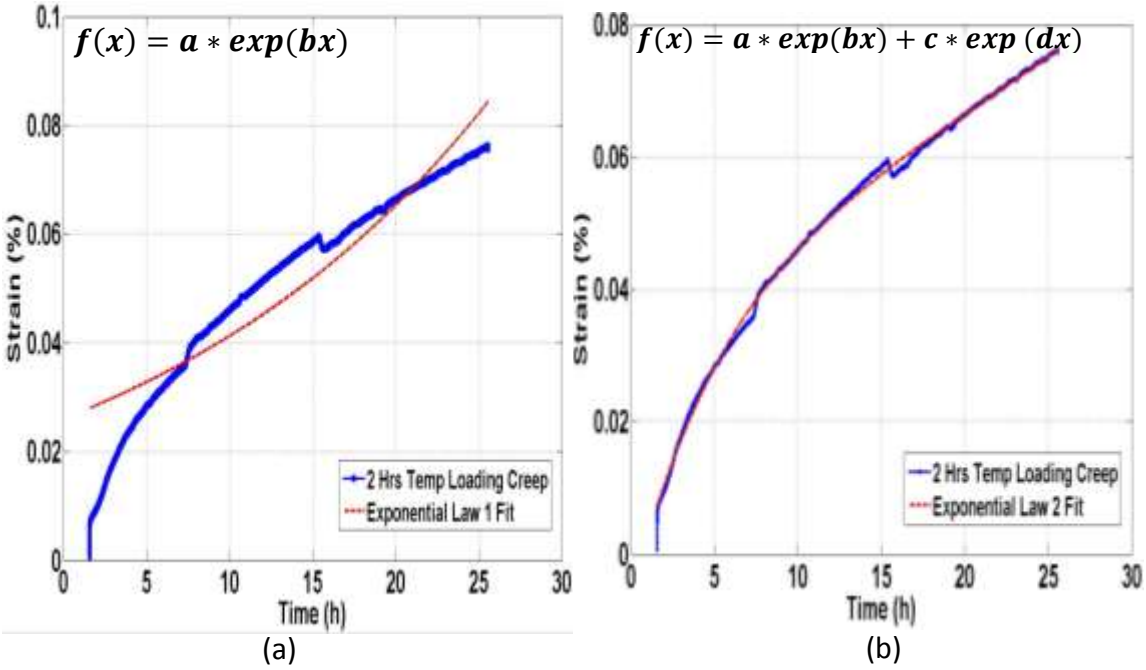

Figure 4.7: Curve fitting of exponential models: (a) power law, (b) modified power law

The exponential model presented in Figure 4.7a did not allow a fit while the modified exponential model fit in Figure 4.7b gave a much better fit for the whole curve. Similar to power law model, this also suggested that at least two regions exist in the creep curve. The exponential model parameters and goodness of fit values are given in Table 4.2.

Table 4.2: Exponential models and goodness of fit parameters

Creep Data	**Model**	**a** (%)	***b***	**c** (%)	**d**	**SSE** (%)	**R^2**	**RMSE** (%)
Preliminary creep test	f(x) $= a * \exp(bx)$	0.0260	0.046	-	-	3.377	0.879	0.0063
	f(x) $= a * \exp(bx) + c * \exp(dx)$	0.0438	0.022	0.004	0.178	0.041	0.998	0.0006

4.3.2.3. The Burger model

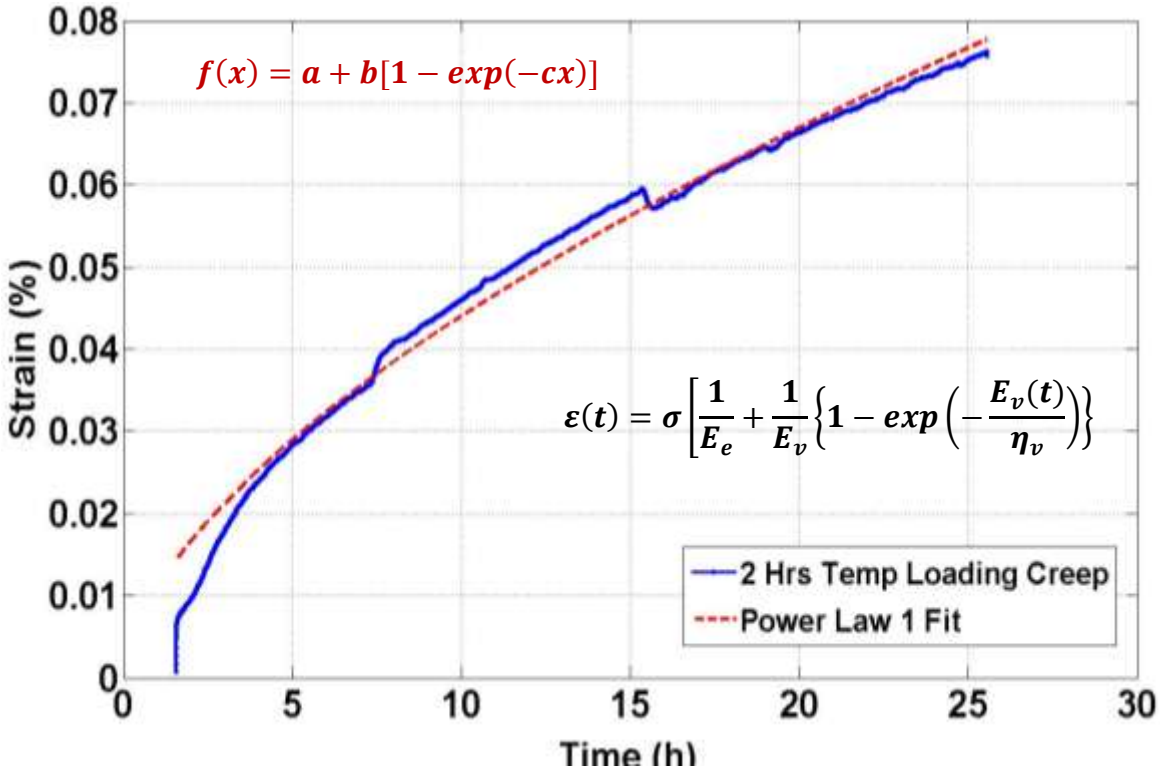

Figure 4.8: Curve fitting of preliminary creep data with Burger model

The Burger model, previously described in chapter 2, was also fitted to the preliminary creep curve data (Figure 4.8) using an exponential function ($f(x) = a + b[1 - exp(-cx)] + dx$) to represent parameters of the Burger´s equation given in Equation 2.8.

The Burger model in Figure 4.8 reveals a good fit for all region of the creep identified. The identified model parameters and goodness of fit values are given in Table 4.3.

Table 4.3: Burger model and goodness of fit parameters

Creep Data	**Model**	**a** (%)	***b*** (%)	**c**	**d** (%)	**SSE** (%)	**R^2**	**RMSE** (%)
Preliminary creep test	$f(x) = a + b[1 - exp(-cx)] + dx$	0.0074	0.043	0.209	0.002	0.043	0.999	0.0007

These identified parameters of the fitted Burger model can be used to obtain some mechanical properties of the experimental creep specimen where parameters are defined such that $a = \frac{\sigma_0}{E_e}$; $b = \frac{\sigma}{E_v}$; $c = \frac{E_v}{\eta_v}$; and $d = \frac{\sigma}{\eta_p}$. Hence the creep equation can be determined for the preliminary creep test data as:

$$\varepsilon(t) = 7.417 * 10^{-5} + 42.67 * 10^{-5}[1 - \exp(-0.2091t)] + 1.597 * 10^{-5}t \quad (4.1)$$

The mechanical parameters are given in Table 4.4.

Table 4.4: Mechanical parameters of preliminary creep test curve.

Stress levels (MPa)	**Elastic Mod. E_e (GPa)**	**Viscous Mod. E_v $(GPa.h)$**	**Visc. Coeff. η_v $(GPa.h)$**	**Visc. Coeff. η_p $(GPa.h)$**
1	**13.483**	**2.344**	**11.208**	**62.617**

4.3.3. Main creep test – long duration

From the results obtained in the preliminary creep test, regions of primary or secondary creep could not be easily determined. Acquiring more data was necessary to understand the creep behaviour over a long period of time. Hence, the creep test duration was extended for a longer period of up to 250 hours. The test was carried out at constant temperature of 900 °C and at four different stress levels as shown in the following figures.

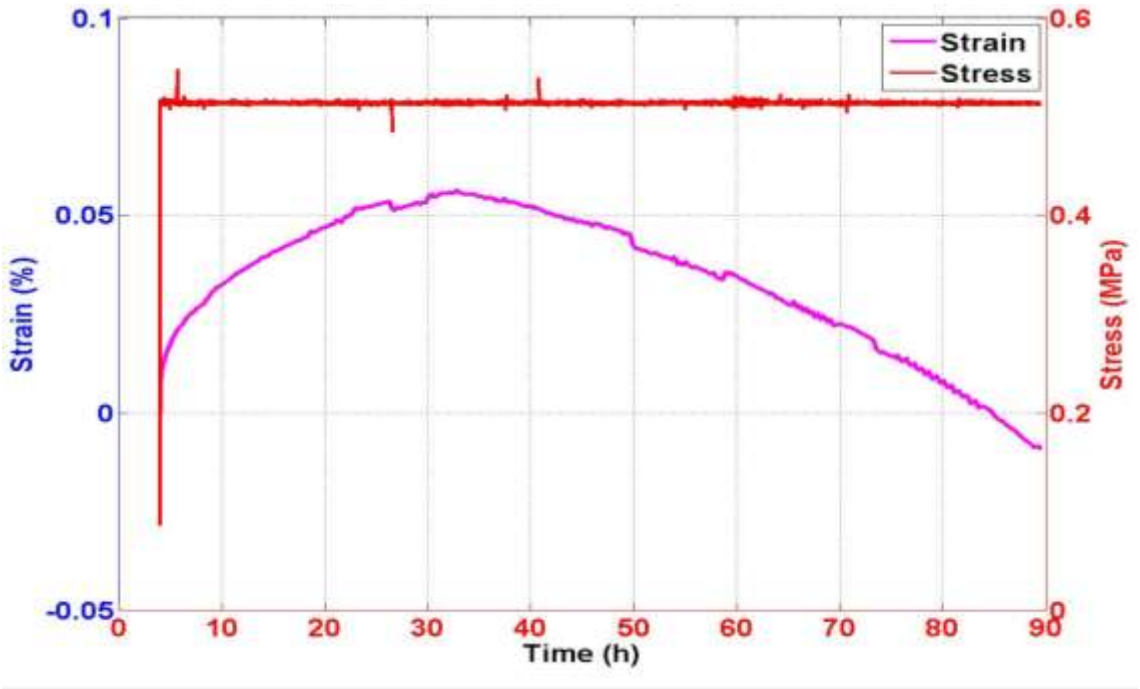

Figure 4.9: Creep test data at 900 °C, at a stress level of 0.5 MPa

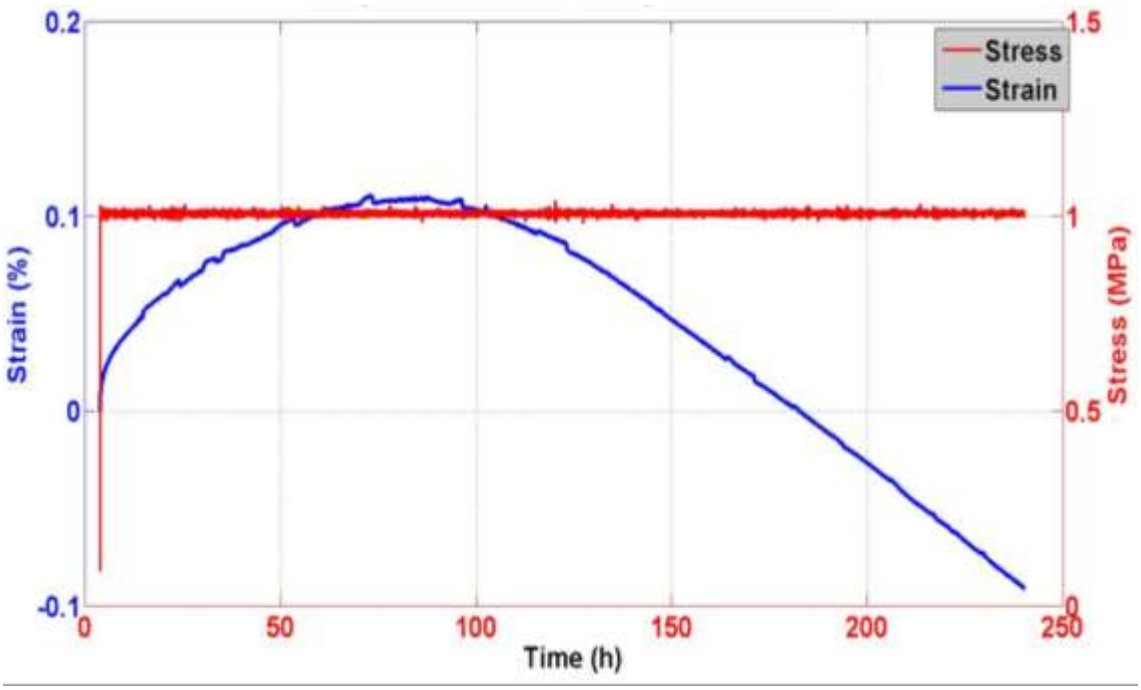

Figure 4.10: Creep test data at 900 °C, at a stress level of 1 MPa

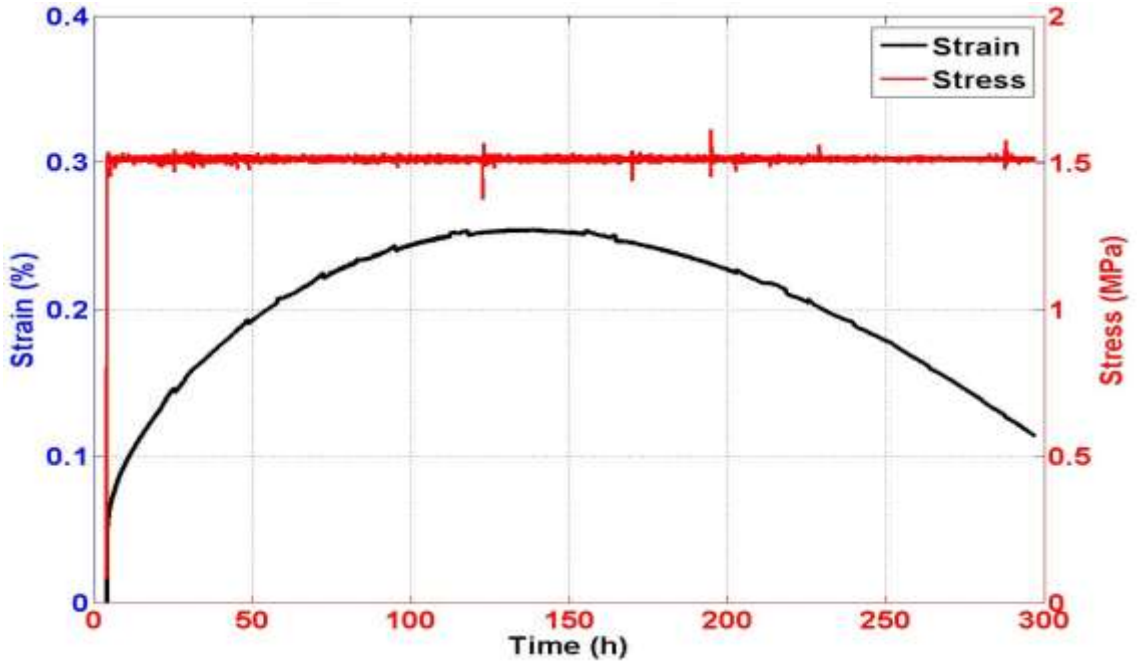

Figure 4.11: Creep test data at 900 °C, at a stress level of 1.5 MPa

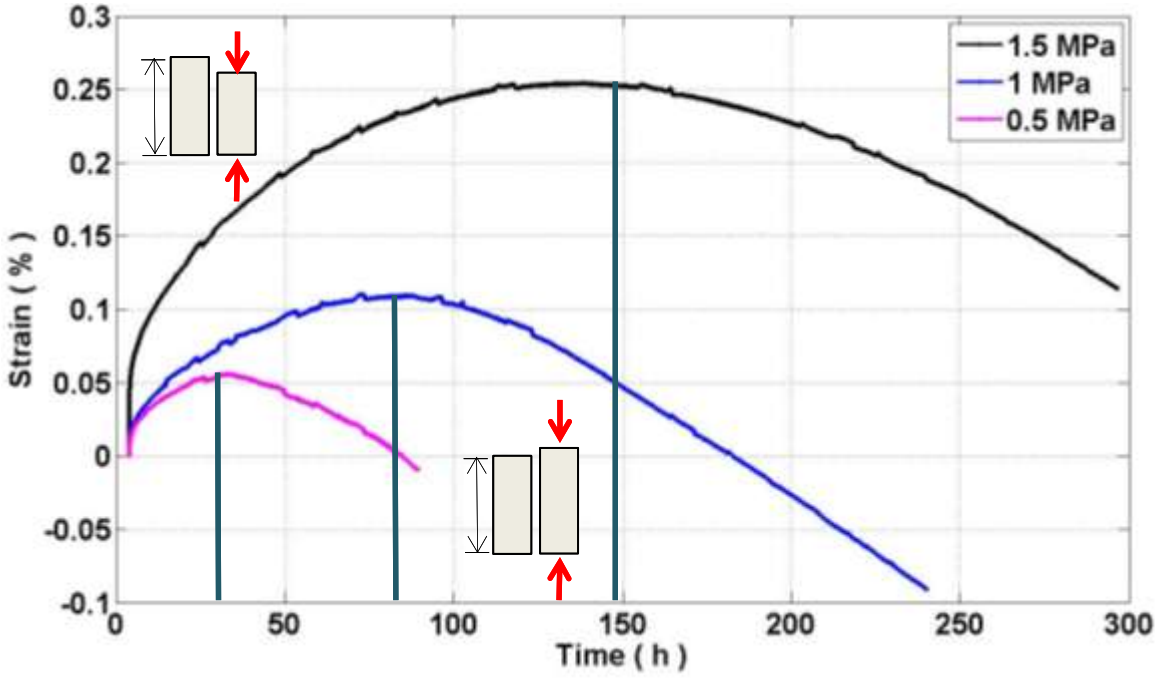

Figure 4.12: Comparison of creep test data at 900 °C and three stress levels (0.5, 1, 1.5 MPa)

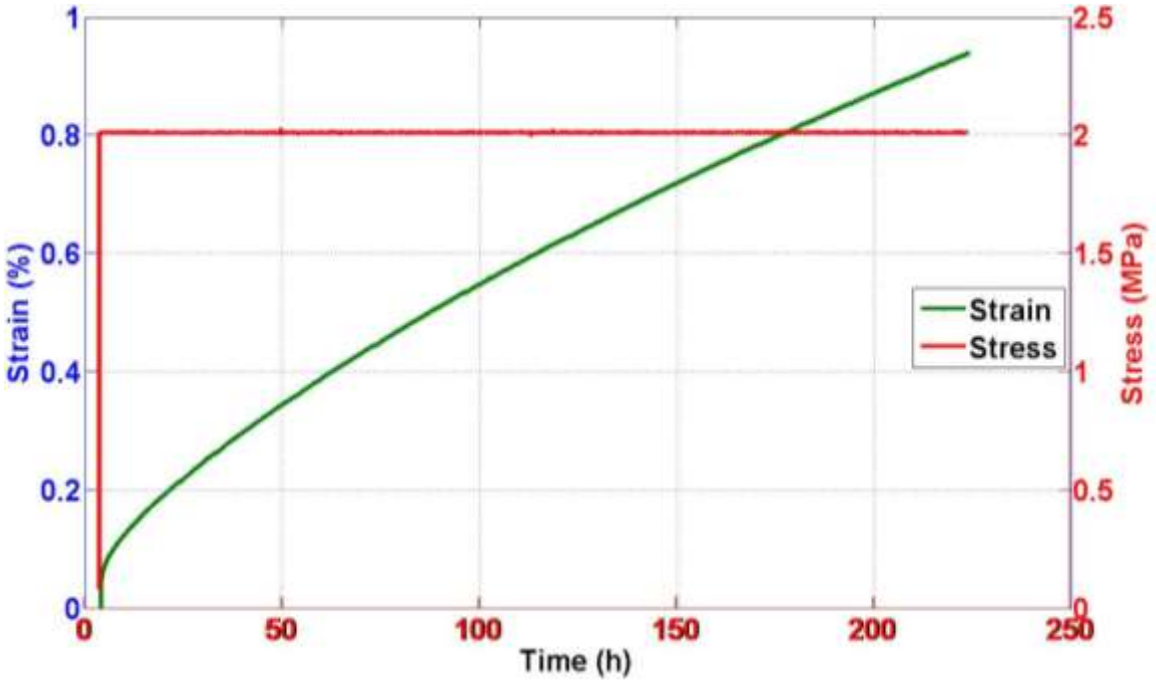

Figure 4.13: Creep test data at 900 °C, at a stress level of 2 MPa

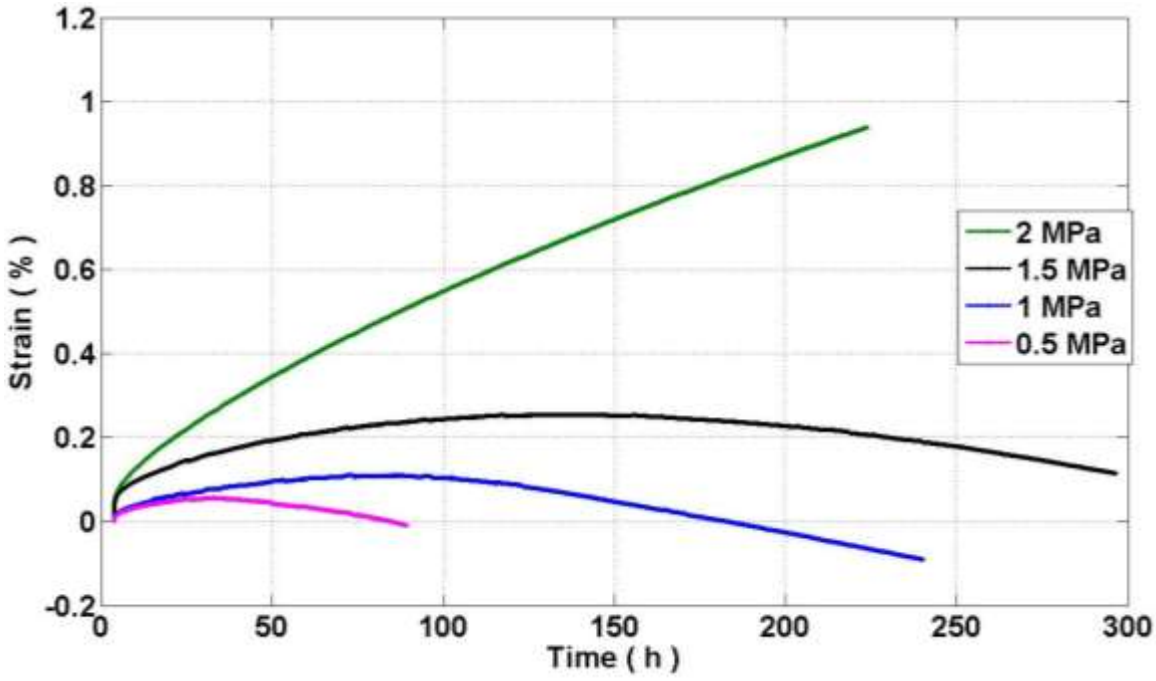

Figure 4.14: Comparison of creep test data at 900 °C and all stress levels (0.5, 1, 1.5, 2 MPa)

Figures 4.9 - 4.14 present the time-dependent strain data for the four stress levels at 0.5, 1, 1.5 and 2 MPa. For the first three stress levels (0.5, 1 and1.5 MPa), unconventional behaviour being characterized by time and the applied stress level was observed. At 0.5 MPa (Figure 4.9), obtained strain showed that the sample continued to deform in compression for duration of about 30 hours after which it tends to change behaviour with expansion occurring in the sample as time increases. Similar behaviour was observed for strain obtained at 1 and 1.5 MPa (Figure 4.10 - 4.11). At 1 MPa, this change in behaviour was seen to occur after about 100 hours and for 1.5 MPa, after 150 hours where each peak was seen (Figure 4.12).

After each peak, the material tends to experience a time-dependent expansion, the rate of this expansion seemed to reduce with increasing stress level (Figure 4.12). A higher expansion rate was observed at 0.5 MPa to that of 1 MPa. Similarly, the expansion rate at 1 MPa was also higher to that of 1.5 MPa. From all indication, this behaviour seems to be time-dependent and a function of the applied stress level.

The case was different for creep test data at stress level of 2 MPa, where a conventional creep curve, characteristically dominated by secondary creep region was obtained (Figure 4.13). A comparison of the whole creep data at different stress levels showed the creep profile at 2 MPa to be completely different from those obtained for lower stress levels right from onset (Figure 4.14).

Similar to the preliminary creep test data, an exponential function ($\boldsymbol{f(x) = a + b[1 - exp(-cx)] + dx}$) was used to obtain the creep strain rate and the parameters of the burger model respectively. Hence, evaluation of the mechanical properties of the creep curve data at 2 MPa (Figure 4.15)

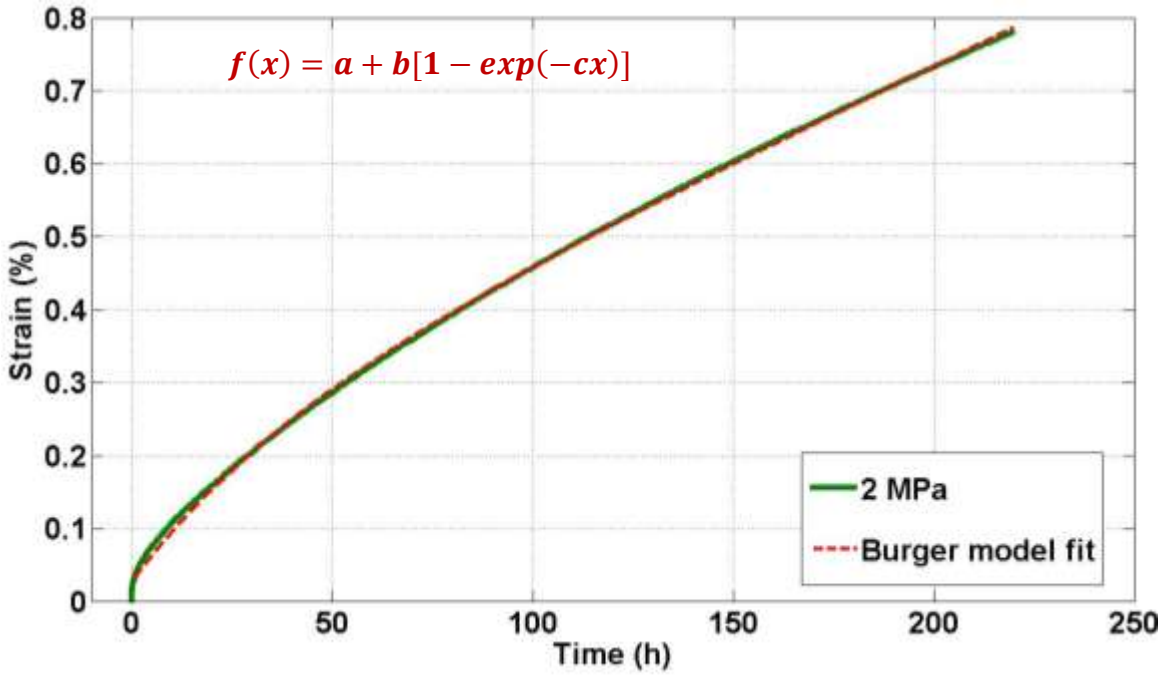

Figure 4.15: Curve fitting of the creep data at a stress level of 2 MPa with Burger model

The model gave a good representation of the creep data and the mechanical properties obtained are presented in Table 4.5.

Table 4.5: Mechanical parameters of Burger model at a stress level of 2 MPa.

Stress levels (MPa)	Elastic Mod. $E_e\ (GPa)$	Viscous Mod. $E_v\ (GPa.h)$	Visc. Coeff. $\eta_v\ (GPa.h)$	Visc. Coeff. $\eta_p\ (GPa.h)$	Creep Strain Rate $\dot{\varepsilon}^{cr}$ (% / h)
2	10.752	1.106	7.667	75.873	0.0037

However, at this point, this data are considered inconclusive as an unknown parameter, oxidation, observed to affect creep at low stress levels could also in theory have minor influence at high stress levels. This effect may occur at smaller magnitude, masked by the applied high stress and not easily observed in the creep curve. Hence, further consideration and tests were carried out with a modified approach to the experimental set-up (to reduce the effect of oxidation) as later discussed in section 4.5.

4.4. Microstructural Investigation

Microstructural inspection was carried out on virgin samples and creep test samples by method described in Chapter 3 in an effort to understand the unconventional behaviour obtained at stress levels below 2 MPa. The circumferential surface of a virgin sample and creep tested samples were inspected. Inspection was also carried out on the cross sectional edges of the creep tested samples as described (Chapter 3) for creep test samples at three different stress levels. All inspections carried out are as summarised in Table 4.6 and discussed further below.

Table 4.6: Summary of microstructural inspection carried out

Inspected area (Figure 3.4)	**Sections and Figures**
Circumferential surface	**Section 4.4.1**
Virgin bar	Figure 4.16
Creep tested sample at 2 MPa	Figure 4.17
Creep tested sample at 1.5 MPa	Figure 4.18
Contact surface edge	**Section 4.4.2**
Virgin bar	Figure 4.19
Creep tested sample at 2 MPa	Figure 4.20
Creep tested sample at 1.5 MPa	Figure 4.21
Creep tested sample at 1 MPa (240 h)	Figure 4.22
Creep tested sample at 1MPa (72 h)	Figure 4.23
Contact circumferential edge	**Section 4.4.3**
Virgin bar	Figure 4.19
Creep tested sample at 2 MPa	Figure 4.20
Creep tested sample at 1.5 MPa	Figure 4.21
Creep tested sample at 1 MPa (240 h)	Figure 4.22
Creep tested sample at 1MPa (72 h)	Figure 4.23

4.4.1. Initial inspection on the circumferential surface

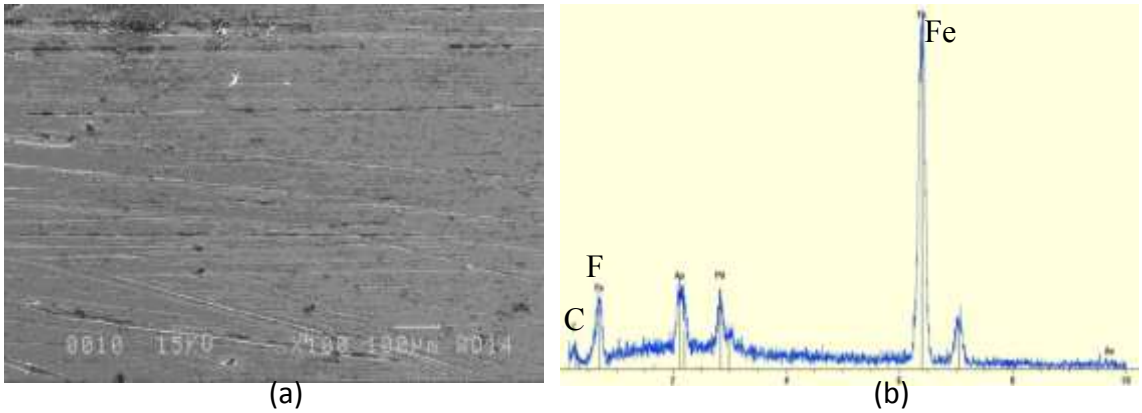

Figure 4.16: Inspection on the circumferential surface of a virgin sample

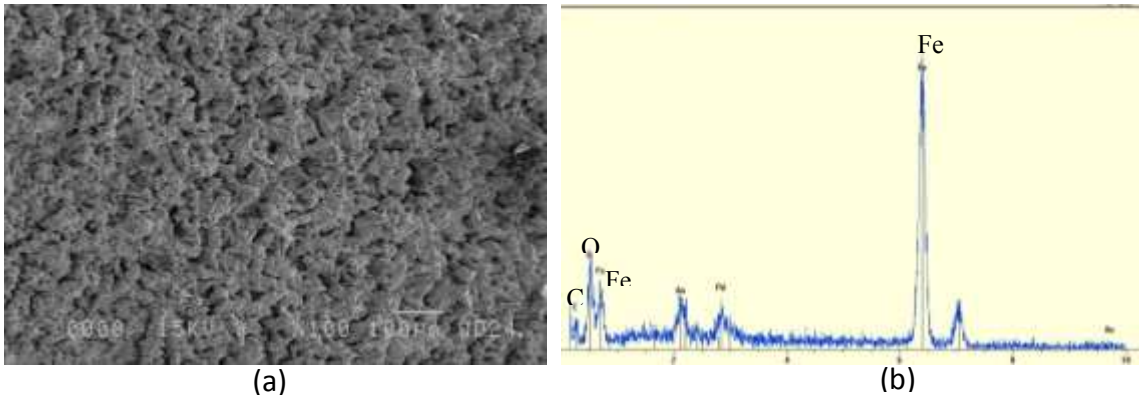

Figure 4.17: Inspection on the circumferential surface of a creep tested sample at 900 °C, at 1.5 MPa for 280 h

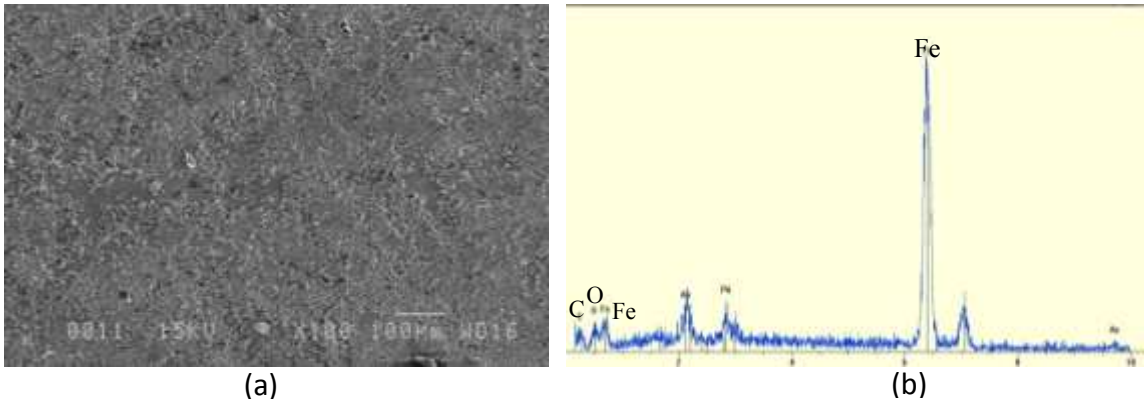

Figure 4.18: Inspection on the circumferential surface of a creep tested sample at 900 °C, at 2 MPa for 230 h

Figures 4.16, 4.17, and 4.18 show results of inspection carried out on the circumferential surface of virgin and creep test samples at 2 and 1.5 MPa respectively. Each figure shows the topographic view, elemental analysis and chemical characterisation of the inspected surface using the energy dispersive x-ray spectroscopy (EDS). Figure 4.16 shows the plain surface of the virgin bar and a composition of mainly iron (Fe). Figure 4.17 for test sample at 2 MPa after 230 h, shows formation of oxide on the surface of the specimen while also showing small presence of oxygen in the composition analysis. Figure 4.18, for test sample at 1.5 MPa after 280 h shows even more intense oxide formation on the surface and a greater presence of oxygen in the composition analysis. All sample analysis and images were taken at the same reference point (Figure 3.4) and zoom at 15kV, X100 and 100 μm.

4.4.2. Inspection on contact surface edge

Figures 4.19 – 4.23 show the topographic view and the compositional analysis of the microstructural inspection carried out at the cross sectional surfaces of a virgin and creep tested samples at 2, 1.5, 1 MPa after a certain duration of time. The edge of the top surface directly in contact with the alumina when stress was applied, was examined. The figures show the sample, majorly as the pale region representing the iron (Fe), a black region which represents the resin used in the material preparation and the interface between the sample and the resin.

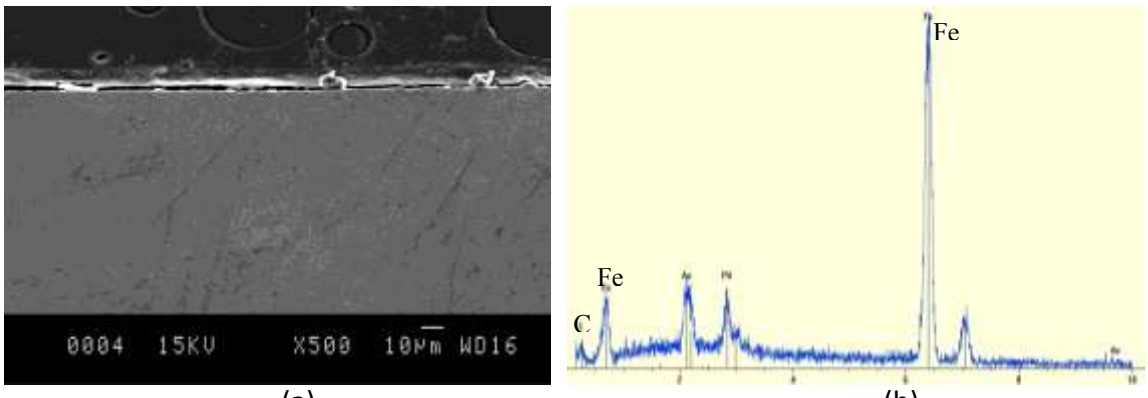

(a) (b)

Figure 4.19: Inspection on the top contact surface edge of a virgin sample

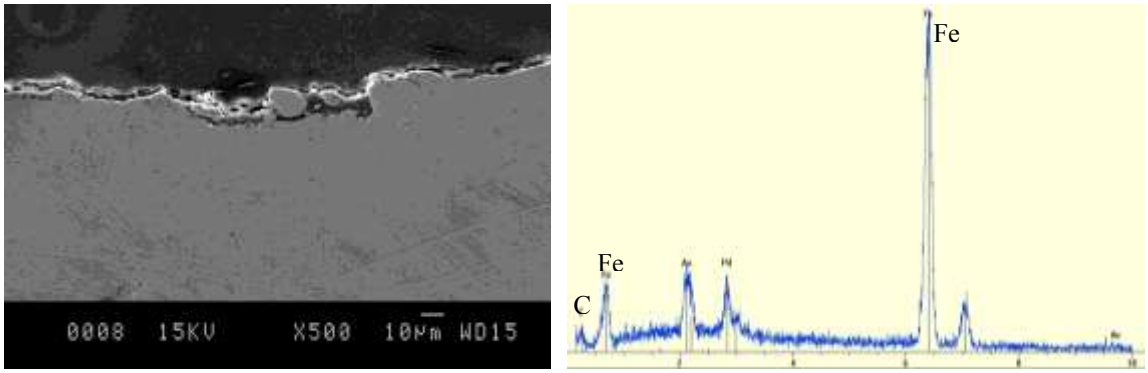

Figure 4.20: Inspection on the contact surface edge of a creep tested sample at 900 °C, at 2 MPa for 230 h

Figure 4.19 show the inspection results of the virgin sample which had a smooth surface at interface with the resin and a compositional analysis showing presence of mainly iron and carbon. Figure 4.20 shows microstructural inspection on a creep test sample at 2 MPa after 230 h, where a rough surface is seen at the interface between the sample and the resin with no particular oxide formation. Composition analysis at this surface showed majorly the presence of iron and small content of carbon similar to the virgin bar.

.

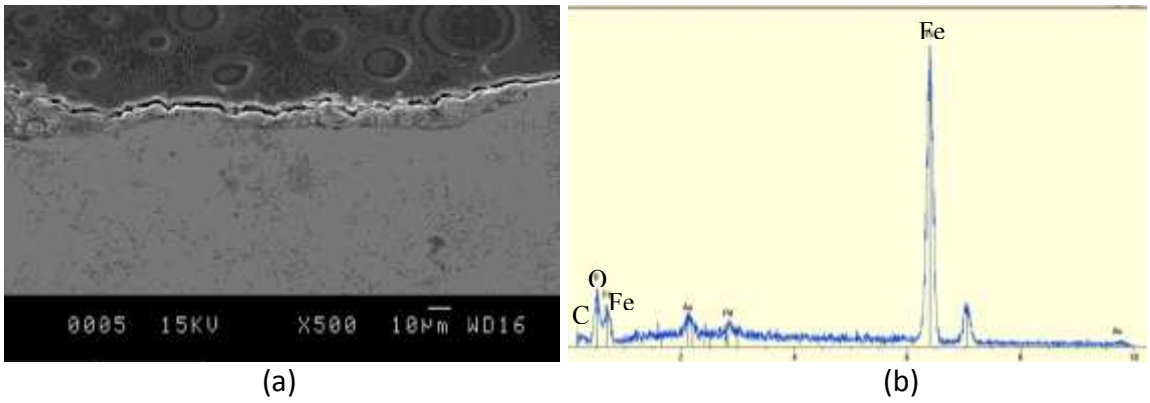

Figure 4.21: Inspection on the contact surface edge of a creep tested sample at 900 °C, at 1.5 MPa for 280 h

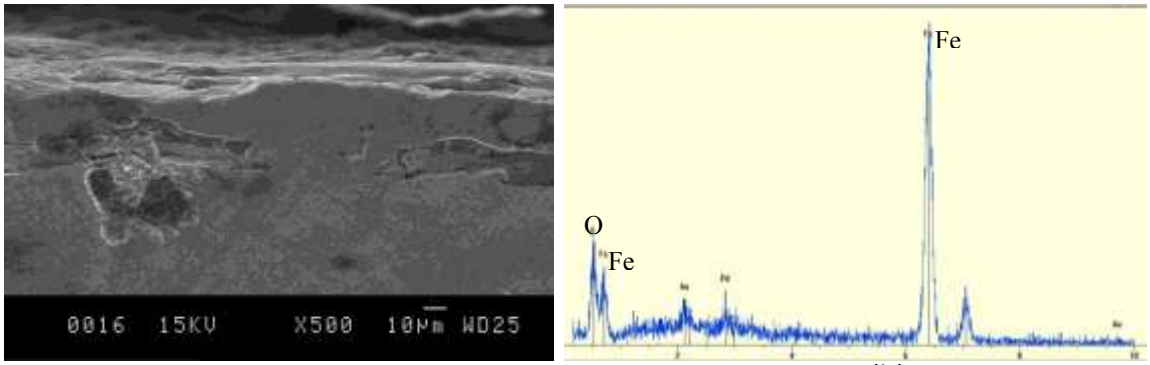

(a) (b)

Figure 4.22: Inspection on the contact surface edge of a creep tested sample at 900 °C, at 1 MPa for 240 h

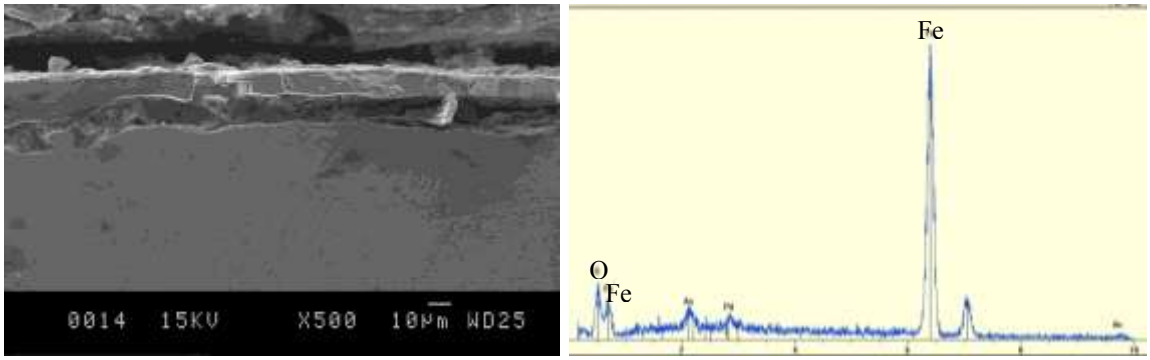

(a) (b)

Figure 4.23: Inspection on the contact surface edge of a creep tested sample at 900 °C, at 1 MPa for 72 h

Inspection on creep tested samples at 1.5 MPa after 280 h shows rough surface and formation of oxide to some small extent at this surface (Figure 4.21). The compositional analysis of this surface also showed the presence of little oxygen. Inspected creep tested samples at 1 MPa after 240 h and 72 h respectively showed a much intense rough edge, more presence of the oxides and a thicker penetration layer into the sample (Figure 4.22 and 4.23). The compositional analysis of these surfaces also showed presence of oxygen at higher level compare to that of 1.5 MPa.

In summary, the microstructural inspection at this edge showed a smooth surface for a virgin sample, rough surface due to applied stress for tested sample at 2 MPa but without

oxide formation. Material composition analysis showed presence of mainly iron and small carbon content for both virgin and tested sample at 2 MPa. Oxide formation and penetration was observed for test samples at lower stress levels below 2 MPa and the presence of oxygen was detected in the material composition analysis. The level of oxide penetration, its thickness and the amount of oxygen detected in the composition analysis was observed to increase with reducing stress levels and or longer test duration.

The circumferential edge was also further inspected and described in the next section.

4.4.3. Inspection on contact circumferential edge

Figures 4.24 – 4.28 shows the topographic view and the compositional analysis of the microstructural inspection carried out at the cross sectional surfaces (Figure 3.4) of a virgin and creep tested samples at 2, 1.5, 1 MPa after a certain duration of time. The edge at the circumference directly exposed to the furnace temperature was examined. Similar to previous results, the black section is as a result of the carbon resin used in preparing the sample, the pale section as the iron (Fe) in the sample and the interface between the sample and the resin was also seen.

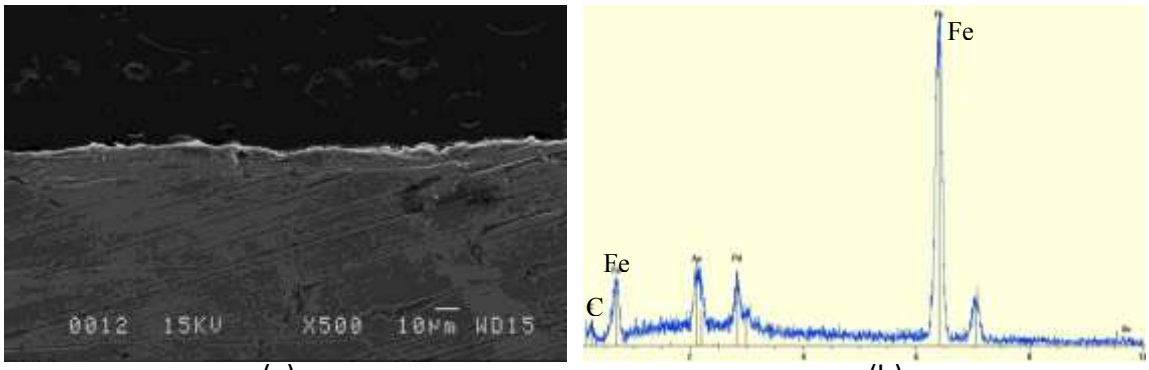

Figure 4.24: Inspection on the circumferential edge of a virgin sample

Figure 4.24 showed the inspection on the circumferential edge of the virgin sample. There is a smooth surface at the interface between the sample and the resin. The compositional analysis also showed the presence of mainly iron and small carbon content.

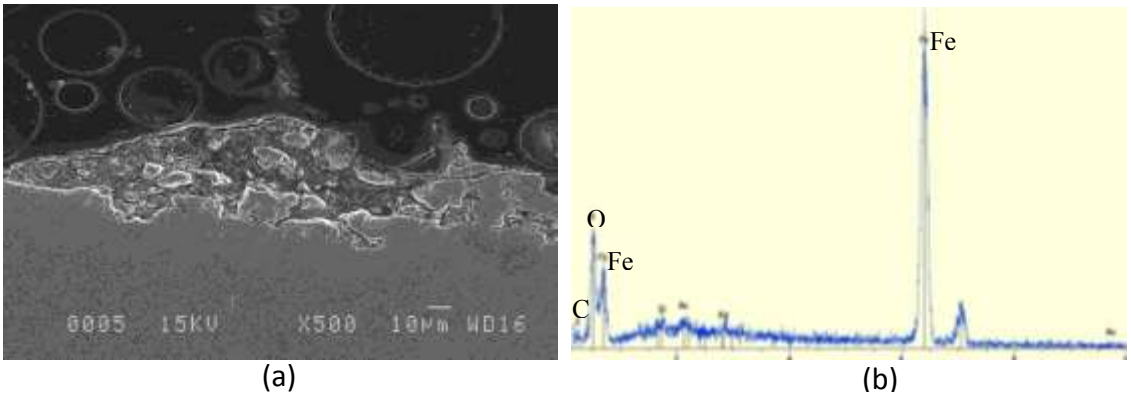

Figure 4.25: : Inspection on the circumferential edge of a creep tested sample at 900 °C, at 2 MPa for 230 h

Figure 4.25 shows the microstructural inspection on the circumferential edge of a creep test sample at 2 MPa after 230 h. A slightly rough surface was seen at the interface between the sample and the resin with the presence of some oxide formation to some small extent. Composition analysis at this surface showed majorly the presence of iron, small content of carbon and the presence of oxygen.

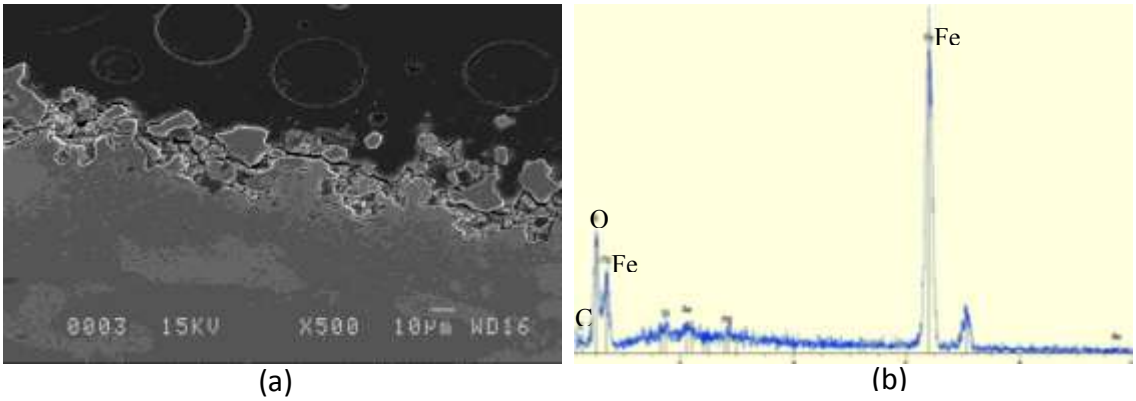

Figure 4.26: Inspection on the circumferential edge of a creep tested sample at 900 °C, at 1.5 MPa for 280 h

Inspection on creep tested samples at 1.5 MPa after 280 h showed increased rough surface and oxide layer slightly higher in compare to that of 2 MPa (Figure 4.26). The

compositional analysis of this surface also showed the presence of slightly increased presence of oxygen level.

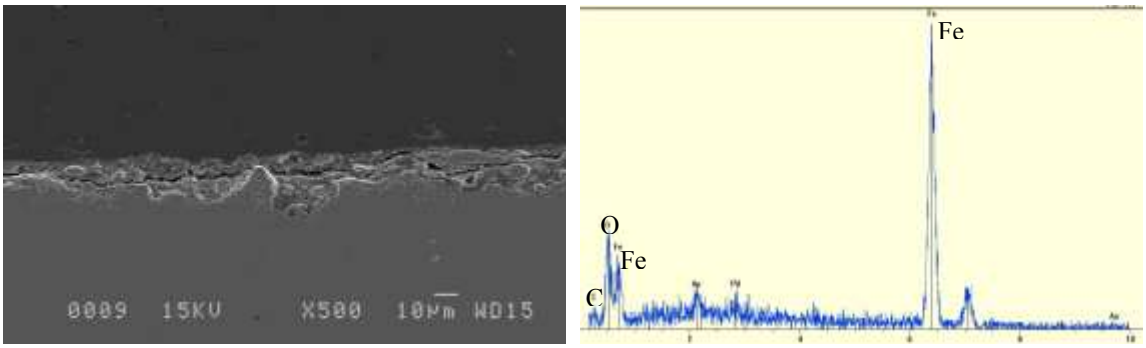

Figure 4.27: Inspection on the circumferential edge of a creep tested sample at 900 °C, at 1 MPa for 240 h

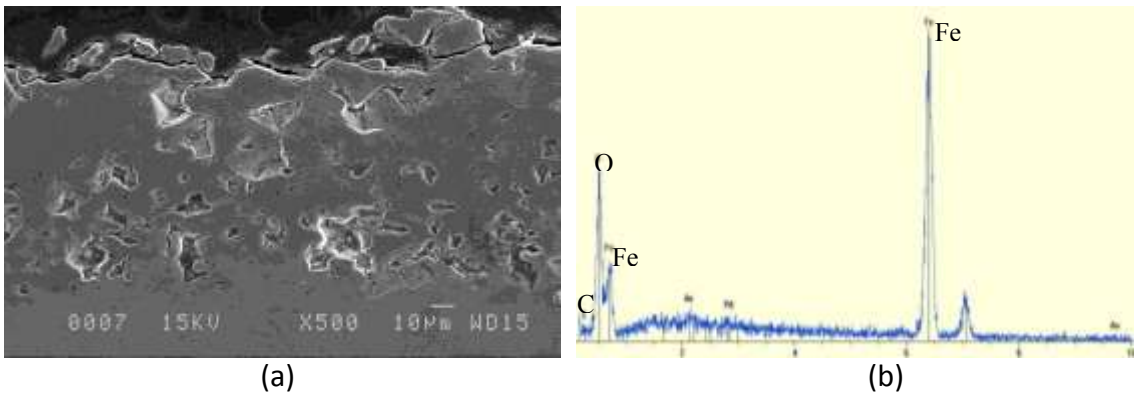

Figure 4.28: Inspection on the circumferential edge of a creep tested sample at 900 °C, at 1 MPa for 72 h

Inspected creep tested samples at 1 MPa after 240 h and 72 h respectively showed a much intense rough edge, more presence of the oxides and a thicker penetration layer into the sample (Figure 4.27 and 4.28). The compositional analysis of this surface also showed presence of oxygen at higher level in compare to that of 1.5 MPa or 2 MPa.

In summary, the microstructural inspection at this circumferential edge showed a smooth surface for a virgin sample with composition analysis showing presence of just iron and carbon. Oxide formation and penetration were observed in creep tested samples at all stress levels and the presence of oxygen was detected in the composition analysis at this edge. A slightly rough surface with small oxide layer was observed for test sample at 2 MPa. For creep tested samples at stresses below 2 MPa, the level of oxide penetration, its thickness layer and the amount of oxygen detected in the composition analysis were observed to increase with reducing stress levels and or longer test duration.

4.5. Further Investigation

This subsection communicates the results of further investigation carried out with the aim of reducing or completely eradicating the effect of oxidation occurring the during the creep test. As observed in the results of the microstructural investigation carried out, the effect of oxidation was seen on the creep tested samples. The rate of oxide formation and the level of the oxide thickness layer in the samples appeared to be characterised by the time of exposure to the creep test environment and also as a function of the applied stress. Results of the microstructural investigation gave a matching profile to that of the creep strain data obtained. This led to the conclusion that the unconventional creep strain data obtained were as a result of the oxidation occurring during the creep test.

Therefore, this gave a good headway to an approach to modify and further improve the creep test set up to reduce or completely eradicate the effect of oxide formation in the sample during creep tests at high temperature. Various ideas were discussed and summarised in the next section, one of which was implemented while further creep test was carried out under the new modifications to confirm its benefits.

4.5.1. Suggestions and modification approach to the creep test – set up and methodology

Various ideas and suggestions were considered as an approach towards modifying the test set-up to reduce oxidation effect on test samples. Options in literature [17] suggested the use of pressure pump to create a vacuum. This however was considered an elaborate and expensive approach which does not seem effective solution for our test set up at this time.

Recommendations from the industry (by Dr. Richard Beeler - Alcoa) suggested packing the sides of the sample with coke (carbon), enough to absorb the presence of oxygen around the test samples (as practised within the industry, stating that oxidation is not experienced by the cathode collector bar in the cell).

The final idea considered and implemented was to create a small close section around specimen in the furnace and to directly fill the surrounding of the small section with the weaker gas such as Argon rather than the entire furnace (Figure 4.29). A small cylindrical shaped metal (Inconel) was machined to create an enclosed section (almost air tight) around the specimen after which it was filled with Argon gas to expel other gases that may present (Figure 4.29). An ABB gas analyser was used determine the gas composition within this chamber. By allowing flow of argon into the small section chamber around the specimen at a rate of 3 l/min, the analyser gave zero presence of oxygen after 4 minutes at room temperature.

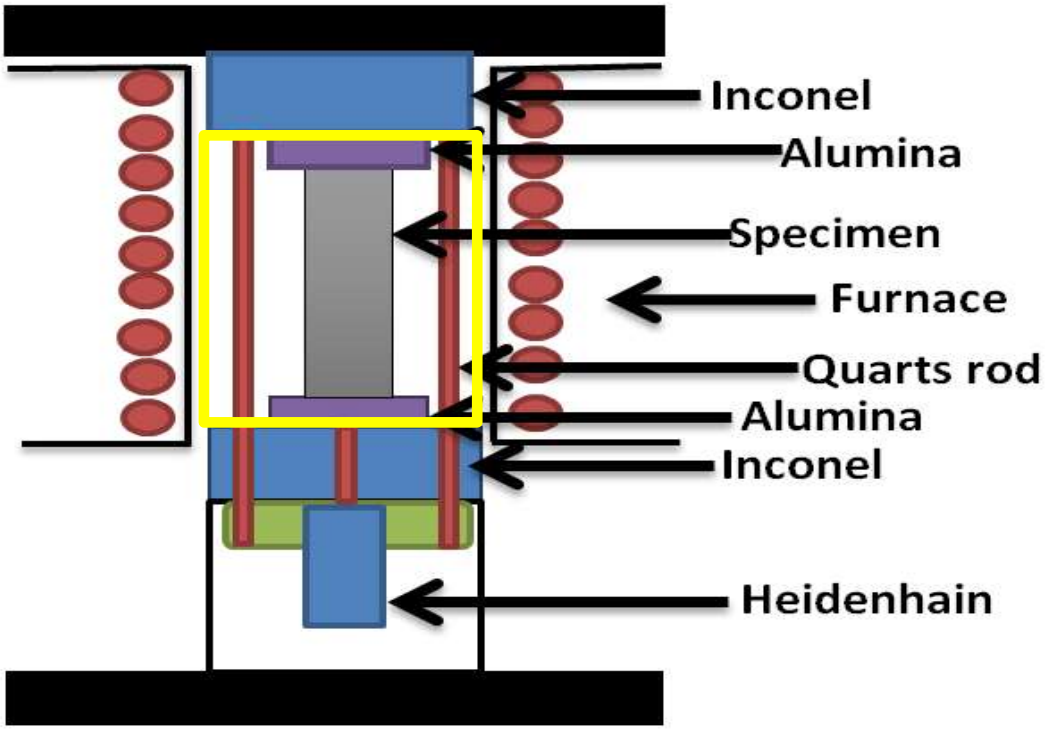

Figure 4.29: Schematic layout of modified creep test set-up

To validate the effectiveness of this modification and approach further compression creep tests were carried out. There was a slight modification in approach as the small section chamber created around the sample and filled with argon gas at a rate of 4 l/min was allowed 15 minutes stability time before commencing the heating stage. This was to ensure that all forms of oxygen present were expelled from the chamber. However, a short limitation existed as even though the temperature of the furnace could be measured, the temperature of the sample in the closed chamber could not be measured directly.

4.5.2. Compression creep tests

Creep tests were carried out on two samples without any coating at 0.1 MPa, (almost at no load) right from the onset, to compare the difference between the old set-up and the effectiveness of the new set- up after a long period of time. Both tests were carried out in an argon filled environment within the furnace at 900 °C (Figure 4.30).

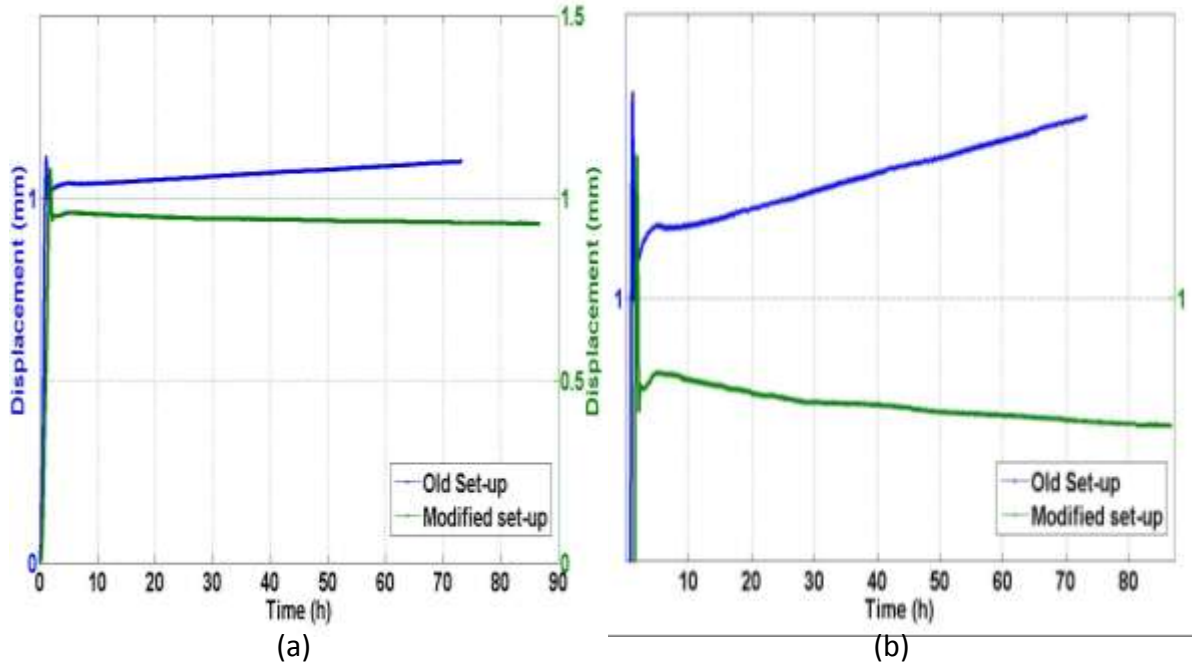

Figure 4.30: Creep test at 900 °C, 0.1 MPa, (a) overall view, (b) zoomed

Figure 4.30 shows the deformation behaviour recorded for the two tests carried out with the old set up and the newly modified set-up at 900 °C and almost zero stress level (0.1 MPa, to ensure contact). Both samples were seen to undergo region thermal expansion and phase change as the previous test had shown. However, after this, at constant temperature of 900 °C, the sample tested with the old set-up approach was seen to continue to deform (expand) reasonably under the applied compressive load of 0.1 MPa. The sample tested with the newly modified set-up remained reasonably constant with slight slow deformation (in contraction), which can be regarded as creep due to the applied compressive load of 0.1 MPa.

Physical inspection was carried out on both samples after the test (Figure 4.31). The circumferential surface directly exposed to the furnace surrounding and the top surface in contact with the alumina (in line with the direction of the applied force) was inspected.

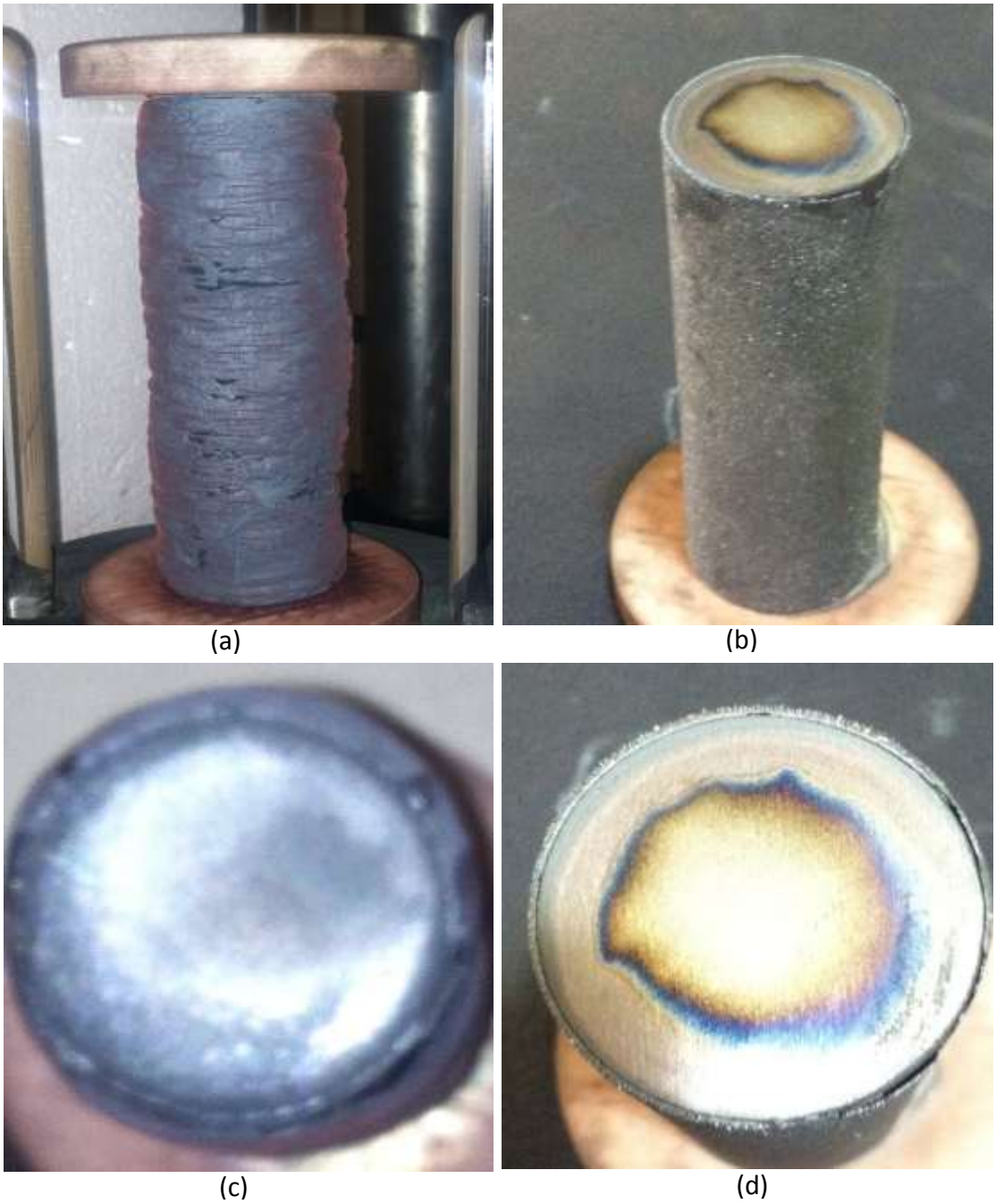

Figure 4.31: Creep test at 900 °C, 0.1 MPa, (a) old setup - side view, (b) modified setup – side view (c) old set up – top view, (d) modified set up – top view

Both samples show the effect of corrosion, however, the sample tested under the previous set-up was greatly affected by oxidation while this was much less in the sample tested under the newly modified set up. Inspection on the top surface of each sample showed

that sample tested under the previous set-up had greater oxidation thickness layer and a very rough surface. While the sample tested under the newly modified set-up showed a less oxidation thickness layer and the surface was as smooth as before the test with some slight colouration.

In summary, the newly modified approach showed reduced rate and effect of oxidation on the test samples but did however not completely eradicate the presence of oxygen in the chamber and its effect on the samples. The results also further clarified the effect of oxidation on the deformation behaviour of the samples. With this slight improvement, further creep tests were carried out at 1 and 2 MPa with the new set up to compare results with previous tests carried out under the old set-up.

4.5.3. Creep test at 1 MPa

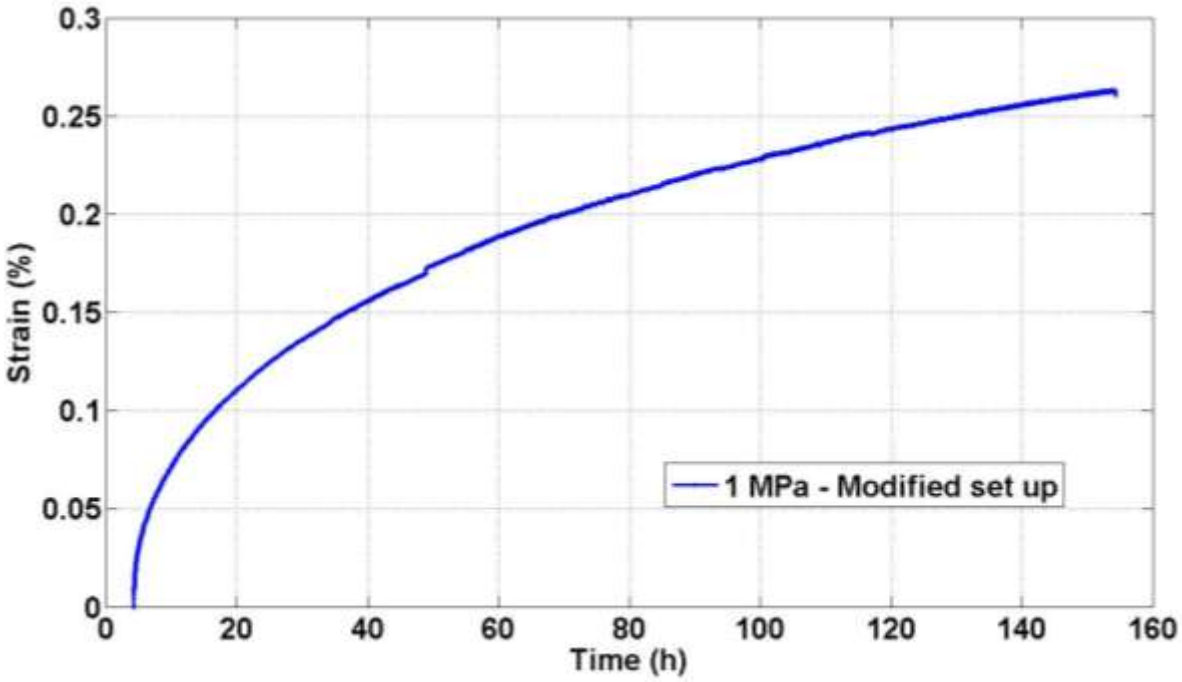

Figure 4.32: Creep test at 900 °C, and a stress level of 1 MPa

Figure 4.32 shows the creep curve for the creep test in compression carried out at 900 °C and at a stress level of 1 MPa. The test was carried out for a period of about 160 hours

where the sample continued to strain in contraction even after 80 hours. Creep test data obtained under the old set-up approach at similar conditions gave an unconventional behaviour where the sample strained in contraction up to about 80 h before it began to expand while under the applied constant compressive load of 1 MPa. The strain behaviour obtained with this modified set-up approach gave quite a different deformation profile as the sample continued to strain in contraction even after 140 h. The creep strain rate versus time plot also gave a minimum creep strain rate of 0.0028 %/h (Figure 4.33).

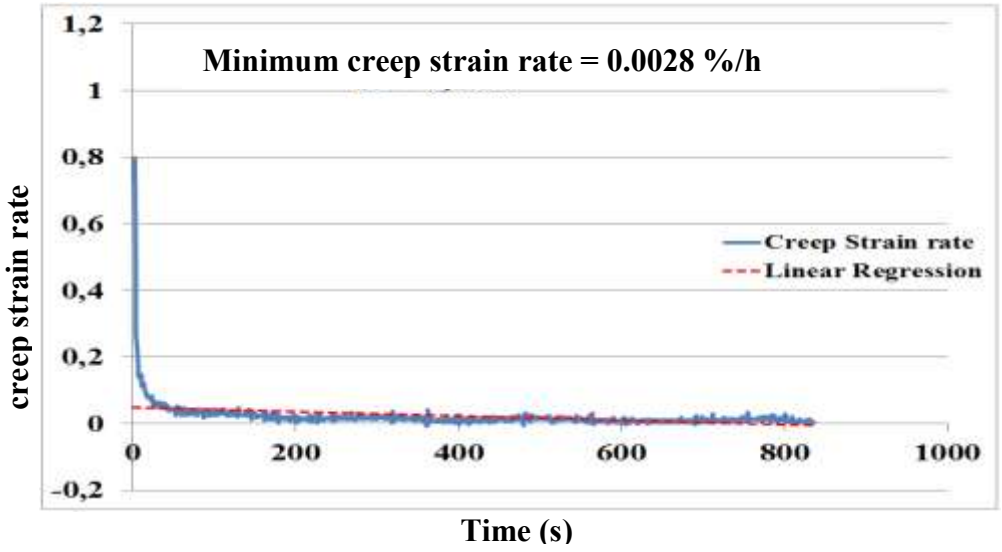

Figure 4.33: Creep strain rate vs time of test at 900 °C, and at 1 MPa stress level

Physical inspection showed the effect of oxidation formation layer on the circumference of the sample after the test (Figure 4.34). The thickness of the oxidation layer was dramatically reduced and can be considered negligible when compared to those of samples tested under the previous set up at similar conditions. The inspection on the top surface showed a smooth surface finish as it was before the test but with some slight colouration. This is also quite an improvement compared to samples tested under the previous set up where rough and non-uniform surface could be seen at the top surface after the test.

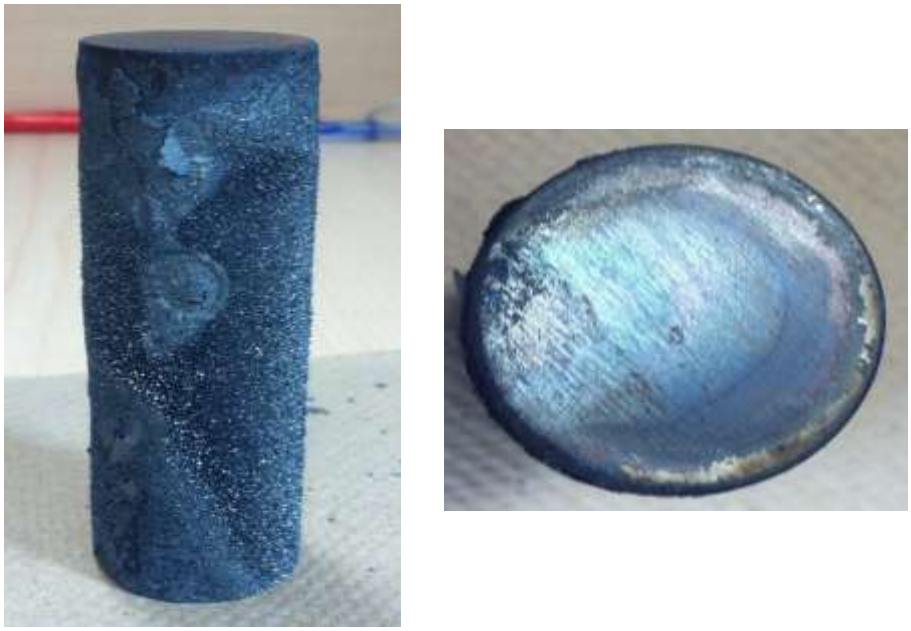

Figure 4.34: Physical inspection on test sample at 900 °C, and a stress level of 1

4.5.4. Creep test at 2 MPa

Further creep test in compression was carried out at at 900 °C and a stress level of 2 MPa (Figure 4.35).

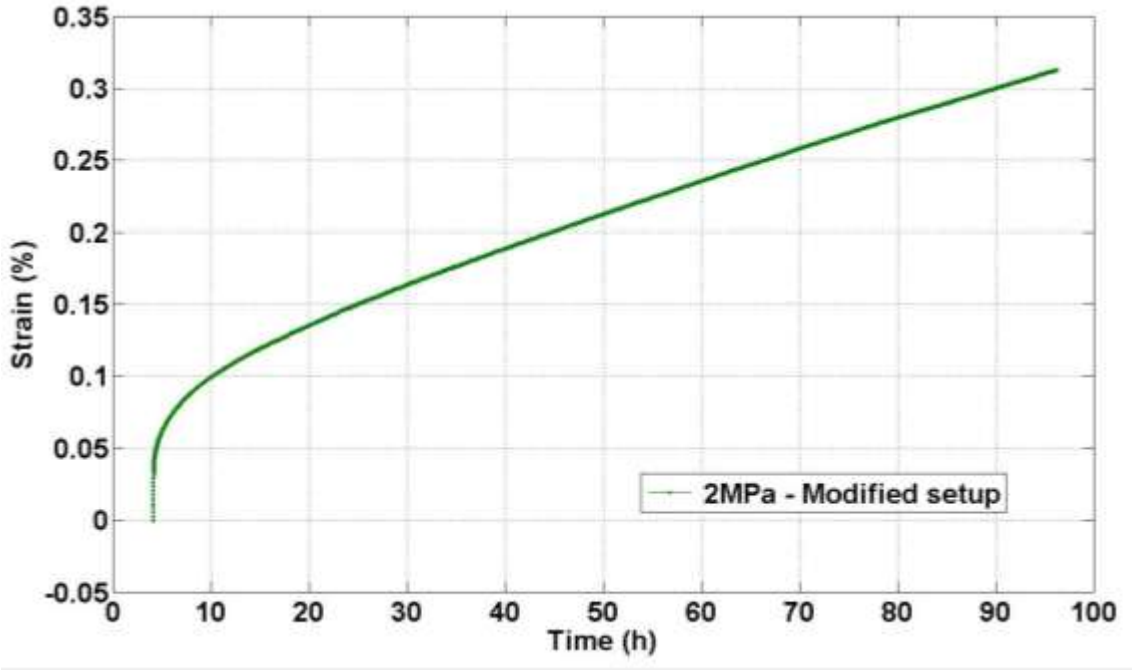

Figure 4.35: Creep test at 900 °C, and a stress level of 2 MPa,

The test was carried out for a period of about 100 hours where a total strain of 0.32 % was obtained. A typical creep curve dominated by steady state creep region right from the onset was also observed. This behaviour was similar to that of the creep strain data obtained for creep test carried out under the previous test-up at similar conditions. The creep strain rate versus time plot also gave a minimum creep strain rate of 0.0033 %/h (Figure 4.36).

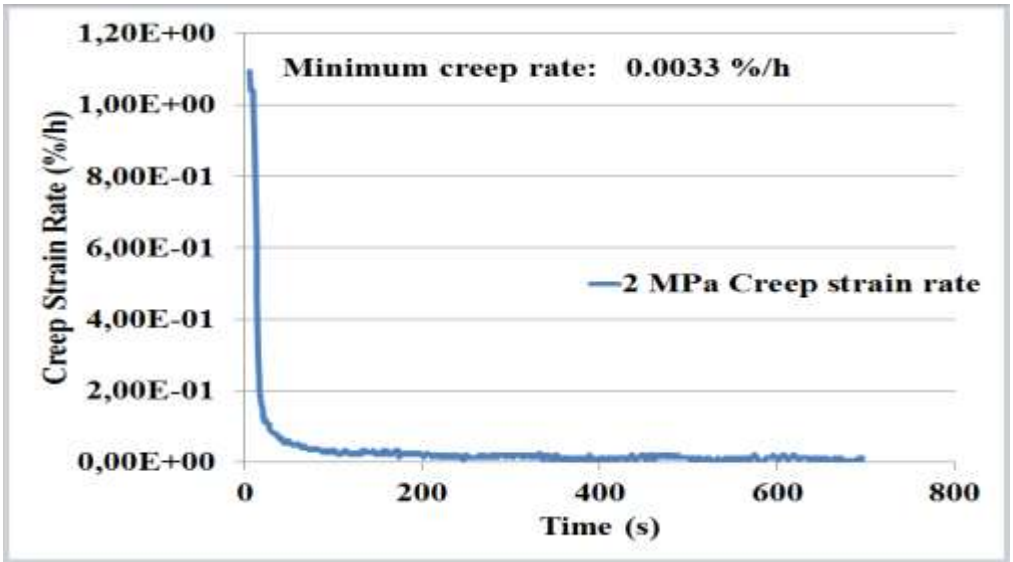

Figure 4.36: Creep strain rate vs time of test at 900 °C, and at 2 MPa stress level

Physical inspection on the sample used in this test also showed similar observation to that of the creep test at 1 MPa sample. There was a slight formation of oxidation layer on the circumference and the thickness of the layer was less to that observed in samples tested under the old test set-up. The inspection on the top surface also showed a smooth surface finish as it was before the test but with some slight colouration. This is also quite an improvement in comparison to samples tested under the previous set up where rough and non-uniform surface could be seen at the top surface after the test.

The strain data of both creep tests at 1 and 2 MPa carried out under the newly modified set-up was plotted on one graphical area to get a good compare (Figure 4.37).

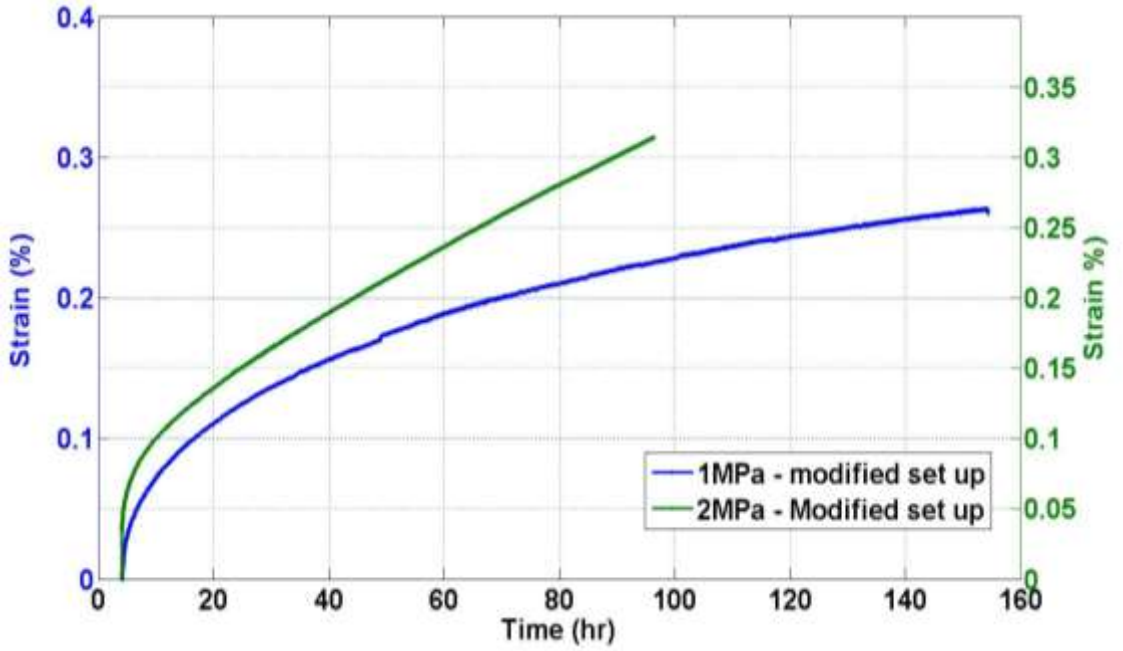

Figure 4.37: Compare of strain data for creep tests at 900 °C, and stress levels of 1 and 2 MPa using modified ted set-up approach

For strain data obtained at constant applied compressive stress of 1 MPa, the material continued to strain in contraction even after 80 h and lasted for a total duration of 160 h. A creep strain rate of 0.0028 %/h was obtained which stands relatively close to data in literature at 0.0025 %/h for low carbon steel.

For constantly applied compressive stress of 2 MPa, the strain data gave a creep curve typically dominated by secondary creep region and continued to strain in contraction for a period of 100 h. A maximum strain of 0.32 % and a minimum creep strain rate of 0.0033 % per hour were obtained which compares relatively well with data in literature.

Finally, the overall summary of the investigation approach, the merits and plausibility of the improvements made to the test methodology based on the analysis of data obtained, observations in microstructural inspection and other factors that appears to affect the accuracy of the investigation, were evaluated and discussed in section 4.6.

4.6. Overview of study

This section presents the overall summary of the approach and results obtained in an investigation carried out to study the deformation behaviour of the cathode collector bar in an aluminium reduction cell. The collector bar is made of low carbon steel and undergoes not only elastic contraction but also creep deformation over the service life of the cell (chapter 1). A good knowledge of the thermal and mechanical properties such as coefficient of thermal expansion, Young´s modulus and creep strain rate were deemed necessary to adequately understand the material behaviour of the collector bar at the operating conditions (high temperature of about 960 °C) within the cell.

The objectives of this investigation were such that a literature review was first carried out on the material properties, creep mechanism, physical laws and representative models of the deformation behaviour of metals at high temperatures (chapter 2). This was followed by an experimental program of compression creep tests carried out on low carbon steel (AISI 1006) at high temperature and low stress levels (chapter 3). Due to the high temperature corrosive environment at which the test was carried out, microstructural investigation on creep tested samples was also included in the experimental program.

Results of the strain data obtained during the test were presented in two stages (chapter During the heating stage, strain obtained due to thermal expansion, the effect of phase change and the evaluated thermal expansion coefficient were looked at. The creep strain data, observations in the deformation behaviour at different stress levels and the sensitivity of the strain to changes in the furnace temperature were also looked at. Obtained data and deformation behaviour at each stage were compared to existing data in literature.

The fit of various creep models identified in literature, their suitability to the obtained creep strain data in this investigation and a comparison of the values of selected model parameters and mechanical properties to those given in literature were summarised this chapter. Results of the microstructural inspection showing the effect of oxide formation on the creep tested samples were also discussed.

Different factors were considered in search of a valid explanation for the deformation behaviour obtained at stress levels below 2 MPa. One of such was the idea of the threshold stress theory previously discussed in chapter 2. It was identified in literature that there is a threshold stress (minimum stress) below which no creep occurs. This theory just describes a plateau level attained in the creep curve at which no deformation (compression or expansion) can be observed for such stress level (Figure 2.5a). Hence, such a theory cannot be used to explain this behaviour.

However, due to the corrosive nature of the test environment, microstructural inspection of the creep tested sample to determine the effect of corrosion and oxide formation on the deformation was considered viable approach. Microstructural investigation carried out the creep tested samples showed the effect of corrosion and oxide formation on the samples with matching profile to the obtained creep data as a function of the test duration and applied stress. This led to further investigations by modifying of the test set-up.

An approach to create a smaller chamber around the location of the specimen within the furnace and fill with Argon rather than fill the whole furnace which is a larger area with Argon was adopted. The test set up was modified to this new approach (Figure 4.29) and further tests were carried out using this method.

Comparison of tests carried out on samples using the old test set-up and the modified test set up at same condition (900 °C and at stress of 0.1 MPa) showed the occurrence of oxidation in both approach. However, the sample of the modified test set-up showed dramatically less effect of oxidation formation and thickness layer in comparison to the sample of the old test set up (Figure 4.31). Physical inspection on the top surface of both samples showed that the surface of the modified test-set up sample had a relatively smooth surface as before the test compared to that of the old test set-up which showed a rather rough surface due to the oxidation effect.

Maintaining a uniform (smooth) surface at the top and bottom surface where the sample is interfaces (in contact) with the alumina and in the direction of the applied load is very important to maintain uniform contact and uniform stress distribution within the sample. Otherwise, this may affect the deformation behaviour of such samples over time.

The strain data obtained (Figure 4.30) for both samples also showed that, at constant temperature, the sample tested under the modified test set up approach remained almost in a constant state over time with slight strain in contraction considered as creep due to the constantly applied 0.1 MPa load. While the sample tested under the old set-up approach continued to strain in expansion (at constant temperature) to a reasonable large extent over time. This further displayed the effect of oxidation on strain behaviour of the sample.

The modified test set up approach did not completely eradicate the effect of oxidation, however, major improvements were observed. Therefore, further creep test were carried out at 900 °C and applied compressive load of 1 MPa and 2 MPa (Figure 4.37) using the modified test set-up approach. A typical creep curve was obtained at both stress levels.

5. Conclusion

5.1. Strain behaviour during the heating stage

During the heating stage, a linear thermal expansion was observed at increasing temperatures from ambient up to about 750 °C with a maximum strain of 1.25 %. This was followed by a stage of short contraction at increasing temperatures from 750 °C to 900 °C signifying region of phase change from ferrite to austenite (Figure 4.1). The evaluated thermal expansion coefficient value was 18 x 10^{-6} per °C. The deformation profile and the obtained values for maximum strain and thermal expansion coefficient at this stage was comparable to given data in the literature for a low carbon steel material (see chapter 2 – subsection 2.2.3 – Figure 2.2).

The iron-carbon phase diagram (Figure 2.2b) showed that for a low carbon steel with carbon content of 0.08 %, a phase change from ferrite to austenite begins to occur at about 750 °C, where both phase can coexist and only reaches a full austenite region at 915 °C. During the test, the sample was left at isothermal condition (at 900 °C) for four hours where a steady state (constant value of strain) was reached (Figure 4.2). However, at this test temperature, the material is in a region where both ferrite and austenite phase still coexists and suggests that the microstructure of the material is not in a completely steady austenite region. This could have some effect on the value and behaviour of strain data obtained during the creep test.

5.2. Strain behaviour during creep test

Analysis of the preliminary creep test curve at 1 MPa – 900 °C (Figure 4.4), gave data which in terms of the elastic modulus of 12 GPa were comparable to those obtainable in literature (chapter 2 – subsection 2.2.5). However, the obtained value of the creep strain rate data at 0.006 %/h differs to that given in literature (chapter 2 – subsection 2.2.5). A clear elastic and creep strain region were observed in the creep data (Figure 4.4), but the region of primary and or secondary creep could not be easily distinguished and the controlling creep mechanism was not determined.

This preliminary test was carried out for a short duration of 24 hours and could not be considered long enough to accurately characterize the long-term behaviour of the

collector bar at operating conditions. Though the value of Young´s modulus compared well with literature, but the obtained creep strain rate data differs and could not be properly compared as information on the creep test duration, creep regions in the curve and the controlling creep mechanism were not provided (Figure 2.4).

Further creep tests were carried out at 900 °C and at four different stress levels of 0.5, 1, 1.5 and 2 MPa for longer duration of 250 h. Analysis of the creep test data at stress levels below 2 MPa did not produce a typical creep curve as expected and described in the literature. The material while under constant compressive force at high temperature in the furnace, produced a time-dependent deformation behaviour first in contraction up to a certain peak after which it began to expand (Figure 4.12). The behaviour could be characterised by time and the applied stress level. The lower the applied stress level, the quicker the peak was reached in contraction before expansion began to occur (after the peak), as it took 30, 80, and 150 hours to reach each peak for compressive creep test at stress levels of 0.5, 1 and 1.5 MPa respectively.

However, for the analysed strain data of creep test carried out at stress level of 2 MPa, a typical creep curve characteristically dominated by a region of secondary creep was obtained. The deformation behaviour observed at lower stress levels earlier could not be seen for the creep test data at stress level of 2 MPa even after a long period of time (Figure 4.13). Similar to process described during analysis of the preliminary creep test data was used to obtain a Young´s modulus of 11 GPa and a creep rate of 0.0037 %/h was obtained for the creep strain data at stress level of 2 MPa (Figure 4.15). This result compared well to data found in literature.

5.3. Models and parameters

Three creep models including power law model, exponential models and Burger rheological model were fitted to the obtained preliminary creep test data. The Power law and exponential model in their natural form did not suitably represent the whole creep region (Figure 4.6a, 4.7a) but had to be slightly modified to accommodate for more parameters which produced a much better representation (Figure 4.6b, 4.7b). The good fit of the modified power and exponential model suggested that at least two creep regions

existed within the obtained experimental creep data and provision to accommodate the elastic region should also be considered.

A linear Burger model was also fitted to the preliminary creep test curve and was considered the most suitable model to give a better representation of the creep curve for its ability to combine the elastic, the primary and the secondary region of the creep curve with more parameters using exponential functions (Figure 4.8). The model was also applied to the creep curve for test at stress level of 2 MPa (Figure 4.15). The model parameters were obtained and used to determine the mechanical properties of the material as presented in Table 4.4 and Table 4.5 for the preliminary creep test data at a stress level of 1 MPa and the creep test data at a stress level of 2 MPa respectively.

5.4. Microstructural inspection

Results of the microstructural investigation carried out on virgin bar and the creep tested samples at different stress levels were presented in section 4.4 of the previous chapter. The inspection was carried out at the circumferential surface, and two edges of the cross sectional surface to investigate the effect and level of oxide formation on the samples.

Initial inspection at the circumference surface of the samples showed formation of oxides to be more intense with increasing time of exposure of sample to test environment. Further inspection at the cross sectional surface (i.e. edge of the top surface where the sample was in contact with the alumina) showed a rough surface for creep tested sample at 2 MPa but without any oxide formation/layer.

However, the inspection on creep tested samples at stress levels below 2 MPa (at 1.5 and 1 MPa) showed the presence of oxide layer formed at this surface. Final inspection on the circumferential edge of the cross – sectional surface gave similar results and observations to those obtained at the edge of the top surface of the cross- section.

In conclusion, the effect of oxide formation and the presence of oxygen could be seen in all creep tested samples. The presence of the oxygen and the level of penetration of the oxide layer in the samples was seen to be dependent on time of exposure to creep test environment and characterised by the applied stress.

5.5. Modifications and improvements to approach

During the heating stage of all samples and for creep tests at a stress level of 2 MPa, the strain profile and obtained data were as expected and in good correlation with literature. However, creep strain profile obtained for tests at stress levels below 2 MPa gave a different characteristic to expectation. This unconventional behaviour was characterised as being dependent on the time of the creep test and as a function of the applied stress.

Findings of the microstructural investigation showed the effect of oxidation on the creep tested samples, these findings correlate well and gave a relatively good explanation for the creep strain behaviour obtained at stresses below 2 MPa. Hence, further modifications and improvements were made to the test bench set-up and test procedure to help reduce the effect of oxidation on the sample by trying to eradicate the presence of oxygen in the furnace during the test. Further creep tests were carried out with these new modifications. These changes and obtained results of repeated tests were presented in section 4.5.

The creep rate of 0.0033%/h obtained at 2 MPa test after modification and improvement to test approach is similar and comparable to the creep rate of 0.0033%/h obtained in the initial approach. Hence it can be concluded that the effect of oxidation is less on the specimen at higher stress levels above 2 MPa.

In conclusion, major improvements were seen in the data obtained from the modified test set-up approach in compare to the old test set up approach. The effect of oxidation could be seen by physical inspection on the sample and also in the deformation behaviour given by the obtained strain data. Though the modified test set up presently provides a better approach to that of the old test set up, the presence of oxygen and the effect of oxidation has not been completely eradicated and continues to limit the accuracy and the objective of the study.

In recommendation, the modified test set-up approach gave a good headway but further modification is required to the test set-up. More effort and further approach should be focused on creating a complete airtight vacuum chamber, filled with argon, around the sample within the furnace. With the ability to carry out these tests without the effect of

oxidation, more accurate results can be obtained. This will go a long way towards proper study of the deformation behaviour of the collector bar.

Bibliography

1. Prasad S. Studies on the Hall-Heroult aluminum electrowinning process. Journal of the Brazilian Chemical Society. Brazilian Chemical Society, 2000;11(3):245–51.

2. Tschope K. Degradation of Cathode Lining in Hall-Heroult Cells. Ph.D. Thesis, Institute of Material Technology, Norwegian University of Science and Technology; 2010.

3. Jessen SW. Mathematical Modelling of a Hall Héroult Aluminium Cell. Masters Thesis, Technical University of Denmark; 2008.

4. Beeler R. An Analytical Model for Cathode Voltage Drop in Aluminium Reduction Cells. TMS (The Minerals, Metals and Materials Society). 2003.

5. Hop J.G. Sodium Expansion and Creep of Cathode Carbon. Ph.D. Thesis, Institute of Material Technology, Norwegian University of Science and Technology; 2003.

6. Picard D, Fafard M, Soucy G, Bilodeau J-F. Room temperature long-term creep/relaxation behaviour of carbon cathode material. Materials Science and Engineering A, 2008;496(1):366–75.

7. Wilkening S, Winkhaus G. Material problems in electrowinning of aluminium by the Hall-Heroult process. Journal of Applied Electrochemistry, 1989;19(4):596–604.

8. Kodur V, Dwaikat M, Fike R. High-Temperature Properties of Steel for Fire Resistance Modeling of Structures. Journal of Materials in Civil Engineering American Society of Civil Engineers, 2010;22(5):423–34.

9. Norman ED. Mechanical Behaviour of Materials. 3rd editio. Pearson Prentice Hall; 2007. p. 23–45; 772–836.

10. Weinberg F. The strength and ductility of continuouslycast steels above 800°C. Metallurgical Transactions B, 1979;10(4):513–22.

11. Wray PJ. Effect of carbon content on the plastic flow of plain carbon steels at elevated temperatures. Metallurgical Transactions A, 1982;13(1):125–34.

12. Pines, Y. A., Sirenko, A. F. Physics – Solid State. SOV. 1962;6:1336–9.

13. Ruano OA, Wadsworth J, Sherby OD. Harper-dorn creep in pure metals. Acta Metallurgica, 1988;36(4):1117–28.

14. Chen, J., Young, B., Uy, B. Behavior of high strength structural steel at elevated temperatures. Journals of Structural Engineering, 2006;132(12):1948–54.

15. European Committee for Standardization. Eurocode 3: Design of steel structures - Part 1-2: General rules - Structural fire design. Brussels: European Committee for Standardization; 2005. p. 4–76.

16. Xinbo L, Fubao Z, Jianhua F, Zhiliang Z. Research on the flow stress characteristics of AISI 1006 and AISI 5140 in the temperature range of warm forging by means of thermo-mechanical experiments. Journal of Materials Processing Technology, 2002;122(1):38–44.

17. Mishra, R.S., Jones, H., Greenwood, G.W. Creep of Low Carbon Steel at Low Stresses and Intermediate Temperatures. Acta metal material. 1990;38(3):461–8.

18. Harold, J.F., Ashby, M.F. Deformation – Mechanism Maps, the Plasticity and Creep of Metals and Ceramics. First edit. Pergamon Press; 1982.

19. Kassner, M.E. Fundamentals of Creep in Metals and Alloys. Second edi. Elsevier Science; 2009. p. 95–115.

20. Odqvist FKG. Mathematical Theory of Creep and Creep Rupture. 2nd Editio. Oxford University Press; 1974.

21. Brehm H, Daehn GS. A framework for modeling creep in pure metals. Metallurgical and Materials Transactions A, 2002;33(2):363–71.

22. Chandler HD. Creep modelling using semiempirical deformation and damage equations: f.c.c. metals. Materials Science and Engineering: A, 1991;131(2):177–85.

23. Nilsson J-O, Howell PR, Dunlop GL. Interfacial microstructure and low stress, high temperature creep of an austenitic stainless steel. Acta Metallurgica, 1979;27(2):179–86.

24. Wilshire B. Creep and Fracture of Engineering Materials and Structures. Maney Pub;1993 p. 812.

25. Naumenko K, Altenbach H. Modeling of Creep for Structural Analysis, Berlin, Heidelberg: Springer Berlin Heidelberg; 2007.

26. Parker JD, Wilshire B. Deformation and fracture processes during creep of 12Cr12Mo14V ferritic steel. Mechanics of Materials, 1982;1(2):113–21.

27. Solberg, J.K. A semi-empirical model for stress relaxation including primary and secondary creep stages [online]. Blindern: Chapman and Hall Ltd; 1986. p. 630–6.

28. Walser B, Sherby OD. The Structure dependence of power law creep. Scripta Metallurgica, 1982;16(2):213–9.

29. Cottrell, A.H., Aytekin, V. Andrade's Creep Law and the Flow of Zinc Crystals : Abstract : Nature. Nature, 1947;160:328–9.

30. Garofalo F, Zwell L, Keh A., Weissmann S. Substructure formation in iron during creep at 600°c. Acta Metallurgica, 1961;9(8):721–9.

31. Picard, D., Fafard, M., Soucy, G., Bilodeau, J.F. Three-Dimensional Constitutive Creep/Relaxation Model of Carbon Cathode Materials. Journal of Applied Mechanics. American Society of Mechanical Engineers, 2008;75(3):031017.

32. Yang L, Luo Y, Tang X. Rheological properties of carbon constructional quality steels. Journal of Central South University of Technology, 2007;14(S1):285–8.

33. Yu M, Luo Y, Peng X. Creep testing and viscous behavior research on carbon constructional quality steel under high temperature. Journal of Central South University of Technology, 2010;15(S1):206–9.

34. Tschoegl NW. The Phenomenological Theory of Linear Viscoelastic Behavior, Berlin, Heidelberg: Springer Berlin Heidelberg; 1989.

35. Findley W. Creep and relaxation of nonlinear viscoelastic materials : with an introduction to linear viscoelasticity. New York: Dover; 1989.

36. Birosca S. The microstructural development of oxide scales on low carbon steels [online]. Loughborough University Institutional Repository; 2006 Available from: https://dspace.lboro.ac.uk/dspace-jspui/handle/2134/5852 [accessed 2013 Aug 4].